Bioartificial livers: theoretical methods to improve and optimize design

Davidson, Adam

Award date:
2011

Awarding institution:
University of Bath

Bioartificial Livers: Theoretical Methods to Improve and Optimize Design

Adam James Davidson

A thesis submitted for the degree of Doctor of Philosophy

University of Bath

Department of Chemical Engineering

June 2011

Acknowledgements

I would like to acknowledge the tremendous contribution made to this work by my supervisors, Professor Julian Chaudhuri and Dr Marianne Ellis. Each of them has given me a lot of time and valuable guidance, and their feedback has been essential to the completion of the thesis. Additionally, I have had very productive discussions with Kawai Chan, Dr Rebecca Shipley and Dr Sarah Waters at the Department of Mathematics at the University of Oxford, and also Michael Buccholz and Dr David Tosh of the Department of Biology here at the University of Bath.

On a personal level, my colleagues here in the Department of Chemical Engineering have always been a source of both inspiration and laughter at times. I would like to dedicate this work to them and also to my beloved fiancée Yui and fantastic parents who have supported me throughout my university career.

Table of Contents

List of Figures

List of Tables

Nomenclature

B_1	Empirical constant, relating k_{hyp} to R_l (s/m)
B_2	Empirical constant, relating k_{hyp} to R_l (s)
c	Concentration of oxygen in convection-diffusion equation (mol/m^3)
C_x	Empirical constant, relating k_x to R_l (s)
C_L	Number of cell layers surrounding each hollow fibre
D	Diffusion coefficient in general convection-diffusion equation
d_{cell}	Thickness of cell layer (m)
D_{Hb}	Diffusion coefficient for haemoglobin (m^2/s)
D_{hep}	Diffusion coefficient for oxygen in hepatocyte layer (m^2/s)
D_{plasma}	Diffusion coefficient for oxygen in plasma (m^2/s)
$f_{PP/PC/PV}$	Size of each liver zone expressed as a fraction of the cell volume
Hb	Concentration of haemoglobin in the blood stream (mol/m^3)
K	Empirical constant in Margaria equation (mmHg^{-1})
k_{hyp}	Proportionality constant between Z_x and $\bar{u}$ (s)
k_l	Proportionality constant between L_x and $\bar{u}$ (s)
K_m	Michaelis-Menten constant (mol/m^3)
L	Fibre length (m)
L_{hyp}	Axial position of partial pressure contour (m)
L_x	Axial position of partial pressure contour (m)
N	Number of fibres
N_{cell}	Number of cells in the BAL
k_{O2}	Reaction rate term for release of oxygen from haemoglobin (s^{-1})
$N_{cell(max)}$	The maximum number of cells that can be supported in the BAL for a given flow rate
N_{eq}	Fibre number that will result in equally sized periportal and perivenous zones
N_{max}	Maximum allowable number of fibres according to the anoxia constraint
N_{min}	Minimum allowable number of fibres according to the cell number constraint
m	Empirical constant in Margaria equation
M_x	Empirical constant, relating k_x to R_l (s/m)

pO_2	Partial pressure of oxygen (mmHg)
$pO_{2(in)}$	Partial pressure of oxygen at the entrance of the BAL (mmHg)
Q	Plasma flow rate to the BAL (ml/min)
Q_{eq}	Plasma flow rate that will give equally sized periportal and perivenous zones (ml/min)
Q_{min}	The minimum flow rate required to support a given cell population in the BAL (ml/min)
r	Radial coordinate (m)
R_l	Fibre lumen radius (m)
R_m	Radial position of outer fibre membrane surface (m)
R_e	Radial position of outer cell layer surface (m)
u	Fluid velocity vector (m/s)
$\bar{u}$	Mean axial velocity (m/s)
V	Generation/uptake term in the convection-diffusion equation (mol/m^3/s)
V_{max}	Maximum oxygen consumption term in Michaelis-Menten equation (mol/m^3/s)
w	Thickness of hollow fibre membrane (m)
x	Subscript denoting the relevant partial pressure of oxygen
z	Axial coordinate (m)

Greek Letters

α	Solubility constant for Henry's Law (mmHg/mol m^{-3} s^{-1})
ρ_{cell}	Cell surface density on hollow fibre (cells/m^2)

Abbreviations

BAL	Bioartificial Liver
BLSS	Bioartificial Liver Support System
ECS	Extracapillary Space
ELAD	Extracorporeal Liver Assist Device
HFBR	Hollow Fibre Bioreactor
MARS	Molecular Adsorbent Recycling System
SPAD	Single Pass Albumin Dialysis

Abstract

In this work, a mathematical modelling approach is taken to improve and optimize the designs of bioartificial liver (BAL) systems. BALs are an alternative therapy for the extremely serious condition of liver failure where liver transplant is currently the only viable option. As yet, large-scale clinical trials have not been successful enough in order for BALs to gain regulatory approval. Through the work in this report, it is envisaged that BAL design can be improved to the point where they can gain clinical acceptance

One of the main issues in BAL design is the provision of adequate oxygen to the cell mass. To this end, a mathematical model to describe oxygen mass transport is developed based on the principle of Krogh cylinders. The results of this model are subsequently interpreted and presented in Operating Region charts, an image of a parameter space that corresponds to viable BAL designs. These charts allow several important design trends to be identified, e.g. numerous short and thin hollow fibres are favourable over fewer thicker, longer fibres. In addition, it is shown that a physiologically relevant cell number of more than 10% of the native liver cell mass can be supported in these devices under the right conditions. Subsequently the concept of the Operating Region is expanded to include zonation, a metabolic phenomenon where local oxygen tension is a primary modulator of liver cell function. It is found that zonation profiles can be well controlled and under standard conditions a plasma flow rate of 185 ml/min to the BAL would distribute the three metabolic zones evenly. Finally, the principles of the Operating Region charts and zonation are applied to three existing commercial BAL designs; the HepaMate, BLSS and ELAD systems. In each case it could be seen that the default designs of each system did not present ideal environments for liver cells. Through consideration of zonation profiles, each device design and operating parameters could be optimized to produce *in vivo*-like environments. In the case of the ELAD, reducing the plasma flow rate from 500 to 90 ml/min resulted in a balanced zonation profile. Overall, the work in this report has developed and detailed a series of tools that will assist a BAL designer in making judicious choices over bioreactor design and operating parameters. As a result, it is hoped that BALs can take a step forward towards clinical practice and ultimately saving lives.

Chapter 1: Introduction

This report describes a novel, innovative method to improve the design of bioartificial livers (BALs). These are devices that seek to sustain a patient suffering from liver failure until they can receive a transplant or recover naturally. Given the scarcity of donor livers and the length of transplant waiting lists, BALs could be vital tools to save the lives of many people suffering from liver failure.

BALs are extracorporeal devices containing liver cells that support patients whose liver has failed, until they can either receive a transplant or spontaneously recover. Many designs of BALs currently exist in various stages of development, some now in the process of or having already been evaluated in clinical trials. To date, clinical trials have not conclusively shown that BAL therapy can improve survival rates in liver failure patients over standard medical therapy.

As BALs have thus far failed to gain regulatory approval and clinical acceptance, a theoretical framework to improve and optimize BAL design is outlined in this work. This is necessary as adequate oxygen provision to the cell mass is one of the main challenges in BAL design. This framework is based on the use of mathematical modelling techniques to describe mass transport in BAL. Initially an extensive literature review has been performed in Chapter 2, providing background on liver physiology, liver failure and the various methods being developed to treat it. The current key issues facing artificial liver support are then outlined. In addition, the various approaches in the past to mathematically model hollow fibre bioreactors are summarized, making note of particular cases where BALs have been modelled.

As BALs are often based on hollow fibre bioreactors where oxygen depletion is an important issue, BAL design must take account of oxygen availability to the liver cell mass. Using various models described in literature as a starting point, a mathematical model is developed in Chapter 3 to represent oxygen mass transfer within a hollow fibre bioreactor for use as a BAL. The results obtained from the mathematical model are then connected to BAL design. By also defining two operating constraints on the BAL, useful

design trends can be identified. These constraints can be plotted to define an 'Operating Region' within which both constraints are satisfied. These Operating Region charts act as visual design tool that allow design parameters to be chosen to create a viable BAL design. The sensitivity of the Operating Regions to these parameters can also be established. In addition, the operating constraints allow data regarding maximum cell loadings, minimum required plasma flow rates and priming volume of the BAL to be ascertained. These findings allow certain design trends to be identified that point towards better and more functional BALs.

In order to increase the effectiveness of any BAL, the cell environment should closely match the *in vivo* conditions they are normally exposed to. As such another objective can be defined; the Operating Region concept can be expanded by considering liver physiological phenomena, to further improve BAL design. In particular, gradients of oxygen tension within the liver lobule play a large role in defining the functions carried out by hepatocytes. By defining metabolic zones in the liver according to the range of local oxygen tension, mathematical modelling can allow the size of each zone within a BAL to be determined. This is seen in Chapter 4. The size of each zone in the bioreactor will be affected by operating and design parameters. A detailed analysis of how each design parameter impacts on the zone distribution will be carried out. Similar to the Operating Regions of Chapter 3, this will give insight into how more effective BALs can be designed.

Upon establishing a framework of mathematical modelling and BAL design, this framework can then be applied to existing BAL systems that are currently undergoing development and clinical trials. Chapter 5 builds on the work of previous chapters by applying the same principles to specific BAL designs. This allows any potential oxygen mass transport issues to be identified and possibly remedied through alterations to each BAL's design.

Overall, this work seeks to use mathematical modelling techniques to create a framework whereby deficiencies in BAL designs can be identified and more effective designs can be found. Chapter 6 outlines in detail the conclusions that have been made in this work, along with the potential impact on the field as a whole. It is hoped that the work presented here and the lessons gained from it will aid the development of more effective BALs. This

in turn should translate to greater survival rates among liver failure patients, which serves to highlight the importance of this work.

Chapter 2: Mathematical Modelling of Artificial Livers – Literature Review

2.1 Liver physiology

Weighing 1200-1500g in an adult, the liver is the largest internal organ of the human body (Fig. 2.1). It is essential to life and responsible for a myriad of physiological functions. Its metabolic activity is such that it produces 20% of the body's heat at rest (Scanlon and Sanders, 2003). Its removal in animal models invariably leads to death and liver failure in humans is associated with high mortality rates. The following sections will describe the physical structure, functions and physiology of the liver.

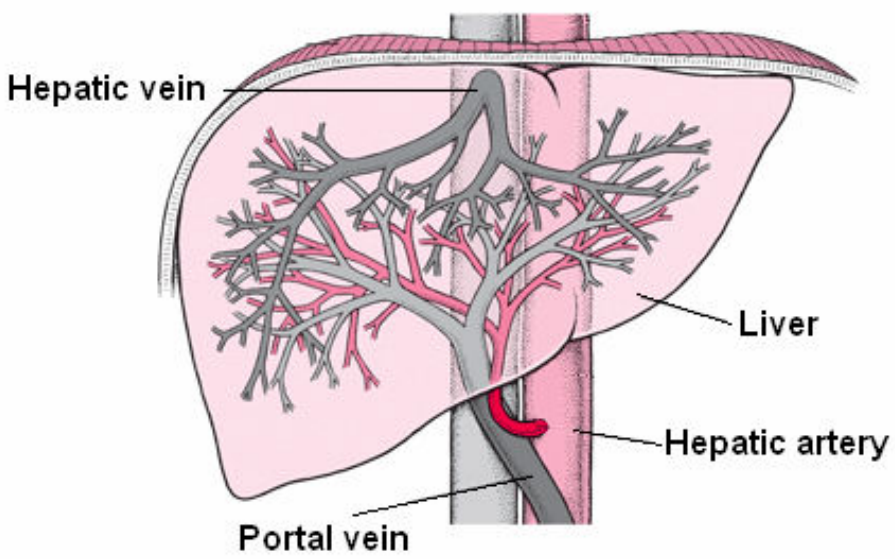

Figure 2.1: The liver is the only organ in the body to receive a dual blood supply. Blood enters the liver through the hepatic artery and portal vein from the small intestine. Diagram adapted from Merck website (Shaffer, 2007)

2.1.1 Structure of the liver

The liver is located below the diaphragm in the upper right and centre of the abdominal cavity. At a macroscopic level it can be seen to consist of two large left and right lobes.

The structural unit of the liver is the liver lobule, a roughly hexagonal column of liver cells about 0.7-2 mm in diameter that surrounds a central vein (Fig. 2.2). The liver receives blood from both the hepatic artery and portal vein, the only organ with such a dual blood supply. The branches of these vessels are situated between each lobule (Scanlon and Sanders, 2003). Two thirds of the supply is from the hepatic portal vein, originating from the small intestine carrying nutrient rich blood. The rest is oxygenated blood supplied by the hepatic artery. The total supply is approximately 1.5 L/min, a quarter of the resting cardiac output (Telford and Bridgman, 1995, Saxena et al., 2003). The capillaries of each lobule are in the form of sinusoids, highly permeable vessels located between each row of liver cells.

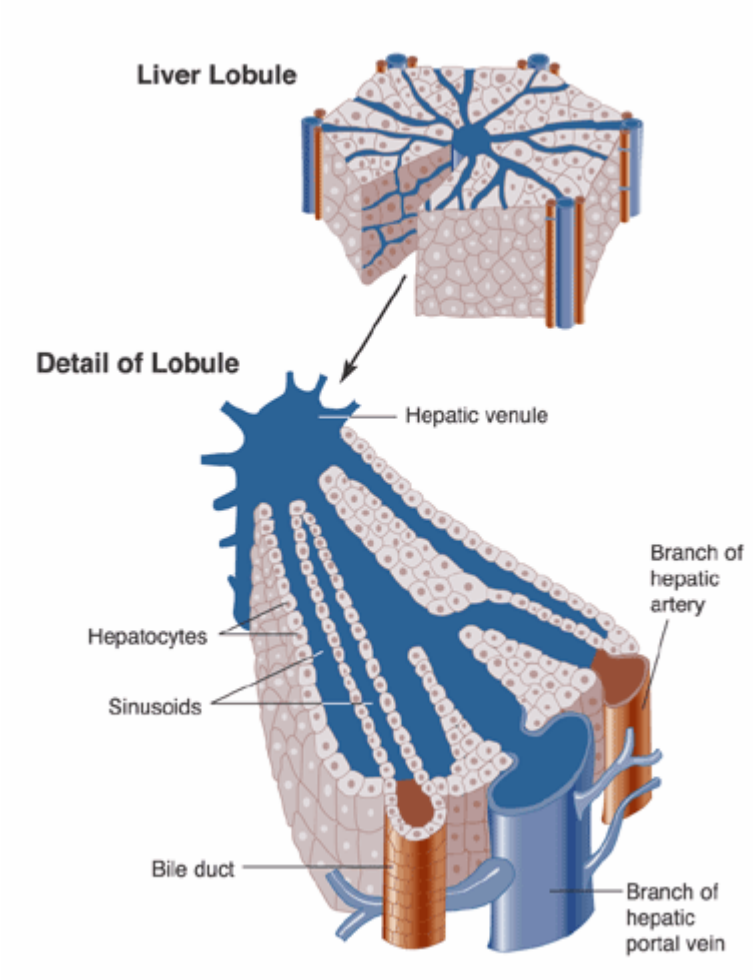

Figure 2.2: A diagram of the liver lobule (Shipley et al., 2011).

2.1.2 Functions of the liver

As stated previously, the liver is responsible for a number of physiological processes in the body. These encompass the regulation of glucose in the blood, synthesis of serum proteins and the detoxification of harmful substances to name a few. Some of these processes are listed below (Scanlon and Sanders, 2003):

- Detoxification of harmful substances. For example, alcohol is broken down into acetate and ammonia is converted into urea
- Xenobiotic metabolism
- Regulation of blood glucose levels
- Synthesis of blood proteins, e.g. albumin, the most abundant plasma protein and clotting proteins such as Factor VIII
- Synthesis of all 12 non-essential amino-acids
- Bile production for the emulsification of fat in the small intestine

In the case of liver failure in a patient all of these processes will be hampered. To aid survival of the patient some of these functions can theoretically be replaced through artificial means. Some of the approaches to achieve this are explained in Section 2.2.

2.1.3 Hepatic microvasculature

The location for the exchange of material between the blood stream and liver cells is the sinusoid (Fig. 2.3). The sinusoids receive venous blood through short venules connected to the portal vein, and oxygenated blood through branches of the hepatic arterioles. As these vessels have the ability to contract, blood supply to each sinusoid is variable. The sinusoid network exhibits a heterogeneity that is determined by its position in the liver. Near the portal vein, the network displays a large degree of interconnectivity whereas vessels become organised in parallel as they terminate in the central venules.

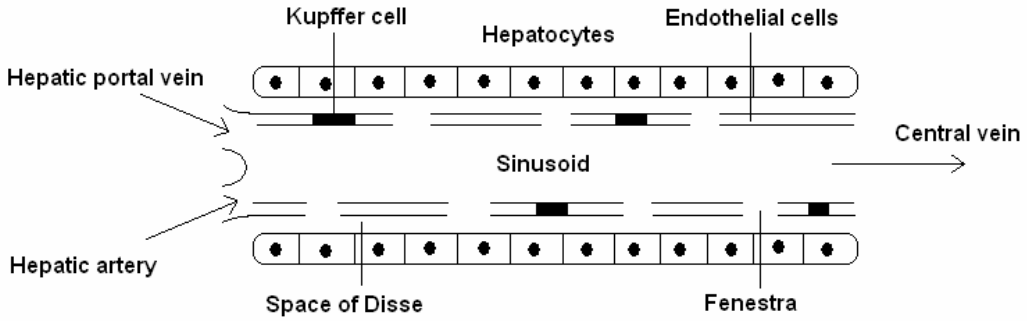

Figure 2.3: A representation of the liver sinusoid.

Each sinusoid vessel has a variable internal diameter of 9-12 μm, the diameter being generally smaller at the periportal end of the network. Similar to a normal capillary, the vessel wall consists mainly of a single layer of endothelial cells. However, loose overlapping of these cells creates a number of fenestrae in the sinusoidal wall. These openings allow contents of the blood (but not platelets or cells) to enter the extraluminal space, known the space of Disse, and interact with hepatocytes (Telford and Bridgman, 1995). Fenestrae account for 6-8% of the sinusoidal surface and are dynamic structures that can vary their diameter in response to a number of stimuli, such as blood pressure or vasoactive substances. In this way they can influence the plasma levels of larger molecules such as cholesterol. The fenestrae also tend to be larger and fewer in number towards the periportal end of the sinusoid.

In addition to endothelial cells, which represent 50% of the cells in the sinusoid, three other cell types are present. Phagocytotic Kupffer cells form part of the sinusoid lining, fat-storing stellate cells reside in the space of Disse and pit cells are attached to the luminal surface. Endothelial and Kupffer cells are able to swell and contract selectively to control the sinusoid diameter, while stellate cells also display some contractile properties to regulate blood flow (McCuskey, 2008).

2.1.4 Hepatocytes and zonation

The liver consists of 80% hepatocytes by cytoplasmic mass (Saxena et al., 2003). Hepatocytes are polyhedral and highly polarized, consisting of 2 specialized membrane

domains. The sinusoidal (or basolateral) membrane faces the sinusoid and is coated with microvilli (micron-scaled projections). The canalicular membrane forms the bile canaliculus along with bordering hepatocytes. These cells are among the most metabolically active and versatile within the body, with numerous functions as described in Section 2.1.2. However, heterogeneity exists in the liver so that functions can differ between the hepatocytes. This is known as liver zonation.

The metabolic functions carried out by hepatocytes vary significantly between the different regions of the liver lobule. This is partly due to the availability of substrates within the blood, with solute uptake normally being greater in the region of the lobule proximal to the hepatic artery and portal vein (Saxena et al., 2003). This is known as the periportal zone. It is also suggested that the functional heterogeneity of hepatocytes is related to differences in the sinusoidal fenestrae between the regions of the lobule as described previously (McCuskey, 2008). Within the periportal region the capacity for oxidative energy metabolism, urea synthesis, bile formation, glucose output and cell protection is greater, whereas the capacity for glucose uptake, glutamine formation, and xenobiotic metabolism is higher in the perivenous area. The perivenous zone is the region of the lobule closest to the central vein of the liver (Jungermann and Kietzmann, 2000, Chan et al., 2004). This zonation of the liver will be an important aspect when considering the design of bioartificial livers as it is desired to replace the full spectrum of liver functions within such a device. Oxygen is one of the primary modulators of hepatocyte function (Gebhardt, 1992, Jungermann and Kietzmann, 2000, Lindros, 1997) and by replicating sinusoid oxygenation *in vitro*, it is hoped this can be achieved.

Mitosis is rare in the adult liver though hepatic cells will divide rapidly to repair a damaged liver. The liver has a remarkable ability to regenerate from serious injury. In animal studies it has been shown that a full recovery is possible after two-thirds of the organ has been removed (Telford and Bridgman, 1995). For humans however, in most cases it not possible for a spontaneous recovery to occur after liver failure. It is this fact that incentivizes the development of an effective liver support device; to provide some way to support a human liver failure patient until a transplant becomes available or recovery can otherwise occur.

2.1.5 Liver failure

In the UK, liver disease is the fifth most common cause of death with up to 13,000 dying from liver related conditions in 2005. Chronic liver disease can progress until liver failure occurs, with orthotopic liver transplant currently the only viable treatment. The waiting list for liver transplants is currently between 6-12 months in the UK for low-risk patients (British Liver Trust – www.britishlivertrust.org.uk). Acute liver failure (ALF) can also occur in patients who have not previously suffered a chronic liver disease and is the primary reason for 9% of liver transplants in Europe in the last 20 years (European Liver Transplant Registry – www.eltr.org).

ALF is broadly described as the onset of encephalopathy (general brain dysfunction) within 8 weeks of a sudden loss of liver function. Variations in the definition of ALF exist in literature, but it can be considered an umbrella term for liver failure that occurs in previously symptom-free patients (i.e. non-chronic). One type of liver failure often referred to in literature is fulminant hepatic failure (FHF), though this can be considered to be a particular case of ALF. It is believed that the build-up of ammonia in the blood stream caused by liver failure is linked to the hepatic encephalopathy and intracranial hypertension which define the onset of ALF (Bernal et al., 2007). There are various causes of the disease, with paracetamol overdose being the leading cause in the developed world while virus strains, particularly hepatitis, is the leading cause elsewhere (Craig et al., 2010).

ALF is associated with significant mortality and morbidity with death rates being between 60-90% (Mareels et al., 2006, de Rave et al., 2002). Despite advances in medicine, therapeutic management of ALF is complicated due to the range of causes and differences in disease progression (Poyck et al., 2007, Lee et al., 2008). Again the only effective treatment is liver transplant but the scarcity of donor organs leads to long waiting lists. In some cases of ALF the liver can spontaneously recover, negating the need for transplant though this occurs in less than 20% of patients (Stadlbauer et al., 2009).

An alternative to organ transplant is the use of engineered liver tissue and research has been conducted to this end. In a recent publication, rat livers were decellularized before

being re-seeded with primary rat hepatocytes (Uygun et al., 2010). It was found that once implanted the graft tissue was able to carry out a number of normal liver functions, providing a proof of concept. A similar approach also using decellularized animal livers but seeded with human hepatocytes and epithelial cells also yielded positive indicators of liver function (Baptista et al., 2009). In another promising approach, 2d cell sheets of hepatocytes were layered to create a three-dimensional construct which was subsequently transplanted into mice (Ohashi et al., 2007). However, these approaches to treating liver failure still require extensive research before they reach clinical trials and eventual practice. In the short term, extracorporeal devices that can bridge patients to transplantation or recovery are being developed (Wigg and Padbury, 2005). Artificial livers can be categorized by whether they use non-biological techniques such as adsorption to detoxify the blood, rely on the natural functions of liver cells, or some combination of both.

2.2 Artificial livers

2.2.1 Non-biological artificial livers

Various detoxification techniques have been employed in attempts to treat the blood of liver failure patients. Hemodialysis and hemofiltration rely on diffusion and convection respectively to remove toxic compounds from the blood, though cannot remove albumin-bound toxins. Plasma exchange has also been explored, where a patient's plasma is removed and replaced with donor plasma. However the availability and cost of plasma render plasma exchange impractical. In addition these techniques have generally been ineffective and had little impact on survival rates (Diekmann et al., 2006, Pryor and Vacanti, 2008). The development of an artificial liver is particularly challenging as unlike other organs, the liver controls many aspects of metabolism and physiologic regulatory processes (Rozga, 2006).

One of the more advanced artificial liver support systems is the Molecular Adsorbent Recycling System (MARS). This involves hemodialysis of whole blood against an albumin dialysate. Albumin-bound toxins in the blood diffuse across a dialysis membrane

to an albumin circuit. From here the albumin is continuously regenerated by adsorption columns and a low-flux dialyser (Fig. 2.4). In one clinical trial, thirteen patients suffering from life-threatening liver failure who had not responded to standard state-of-the-art therapy were treated with MARS. The technology was shown to be safe and nine patients recovered (Stange et al., 1999). More recently, a multicentre clinical trial involving 70 patients was conducted by Hassanein et al. (2007). While an improvement over standard medical therapy in improving hepatic encephalopathy grade was detected, the length of the study meant that an impact on survival rates could not be assessed. This must be considered in future trials in order to fully assess the capabilities of the MARS artificial liver.

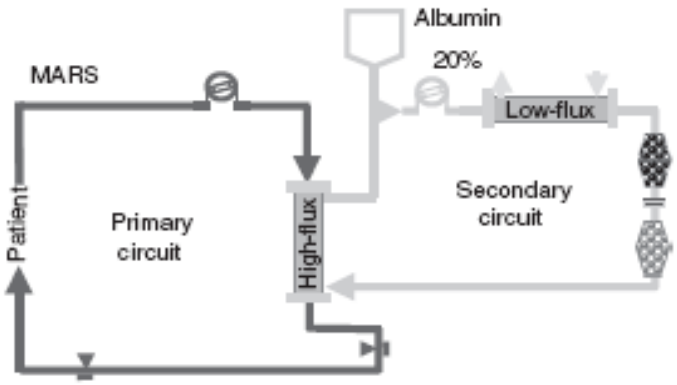

Figure 2.4: A schematic of the MARS artificial liver. The albumin is regenerated by low-flux dialysis and two adsorbers, one of which is charcoal. Diagram taken from Rifai (2008)

A similar system to MARS is Single Pass Albumin Dialysis (SPAD). Rather than regenerating the albumin dialysate it is discarded and fresh albumin added to the circuit. It has been reported that SPAD was significantly more effective than MARS in removing ammonia and bilirubin from the blood stream (Sauer et al., 2004). Another *in vitro* comparison of MARS and SPAD's ability to detoxify human plasma was carried out by Peszynski et al (2001). Contrary to the above findings it was found that MARS more effectively cleared important substances such as bile acids from the blood, while the efficacy of SPAD could only be achieved through a dramatic increase in cost. Without further testing and clinical trial data it is difficult to discern SPAD's effectiveness either relative to MARS or absolutely.

A variation of the artificial livers described previously is the Prometheus system, developed by Falkenhagen et al. (1999). In this system albumin is separated from plasma through a hollow fibre filter before being passed through adsorption columns to remove albumin-bound toxins (Fig. 2.5). The albumin fraction is returned and conventional dialysis is used to remove low molecular weight toxins. The safety of the device was demonstrated in a group of 11 patients (Rifai et al., 2003) and larger controlled multi-centre trials are currently underway (Rifai, 2008).

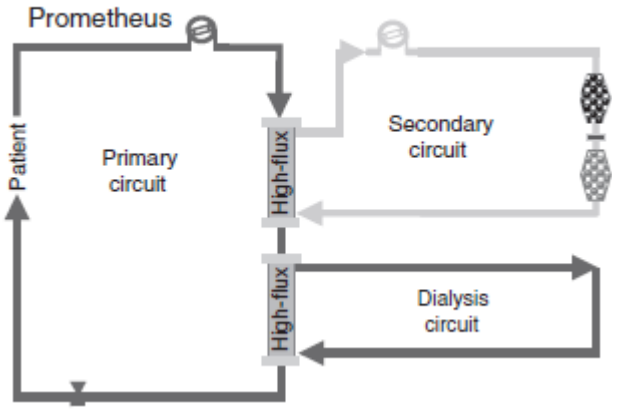

Figure 2.5: A schematic for the Prometheus artificial liver system. Albumin from the patient's blood is filtered into the secondary circuit where it is purified directly using an adsorption technique. Diagram taken from Rifai (2008).

The above systems have demonstrated the ability to clear toxins implicated in liver failure from the blood and improve hepatic encephalopathy grades (Stadlbauer et al., 2008). However, as outlined earlier, detoxification is only one of many important functions carried out by the liver. Artificial methods are also non-selective and may remove beneficial components from the blood. As such, the efficacy of these non-biological systems is still in question. An alternative approach is to incorporate liver cells into the device in an attempt to more effectively replace the native liver's function. These devices are known as bioartificial livers (BALs).

2.2.2 Bioartificial livers

The concept of a BAL is to have a liver failure patient's plasma interact with non-native liver cells or tissue in an attempt to replace the native liver's function until recovery or transplant. A number of attempts have been made to design a bioartificial liver using

various membrane configurations and cell lines though only two (the ELAD and HepatAssist) have reached phase II FDA human clinical trials (Wigg and Padbury, 2005), indicating the difficulty in designing an effective device. In many devices liver cells are contacted with the plasma through hollow fibre modules (Fig. 2.6). Hollow fibres can provide an attachment surface for cells and allow the cells to be protected from fluid shear stresses. In addition the fibres act as an immunological barrier that is important when xenogeneic cells are used in the device. They also resemble the liver lobule and provision of this architecture is hoped to maintain hepatocyte differentiation. As hollow fibre modules are of interest in this report, several BAL designs that incorporate them will be discussed in more detail below.

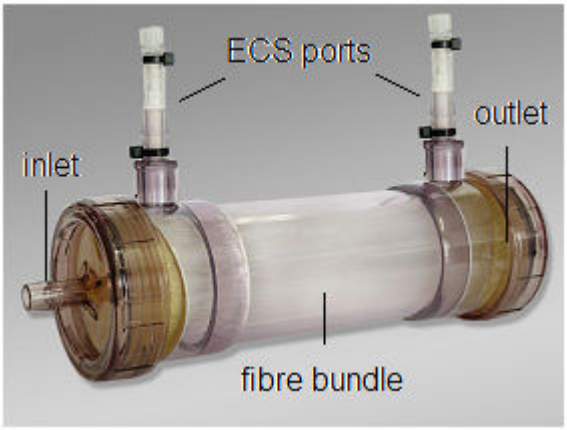

Figure 2.6: A typical hollow fibre bioreactor. This is the Zymax® hollow fibre bioreactor, developed by Spectrum Labs (adapted from an image found at www.spectrumlabs.com). Typically, the patient's plasma travels through the fibre lumens while cells reside in the extracapillary space.

Extracorporeal Liver Assist Device

Originally developed by Sussman et al (1991), the latest version of the Extracorporeal Liver Assist Device (ELAD) system (Vital Therapies Inc.) contains 440g of immortalized, tumour-derived C3A human liver cells inside 4 hollow fibre cartridges (32,000 fibres). This is the only current device to exclusively use human cells, although there are concerns over the tumorigenic potential of the hepatoma-derived C3A cells (Rozga, 2006). Prior to entering the hollow fibre cartridge, plasma is separated from the blood by ultrafiltration and oxygenated (Fig. 2.7). The plasma passes through a filter before being recombined with the cellular fraction of the blood. Previous versions of the ELAD had used whole

blood rather than separated plasma. The plasma and bioreactor are both maintained at body temperature.

The ELAD has been tested in 6 human clinical trials to date. The early trials failed to demonstrate any significant survival benefit or improvement in biochemical parameters (e.g. ammonia clearance) over control cases (van de Kerkhove et al., 2004). However, in the latest clinical trial in China using a modified design, the ELAD was shown to significantly improve survival rates in 17 acute-on-chronic liver failure patients (Hillebrand et al., 2010). According to the Vital Therapies website (as of February 2011), a large multi-centre trial is ongoing in the USA, Europe and UK in an attempt to replicate the results from China. In a poster presentation given in November 2010, significant transplant-free survival benefit in 49 ALF patients treated by the ELAD was revealed.

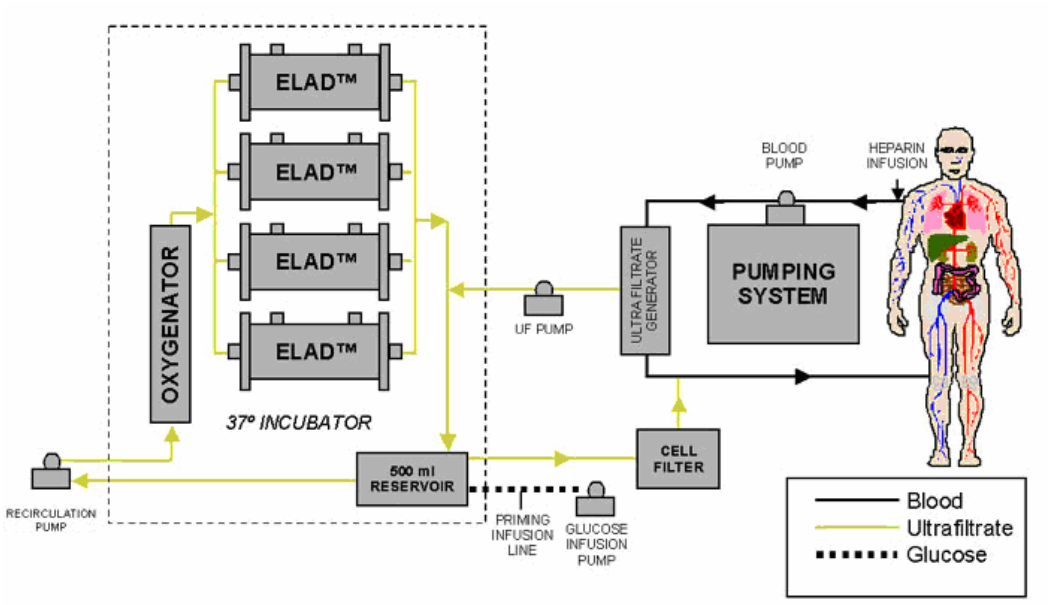

Figure 2.7: A schematic for the ELAD system. The parts labelled 'ELAD' are hollow fibre cartridges containing human C3A liver cells. From Vital Therapies Inc. (2008).

Bioartificial Liver Support System

The Excorp Bioartificial Liver Support System (BLSS) utilises approximately 100g of primary porcine hepatocytes infused into the extracapillary space of a hollow fibre cartridge. In contrast to the ELAD, whole blood perfuses the bioreactor and there is no separation stage. The blood is heated to 37°C and oxygenated before passing through the

hollow fibre bioreactor (HFBR). Nutrient medium is also perfused through the bioreactors extracapillary space in order to maintain the hepatocytes (Mazariegos et al., 2002, Patzer et al., 2002b). To date, the largest clinical trial carried out was a phase I trial in 4 patients. The safety of the device was demonstrated without any indication of efficacy (Mazariegos et al., 2001).

Modular Extracorporeal Liver System

First developed by Gerlach et al. (1994), the hollow fibre configuration in this system is unique in that it consists of three independent hollow fibre bundles woven together. The bundles are used for plasma inflow, plasma outflow, and combined oxygenation and CO_2 removal (Fig. 2.8). The system is also able to accommodate a large mass of cells: up to 600g of hepatocytes are immobilized in the extracapillary space, approximately the same cellular mass as half of an average adult liver (Sauer and Gerlach, 2002). In addition to the hepatocytes some non-parenchymal cells are present. Contact between the cells are said to help maintain the differentiated state of hepatocytes (Diekmann et al., 2006).

The bioreactor section of the device has been named the 'CellModule'. When inoculated with primary porcine hepatocytes, treatment with the CellModule was proven to be safe with 100% survival rate in 8 patients suffering from ALF and waiting for transplant (Sauer et al., 2003).

The Modular Extracoporeal Liver System (MELS) also incorporates non-biological techniques to detoxify the blood similar to those described in Section 2.2.1. As such, the MELS can be described as a 'hybrid' bioartificial liver. MELS combines the bioreactor described above with SPAD (see Section 2.2.1.) and continuous hemodiafiltration. In one instance the system was loaded with primary human hepatocytes from livers unsuitable for transplantation and used to treat 8 patients with liver failure. All patients underwent transplants with a survival rate of 100% after 3 years. As no adverse events occurred, the safety of the treatment was demonstrated (Sauer et al., 2002).

Figure 2.8: A diagram of the bioreactor used in the MELS. Three fibre networks are woven together, each with a different function. Figure adapted from Poyck et al (2007).

TECA Hybrid Artificial Liver Support System

Similar to the MELS, the TECA Hybrid Artificial Liver Support System (TECA-HALSS) is also a hybrid liver support system. In this case the bioreactor is combined with either charcoal adsorption or plasma exchange (Xue et al., 2001, Chen et al., 2001). The bioreactor is perfused with plasma and utilises hollow fibres and porcine hepatocytes (100-300g) as in some of the examples above, however it has one unique feature: rather than being immobilized the cells circulate through the extracapillary space along with nutrient media (Fig 2.9). The viability of the hepatocytes is monitored so they can be replaced when necessary.

In one clinical trial, 6 liver failure patients were treated with the bioreactor described above. In 3 cases, the TECA-HALSS incorporated a charcoal adsorption column while in the others 2-3 litres of the patients' plasma was exchanged for healthy plasma (Xue et al., 2001). The results were promising, with an improvement in neurological function and biochemical parameters (e.g. ammonia clearance) in all patients. In a later trial, the device was applied to 15 patients with severe hepatitis. Each device contained in excess of 5 billion porcine hepatocytes and incorporated plasma exchange before the bioreactor. In 10 patients the necrosis of native hepatocytes was halted when the TECA-HALSS was applied and they subsequently recovered. One patient underwent liver transplant and survived while 4 others died. The treatment was well-tolerated by all patients, displaying the safety of the device (Qian et al., 2003). Further, larger controlled trials will be needed to establish the efficacy of the TECA-HALSS although these initial findings are promising.

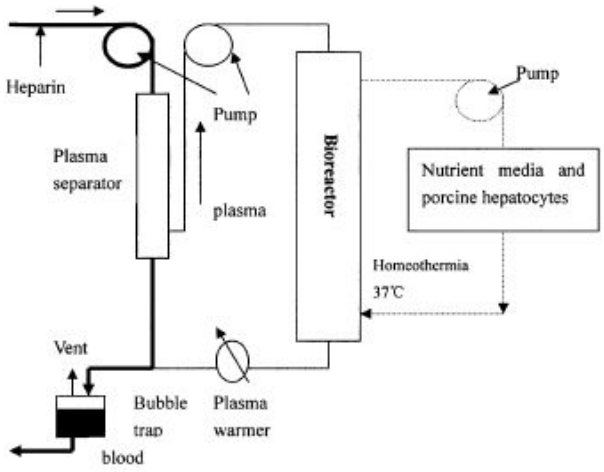

Figure 2.9: A schematic for the BAL section of the TECA-HALSS. The cells and nutrient media circulate through the ECS of the hollow fibre cartridge. The non-biological sections are not shown. Taken from Qian et al. (2003).

HepaMate (formerly HepatAssist)

Now owned by HepaLife Biosystems, Inc., the HepaMate has been in development since the early 90's (Rozga et al., 1992). It is also a hybrid device, incorporating a charcoal adsorption column. Plasma is separated from the blood and then heated and oxygenated before entering the hollow fibre bioreactor. In the initial design of the HepatAssist, approximately 7 billion cryopreserved porcine hepatocytes were immobilized on collagen-coated dextran microcarriers in the extracapillary space (ECS) of the HFBR, which then interact with the plasma (Rozga, 2006). The design has since been updated and according to the manufacturers website now incorporates 14 billion porcine hepatocytes.

Under the guise of the HepatAssist, this BAL has had relatively extensive clinical trials compared to most artificial livers. Phase I trials had demonstrated the safety of the device and subsequently a large randomized controlled multi-centre trial in the USA and Europe took place (Demetriou et al., 2003). Over 170 patients were enrolled to make it the largest bioartificial liver trial to date. Survival rates for patients treated with the HepatAssist were not significantly better when the entire patient group was considered. However by taking several confounding factors into account the patients' survival rate did significantly improve when the HepatAssist was applied. However, given that complex statistical analysis had to be performed to arrive at this conclusion, the efficacy of the HepatAssist is not entirely clear. This point of view is echoed by the US Food and Drug Association who

deemed that the trial had not successfully demonstrated the efficacy of the HepatAssist (Pryor and Vacanti, 2008).

The hollow fibre BALs described above are summarized in table 2.1. Besides these designs, there are other BALs which do not employ hollow fibres in a similar manner. An example is the Amsterdam Medical Centre BAL developed at the University of Amsterdam, in which plasma directly contacts porcine cells in a perfused bed. Hollow fibres are used to oxygenate the bioreactor (Chamuleau et al., 1998). Direct cell perfusion can enhance mass transfer though fluid shear stresses can adversely affect cellular metabolism (Tilles et al., 2001) or cause uneven distribution of cells in the bioreactor (Piret and Cooney, 1990). In another example, a bioreactor consisting of two crossed hollow fibre bundles has been developed. The bundles are responsible for medium inflow and outflow respectively, while human hepatocytes were cultured between the fibres (De Bartolo et al., 2009). In other designs the cells are seeded within the fibres while flow occurs through the extracapillary space (Sielaff et al., 1997).

Apart from hollow fibres, other technologies are being used in bioartificial liver devices. One example is the BioEngine where microelectromechanical systems technology is used to create a 3D structure designed to mimic a single liver lobule. The system has been tested in rats when seeded with both porcine and C3A cells, where it was found the device architecture successfully supported homogenous blood flow through the microchannels and the liver cells remained largely viable (Hsu et al., 2010). A fluidised bed bioreactor containing C3A cells encapsulated in alginate beads has also been proposed (Kinasiewicz et al., 2008a). A review of several novel bioreactor technologies for use in BALs such as a microfluidic polymethylsiloxane bioreactor and a microfabricated grooved bioreactor was carried out by Yu et al (2009).

Table 2.1: Characteristics of five hollow fibre bioartificial livers

	ELAD	BLSS	MELS	TECA-HALSS	HepatAssist
Perfusate	Plasma, previously whole blood	Whole blood	Plasma	Plasma	Plasma
Cell source	C3A human	Porcine	Human or porcine	Porcine	Porcine
Cell mass (grams)	440	100	600	300	70*
Hybrid features	None	None	SPAD, hemodiafiltration	Charcoal adsorption or plasma exchange	Charcoal adsorption
Largest clinical trial (patients)	69	4	8	15	171

* calculated by assuming 1 billion cells is equivalent to a mass of 10g (Hay et al., 2000)

2.2.3 Key issues in BAL development

Bioartificial livers have been in active development for almost 20 years now, but as yet none have successfully demonstrated their efficacy in a large-scale controlled trial. Trials are currently ongoing for several systems, but there are some fundamental issues that confound the development of an effective bioartificial liver. Some of these are technical in nature while others are associated with the practicalities of BAL treatment. Chief among these issues is the fact that BAL treatment can be extremely expensive – between $10,000 and $30,000 per treatment. Some other more technical concerns are outlined below.

A major issue that remains to be addressed is the source of liver cells. Xenogeneic cells, such as porcine hepatocytes are feature in several of the BALs described above. However, a moratorium on xenotransplantation in Europe prohibits the use of these cells (Podger, 1999). There is also concern over disease transmission from the cells, in particular porcine endogenous retrovirus (PERV) though this has not been an issue to date (Kuddus et al., 2002, Sauer et al., 2003, Morsiani et al., 2002). Some work has also suggested that cytochrome P450 expression in porcine hepatocytes is significantly different than human cells, which may limit their clinical applicability (Kleine et al., 2008). Human cells may be ideal however the availability of primary hepatocytes is also limited as healthy organs are mainly donated to transplant patients, leaving only discarded grafts as a source. This may be an adequate source of cells for acute liver failure patients (Sauer et al., 2005) but could prove to be logistically difficult (Gerlach et al., 2002). Immortalized human cell lines such as the C3A cells in the ELAD are another option, but critical functions such as drug and ammonia metabolism are reduced compared to normal cells (Cascio, 2001). There is also a small risk that these cells could cause cancer should they somehow reach the patients blood stream (Rozga, 2006), though no such incidents have yet been reported. A problem associated with all these cell types is the maintenance of their phenotype and associated function *in vitro*. Human stem cells could provide the answer in the future but it is not yet known how to apply them in BAL while maintaining their phenotype (Diekmann et al., 2006). Also of interest are small human hepatocytes, hepatic progenitor cells that have the ability to proliferate *in vitro* and express an array of liver functions (Wurm et al., 2010, Wurm et al., 2009). A further option may be the transdifferentiation of pancreatic cells; this could provide an autologous cell source for use in a BAL (Shen et al., 2003,

Tosh et al., 2002). The choice of cell for use in a BAL is an important question, but is outside the scope of this report.

One aspect of BALs that is also not considered here is the regulatory procedures that must be followed in order for the treatment to be endorsed. These procedures vary according to the global territory and corresponding regulatory agency, for example the Food and Drug Administration in the USA or the European Medicines Agency in Europe. Each regulatory agency has different standards and practices for determining whether a medical product is safe and effective. This evidence is normally obtained through clinical trials, but in the case of BALs it can be difficult to organise large trials as they are concerned only with a specific liver failure mode, acute or acute-on-chronic liver. As such it can be difficult to find the right patients and the trials become lengthy and expensive processes. The use of animal or immortalized cell lines in the devices is also problematic and it is paramount that BALs are demonstrated to be safe, with follow-up studies on treated patients to show no ill-effects have resulted from BAL treatment. The use of hollow-fibre cartridges in BALs is favourable as regulatory bodies already have experience with them through their use in kidney dialysis machines. More complex BAL designs do exist as described in Section 2.2.2, though presumably the use of novel bioreactor designs will be met with more uncertainty on the part of the regulatory agencies.

Besides cell source and regulatory matters, another issue with BAL design is mass transport between the blood/plasma and liver cells (Pless and Sauer, 2005). In particular, oxygen is seen as the most limiting metabolite in HFBR design (Piret and Cooney, 1991). Oxygen is even more critical in BAL designs as hepatocytes can have an oxygen consumption rate around 10 times greater than most other cell types (Cho et al., 2007). For this reason most BAL designs place an oxygenator in the plasma circuit prior to the bioreactor. The mass transport of oxygen to the hepatocytes is critical to the efficacy of a BAL design and is addressed in this report. Mathematical modelling has been employed to this end, so it is useful to outline the various approaches to this problem seen in current literature.

2.3 Mathematical modelling of hollow fibre bioreactors

HFBRs have been studied extensively in the past as a means for cell culture. Only relatively recently has there been an interest in expanding their application to tissue engineering and artificial organs. It is thought that by mimicking the microvasculature present in natural tissues, cells can be cultured more effectively *in vitro*. The hollow fibres provide a large surface area for nutrient transport to the growing tissues, similar to capillaries in the body.

Quantitative mathematical models for practical applications provide a number of benefits. A theoretical framework allows experiments to be guided towards the identification of certain key parameters that characterize the process e.g. membrane permeabilities and diffusion coefficients. Once validated, a theoretical model also provides the opportunity to optimize a process such as oxygenation of a bioreactor. This can be achieved through modelling more quickly and more easily than performing a large number of experiments to obtain empirical relationships. An understanding of the fundamental processes taking place and their mathematical representations is necessary for rigorous scientific study of practical applications, such as hollow fibre bioreactors (HFBRs). To effectively model the HFBR it is necessary to couple various systems of equations describing hydrodynamics, mass transfer and substrate consumption kinetics. A common starting point for many HFBR models is the use of Krogh cylinders to describe the system.

2.3.1 Krogh cylinders

Many attempts to model hollow fibre membrane bioreactors make use of Krogh cylinder geometry (Fig. 2.10). This approach is named after August Krogh (1919) who first used the model to describe capillaries in animal tissues. When this principle is applied to HFBRs, the entire hollow fibre bundle can be described by a single subunit that consists of one fibre surrounded by an annulus of extracapillary space. This approach assumes that all the fibres are identical in terms of properties and internal flow, perfectly straight and equally spaced. Additionally, the interstitial spaces between adjacent Krogh cylinders are ignored. It is important to note that these are unrealistic or inaccurate assumptions as fibres

are often unaligned, moreover the interstitial spaces between fibres may be significant when cells occupy them. The use of a more accurate representative elementary volume to describe the fibre bundle, as is common in fluid dynamics modelling, may be a means to overcome this particular limitation. Despite this, a number of studies use this method to model HFBRs, as will be described below.

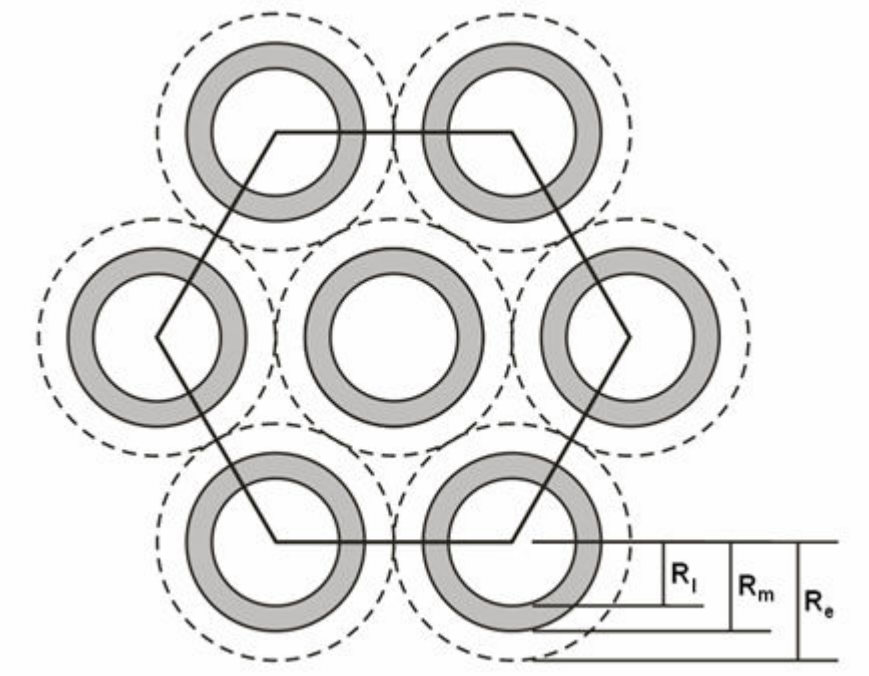

Figure 2.10: A cross-section of some Krogh cylinders. The overall bioreactor can be characterized by summing the contributions of an arbitrary number of identical single fibre subunits. The fibre lumen radius R_l , membrane radius R_m and Krogh cylinder radius R_e are shown.

2.3.2 Hydrodynamics in a hollow fibre bioreactor

Hollow fibres are characterized by having low aspect ratios, i.e. the fibre diameter is small compared to length. Flow in the fibre lumen is typically of a low Reynolds number and in the laminar regime. As a consequence of these facts the entry length is negligible compared to fibre length and so the flow is assumed to be fully-developed on entry to the HFBR (Brotherton and Chau, 1996). A no-slip condition, i.e. zero axial flow velocity at the liquid-solid interface, is also assumed for flow at the fibre inner wall. Surface wettability and roughness are strong factors in determining slip behaviour, and as in this case the interface is porous there may be a degree of slip in practice (Neto et al., 2005). Slip effects in hollow fibres of the size normally seen in dialysis applications are generally

negligible and can be safely ignored (Belfort and Nagata, 1985, Damak et al., 2004, Shipley et al., 2010). Flow is also normally assumed to be incompressible and Newtonian.

It is also often assumed that the HFBR is operating in a diffusion limited regime and radial convection through the membrane is negligible. In this case laminar flow inside the fibre lumen can be described by the Poiseuille equation where flow is solely in the axial direction and velocity is a function of radial position (Kundu and Cohen, 2001). The velocity profile is parabolic as seen in Figure 2.11. Equation 2.1 shows how the axial velocity u is a function of radial position r.

$$u(r) = 2\bar{u}\left(1 - \left(\frac{r}{a}\right)^2\right) \tag{2.1}$$

Where ū is the average flow velocity and a is the radius of the fibre.

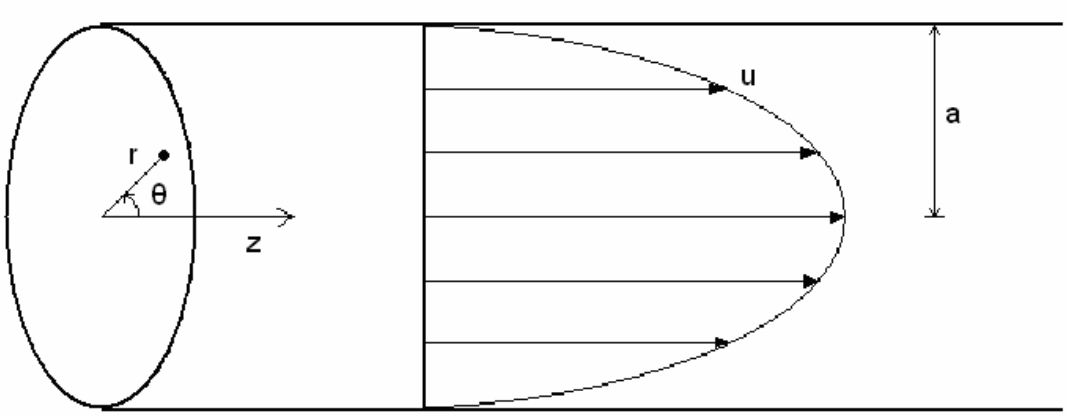

Figure 2.11: Poiseuille flow in a hollow fibre.

2.3.3 Substrate reaction kinetics

Upon passing through the fibre membrane and coming into contact with cells, oxygen will be consumed. Oxygen uptake and how it is modelled therefore have important consequences for the oxygen concentration profiles in the bioreactor and therefore appropriate kinetics must be chosen. In general, Michaelis-Menten kinetics are favoured in literature to describe substrate uptake in mammalian cells:

$$V = \frac{\partial c}{\partial t} = -\frac{V_{\max} c}{K_m + c} \tag{2.2.}$$

The reaction or consumption rate of the substrate is a function of the maximal consumption rate V_{max}, the Michaelis-Menten constant K_m and the substrate concentration c. Most biological kinetics are found to follow this relationship (Davis and Watson, 1985). Zero and first order kinetics are also common, though these are just extreme cases of Michaelis-Menten kinetics when substrate concentration is much greater or much smaller than the Michaelis-Menten constant K_m.

$$\text{Zero-order limit: } c >> K_m \therefore V \approx -V_{\max} \tag{2.3}$$

$$\text{First-order limit: } c << K_m \therefore V \approx \frac{-V_{\max} c}{K_m} \tag{2.4}$$

There is significant difficulty in determining the value of the Michaelis-Menten parameters necessary to characterise oxygen uptake. A cell's metabolism is a function of its surroundings, i.e. the culture conditions. It has been shown that oxygen uptake rate is increased in the presence of high ammonia concentrations (Catapano and De Bartolo, 2002). A cell's environment is also important, such as cell density or whether it is in a 2-D or 3-D culture (Patzer, 2004). Co-culture with non-parenchymal cells also alters hepatocyte oxygen uptake rates (Cho et al., 2007). The physical and chemical properties of the membrane to which the cells are attached is also a factor (De Bartolo et al., 1999). Of course, the cell behaviour also differs according to the cell source. A wide range of values for these parameters are seen in literature, as many cell lines and cell environments are used. The range of oxygen consumption rates observed has been reviewed by Patzer (2004) and examined in Section 4.2.2.

2.3.4 Mass transfer models in hollow fibre bioreactors

Mathematical modelling of HFBRs is complex and various approaches have been used. The methods differ through their assumptions and solution procedures. An overview of some of this work is described below, many of which adopt the modelling starting points described above.

A general mathematical model for mass transport in a permeable tube with radial convection was developed by Ross (1974). A dilute, Newtonian system with low aspect ratio (as is the case for hollow fibres) is assumed with the velocity profile within the fibre consisting of a base Poiseuille flow (Fig. 2.7) superimposed with a small axial position-

dependent radial convective flow. Ross uses this starting point to develop radial profiles for dimensionless concentration and velocity at different axial positions within the tube. The results indicate the exit substrate concentration decreases significantly as tube diameter, length and membrane permeability increase. However the solution presented is only applicable when there is no substrate uptake in the ECS, as this aspect is not included in the model.

An evaluation of the mass transport characteristics in a diffusion-limited hollow fibre reactor was carried out by Davis and Watson (1985). By assuming Poiseuille flow (Eq. 2.1) inside the fibre lumen and neglecting radial convection, a series of equations to derive substrate concentration profiles in the reactor have been presented. The analysis takes account of reduced diffusion through the cells surrounding the hollow fibres and allows any form of substrate reaction kinetics in the cell layer. In order to establish the substrate diffusivity in the cell layer, the diffusion coefficient is chosen so that the sum of squares error between experimental and predicted substrate conversion is minimized. The model can then be solved numerically to predict substrate concentration within the bioreactor.

Another theoretical analysis of a HFBR was carried out by Schonberg and Belfort (1987). Again a Krogh cylinder model is used, although in this case a 4^{th} region that is free of cells occupies the outer layer of the cylinder. The model is simplified into the 1-dimensional case by assuming that axial mass transfer can be neglected with a high flow rate in the lumen. Diffusion of glucose and oxygen through the fibre membrane is assumed to be unhindered as the membrane is thin and porous and the molecules themselves are small. Darcy's Law is assumed to calculate radial velocity through the membrane and cell/enzyme layer. The authors conclude that radial convection could improve the bioreactor's performance, though this may be complicated by cells blocking the convective flux.

Piret and Cooney (1991) analysed oxygen depletion in hollow fibre bioreactors using a mathematical model. In contrast to Schonberg and Belfort (1987), the mass transfer resistance of the lumen is included in the model. In addition, the Krogh cylinder model includes a thin low porosity 'skin' layer on the lumen-side of the fibre which creates a mass transfer resistance in the radial direction. An order of magnitude analysis was performed which led to radial convection being considered negligible. The equations are

then solved using a numerical method. Design criteria for the HFBR are then chosen from plots of an effectiveness factor defined by oxygen penetration depth into the cell layer. Comparison of predicted oxygen limitations to experimental axial cell density profiles led to generally good agreement despite uncertainty over the value of model parameters.

A simplified solution for hollow fibre bioreactor design equations was presented by Jayaraman (1992). The analysis is simplified through a number of assumptions such as zero radial convective flux and using the first order limit of the Michaelis-Menten equation for reaction kinetics. The flow through the lumen is assumed to be Poiseuille flow (Eq. 2.1). The analysis proceeds by decoupling of the membrane and then the ECS equations by treating them as ordinary differential equations. The lumen equation is solved by Kummer's equation to produce a concentration profile in the lumen. However, this analysis only applies when the fairly restrictive assumptions described above have been made and hence the solutions are of limited use.

A comprehensive review of mathematical modelling techniques in HFBRs has been written by Brotherton and Chau (1996). The scope of the review covers Krogh cylinder models that consider the HFBR to be either diffusion-limited or convective-flow dominant. The authors also describe their own model system, including a cell growth term based on Monod kinetics. The systems of equations are non-dimensionalized and solved numerically to create oxygen concentration profiles. The results indicate that convective transport is important to overcome mass transfer limitations that exist during cell growth. However, the application of momentum and continuity equations to describe convective flow in the ECS must be restricted to when cell density is low. When the cells reach tissue-like density, the ECS should be modelled as a porous medium. In addition to these findings, the potential benefits of using alternative flow configurations in the HFBR are explored.

Mass transfer characteristics of a diffusion-limited bioreactor have also been studied by Willaert et al (1999). In this article, analytical expressions for the concentration profiles of a limiting substrate undergoing Fickian diffusion and cell metabolism are derived. The velocity profile inside the fibre lumen is simplified by assuming plug flow and the radial mass transfer resistance in the lumen is ignored by assuming a large axial Peclet number. This allows the lumen concentration profile to be found from an ordinary differential

equation ODE. Radial profiles for substrate concentration in the membrane and ECS are also shown for both the zero and first order limits of Michaelis-Menten kinetics. The influences of diffusion coefficients, membrane thickness and the depth of the ECS region are investigated in order to optimize bioreactor performance.

Cabrera et al (2001) have taken a novel approach to modelling of a HFBR. Their model allows analytical solutions to be found for any arbitrary reaction kinetics (e.g. zero order or Michaelis-Menten). Again, a Krogh cylinder model is used and the bioreactor is assumed to be diffusion-limited with a parabolic velocity profile in the lumen. Similar to Jayaraman (1992), the membrane equation is integrated to provide modified boundary conditions to the non-dimensionalized lumen and ECS equations. In order to solve these equations the appropriate Green's functions are generated. This method had been used previously to solve design equations in dialyzers and packed-bed adsorption. Numerical algorithms are employed to obtain the resulting solutions. The model may be applicable to arbitrary reaction kinetics, but is restricted to diffusion-limited bioreactors and is relatively complicated to use.

Mathematical modelling software can also be applied to solve mass transport equations in HFBR applications. This has been performed extensively by a group at the University of Oxford examining HFBRs for use in bone tissue engineering. They employed the modelling software, FEMLAB, to model the glucose and oxygen partial differential transport equations in a Krogh cylinder representation of a HFBR (Ye et al., 2006, Abdullah et al., 2006). Subsequently the effects on the model due to diffusion at the cellular scale (Das, 2007) and component interaction between oxygen and glucose were examined (Abdullah and Das, 2007). The modelling software employs a finite-element method to solve the relevant systems of partial differential equations.

Table 2.2 summarizes the various approaches described above and how they differ. While this is not an exhaustive list of mathematically models of mass transport in HFBRs, it appears certain trends such as assuming Poiseuille flow and zero radial convection are common. Besides mathematical models of general HFBRs there have been attempts to model HFBRs in the context of a BAL. As this is a significant part of this work's goals, some of these models are outlined below.

Table 2.2: A summary of various approaches to model mass transport in HFBRs.

Reference	Lumen Flow	Radial membrane convection	Reaction kinetics	Model solution method
(Ross, 1974)	Poiseuille with added radial component	Yes	None	Analytical
(Davis and Watson, 1985)	Poiseuille	No	Arbitrary	Numerical
(Schonberg and Belfort, 1987)	Not considered	Yes	1st order	Analytical
(Piret and Cooney, 1991)	Plug flow	No	Zero order	Analytical
(Jayaraman, 1992)	Poiseuille	No	1st order	Analytical
(Brotherton and Chau, 1996)	Plug flow	Yes	Zero order	Numerical
(Willaert et al., 1999)	Plug flow	No	Zero/first order	Analytical
(Cabrera et al., 2001)	Poiseuille	No	General	Numerical
(Abdullah et al., 2006)	Poiseuille	No	Zero/first/second order	Finite-element software

2.3.5 Mathematical modelling of bioartificial livers

As well as general cell culture applications in HFBRs, various attempts have been made to mathematically model BALs in particular. These cases are directly relevant and inform the mathematical modelling carried out in this work. These works vary in terms of the specific systems they are modelling, but also in the modelling assumptions and numerical processes that they employ. In some cases experimental data have been obtained in order to validate the model or identify model parameters.

Giorgio et al (1993) studied the transport of glucose, albumin and fluid in a hollow fibre BAL using both a theoretical model and experimental data. The model is a departure from typical Krogh cylinder models in that it considers the fibre bundle as a whole. It assumes that Poiseuille flow is present in the fibres (Eq. 2.1). Two alternative 'hydraulic geometries' were analyzed. The first configuration considers that the ECS ports of the HFBR cartridge are closed. Hence at low flow rates the pressure in the ECS can be assumed to be constant and the average of the bioreactor inlet and outlet pressures. In the second configuration the distal ECS port is connected to the axial outlet of the bioreactor. The pressure in the ECS is then constant and equal to the outlet pressure. This should increase transmembrane convective flux relative to the first configuration (due to greater transmembrane pressure). Molecular diffusion is ignored and transport of the solutes is assumed to be purely through fluid convection through the membrane. There are also no cells in the model or experiment, so uptake is not included either. Experiments are performed to measure transmembrane flux and parameters are estimated by computer. Predictions of fluid flux in both hydraulic geometries resemble the experimental results. However, the value of the concentration profiles for glucose and albumin is questionable given that no cell behaviour is included in the model. The results indicate that diffusion is important at the low flow rates usually seen in BALs.

Subsequent attempts were made to model a BAL in both diffusion-limited and convection enhanced modes by a group at the University of Strathclyde (Hay et al., 2000, Hay et al., 2001). Both models utilise the familiar Krogh cylinder geometry. In the case of the diffusion limited HFBR, whole blood is assumed to perfuse the device. This necessitates the use of the Margaria equation (Eq. 5.5) to represent the oxygen dissociation relationship with haemoglobin. Poiseuille flow is assumed in the lumen and the hepatocytes consume oxygen according to a Michaelis-Menten relationship. The parameter values are chosen to correspond to the design of the ELAD (see Section 2.2.2) and represent the oxygen uptake of different cell lines. A numerical scheme is used to solve the resulting system of equations. It is concluded that for liver cell lines which consume oxygen at a relatively low rate, the cells could be maintained with an adequately permeable hollow fibre membrane. If primary hepatocytes are used, which have higher oxygen uptake rates, the HFBR is determined to be inappropriate for use in a BAL as it was not possible to adequately oxygenate the cell mass. However, the paper assumes the inlet partial pressure

of blood is 40 mmHg, corresponding to venous blood. It would be possible to increase this by oxygenating the blood before it reaches the HFBR.

By opening the ECS ports to reduce pressure in the shell of the bioreactor and switching to separated plasma instead of whole blood, a convection-enhanced HFBR was also modelled (Hay et al., 2001). In this case, design parameters were taken from the HepatAssist that was undergoing clinical trials at the time. Darcy's law is used to describe radial flow through the fibre membrane and axial flow through the cell region. The intrinsic permeability of the cell-filled ECS is difficult to establish so the model uses a range of values (10^{-12} - 10^{-8} m^2). The radial volumetric flow profile is derived as a second order ODE and solved. Oxygen consumption is then modelled by applying the convective flow profile and assuming Michaelis-Menten kinetics in the cell layer. In this case diffusion of oxygen is neglected. A solution is presented as a first order ODE which is solved through a Runge-Kutta numerical method. Experiments were performed to determine the oxygen transfer rates to the cells for plasma containing different oxygen partial pressures. The parameter values that resulted in the best fit between the results and theoretical predictions were chosen for further modelling. The model predicted that large hypoxic zones would exist in the HFBR regardless of whether a high or low value for maximum oxygen consumption rate V_{max} (Eq. 2.2) was chosen. However, the authors suggest a lack of consistent experimental data may have made any solid conclusions difficult to make. As oxygen is a highly diffusive molecule, neglecting diffusion in the model development is incorrect. This is especially true in the BAL where plasma flow rates are relatively low compared to most commercial applications of HFBRs.

Oxygen consumption in a hollow fibre BAL was also investigated by Patzer (2004). In this work, both mathematical modelling and an experimental approach were taken. The mathematical model is a typical Krogh cylinder model, with Poiseuille flow (Eq. 2.1) in the fibre lumen and Michaelis-Menten kinetics (Eq. 2.2) describing oxygen uptake. The flow of whole blood through the device is also modelled by using the Hill equation to describe oxygen dissociation from haemoglobin. The system of equations was then non-dimensionalized to reduce the number of operating parameters from approximately 15 to 8. Experiments were also carried out in 11 HFBRs containing freshly isolated porcine hepatocytes, each perfused by culture media. As it is not possible to measure spatial oxygen profiles within a HFBR, the model could not be validated against experimental

results but rather was compared with the model solutions from Hay et al described with above. The model proved to be more conservative than Hay's when predicting diffusion-limited regimes. It was determined that the bioreactor would be diffusion-limited rather than kinetically controlled for almost all operating conditions. The results also appear to indicate that the intrinsic, per cell oxygen consumption in the HFBR is a decreasing function of the cell density. This may be due to higher cell densities representing a more *in vivo* like environment and hence reduced cell stress rather than diffusional limitations.

A more recent study was carried out by Sullivan et al (2007). In this work the emphasis was placed not only on supplying enough oxygen to the hepatocytes but also to recreate liver zonation by representing the spectrum of oxygen tension seen *in vivo* (see Section 2.3.4). A Krogh cylinder model was used and the HFBR is assumed to be diffusion-limited i.e. no convection across the fibre membranes. Michaelis-Menten kinetics were used to describe the oxygen uptake though they were modified with a parameter that represents the fractional cell volume in the ECS. The ECS oxygen diffusion coefficient was similarly modified. The effect of haemoglobin-based oxygen carriers in the circulating stream was examined. It has been proposed that their presence may alleviate the problems associated with oxygenation. A second convection-diffusion equation was used to describe the mass transport of oxygenated haemoglobin within the fibre lumen. The Adair equation was applied to describe the saturation of the haemoglobin as a function of oxygen partial pressure. Unlike previous models that have been described above, in this case the system of equations was solved using modelling software, the multiphysics package COMSOL 3.5a. In addition to the mathematical modelling, experiments were carried out in order to validate the model. Two HFBRs were set up, one including bovine red blood cells in the circulating media to act as oxygen carriers, and the oxygen consumption per cell was found. There was good agreement between the experimental results and model predictions for both bioreactors, validating the model. The model was then used to predict oxygen profiles for different operating conditions and in particular, different levels of bovine red blood cells. It was concluded that these oxygen carriers would be able to replicate the zonation of the liver within a BAL through provision of an appropriate spectrum of oxygen partial pressures. Without them, it was found that large hypoxic and anoxic regions would exist within the BAL.

2.4 Summary of Literature

The development of a proven, effective BAL is still a work in progress. Current research focuses mainly upon the practical aspects of their development, experimenting with different bioreactor configurations and cell lines. Pre-clinical and small clinical trials have shown that BAL treatment is safe and potentially effective, but this success has yet to be translated to a large scale trial and so BALs have yet to gain clinical acceptance. Further work and research is needed to identify the final form of a successful BAL design.

Current literature disagrees on several aspects of BAL design such as the type and number of cells required or the design and operating parameters of the bioreactor (Table 2.1). These aspects are crucial to potential effectiveness of any BAL treatment. However, there are also common themes in the literature to suggest a good starting point in improving BAL design. For instance, hollow fibre technology has been widely used in the BAL designs to this point. Alternatives do exist as described previously at the end of Section 2.2.2, but it reasonable to assume that hollow fibres are a suitable building block for any successful BAL design. They allow for high-density cell culture and provide a physical barrier against the patient's immune system and flow-induced shear stresses. There is also the issue over whether to use whole blood or fractionated plasma as the bioreactor medium. In general, BAL designs (e.g. the HepatAssist and MELS) have favoured the latter. This is likely due to the increased risks of blood clotting or fibre pore blockage arising from the use of whole blood, though as a consequence the oxygen-carrying capacity of the medium is greatly diminished. The choice of cells has also largely favoured xenogeneic types, particularly porcine hepatocytes. This is largely due to their availability and their relatively high functionality compared to immortalized cell lines, though they are not without issues relating to safety or regulatory matters.

As stated previously, BAL designs are often based on the use of HFBRs to house the liver cells. There is a wealth of literature describing the use of HFBRs in this manner and in the wider field of cell culture. This includes the use of mathematical models to describe mass transport within such systems. Again, current literature on this topic describes a number of different approaches to the problem while reoccurring themes can also be seen (Table 2.2), for example Poiseuille flow is a reasonable assumption considering the laminar regimes

normally seen in HFBR applications. In some cases radial convection through the membrane is considered while at other times it is ignored. The choice of BAL design will also impact on the modelling parameters used in the model, for example to choice of cell type has implications on the oxygen uptake rate in the BAL.

While mathematical models have been used in the context of BALs before, current literature lacks methods to cohesively connect the results of mathematical modelling to trends in BAL design. In most cases, the HFBRs in BALs are repurposed from other applications such as dialysis. It would appear little thought is given to how the demands of a BAL application can be met through specific HFBR design. Aspects of liver physiology, in particular liver zonation, have not been given a great deal of consideration in BAL design. Individual studies have examined zonation, but not in the context of real BAL designs. The use of mathematical modelling combined with identifiable criteria that the design should meet in terms of operation and zonation profiles, may allow better designs to be created.

2.5 Aims and Objectives

The main aim of this work is to address this gap in the literature, i.e. to use mathematical modelling techniques to develop a framework that will rationalize BAL design. This will involve not only developing a mathematical model to describe mass transport in BALs, but also subsequently identifying design paradigms that will result in more effective liver support. This will involve considering aspects of liver cell behaviour and physiology and relating them to the mathematical model. The framework that is developed can also be used to investigate existing BAL designs to ascertain their likely efficacy.

To achieve this, a number of objectives must be met which are detailed below:

- A mathematical model to describe oxygen transport in hollow fibre BALs will be developed based on existing literature. The model solutions will be obtained using the finite-element software package, COMSOL (Comsol Multiphysics).
- Upon obtaining model solutions, they must be interpreted in such a way as to inform better BAL design. This can be done using an ‘Operating Region’ approach

where modelling results and operating constraints on the BAL can be combined to identify a parameter space that delineates valid BAL designs.

- To increase the physiological relevance of BAL designs, the concept of zonation of liver metabolic functions can be introduced into the design framework.
- The principles established in this work can be applied to current real-world BAL designs as an illustration of both current design deficiencies and the power of the theoretical framework in optimizing BAL design.

Overall, this work seeks to develop a rationale based on mathematical modelling to guide optimization of BALs. This includes the use of Operating Region charts to locate feasible designs and zonation analysis to increase the efficacy of the liver cell population in the device. Upon optimization of the design, the BAL should become a step closer to clinical reality.

Chapter 3: Operating Regions for Bioartificial Liver Design

3.1 Introduction

The liver is responsible for a multitude of important functions in the body (Section 2.1.2) and as a result, liver failure is an extremely debilitating condition. As the only current effective treatment, liver transplantation is beset by a shortage of available organs. Bioartificial livers (BALs) have been proposed as an alternative means to treat liver failure, particularly acute liver failure (ALF) that is associated with mortality rates as high as 90% (de Rave et al., 2002). However, as described in Section 2.2.3 and 2.2.4, BALs have yet to gain clinical acceptance and still face a number of issues that they must overcome to do so.

Chief among these issues is consideration of the mass transport limitations inherent in BALs. As BALs are often based on hollow fibre bioreactors (HFBRs) where the cells are separated from the medium flow by a membrane, provision of adequate oxygen and nutrition to the cells to ensure their survival can be problematic. Oxygen is often considered to be the main limiting nutrient in HFBR cell culture due to its low solubility in culture medium (Piret and Cooney, 1991). For BAL applications where patient plasma is used rather than haemoglobin-carrying whole blood, this will also be true. This is exacerbated by the relatively large oxygen demand from the metabolically active liver cells which consume oxygen up to ten times faster than other cell types (Cho et al., 2007). From this it is possible to define one operating constraint on the BAL; sufficient oxygen should be supplied to ensure survival of the cells.

In addition to the constraint on oxygen supply, two other main constraints exist on the system. In order to be effective, the cartridge must contain a cell loading of 10-40% of the liver's mass (Sullivan et al. 2007) or approximately to 10-40 billion cells for an average adult. The exact figure depends largely on whether the patient has any residual liver function. The range of blood/plasma flow rates entering the BAL is also limited; this is generally between 100-300 ml/min due to technical constraints relating to red blood cell lysis that can occur during plasma fractionation (Pless and Sauer, 2005).

In order to design the hollow fibre cartridge within the three constraints outlined above, an 'Operating Region' method is proposed. The concept is similar to a 'windows of operation' approach; a graphical method for determining operating parameters for a bioprocess (Woodley and Titchener-Hooker, 1996, Zhou and Titchener-Hooker, 1999). In windows of operation, design constraints are represented by lines on a chart where the axes are design variables. The region or 'window' bounded by the constraint lines defines a viable parameter space. This process can also allow optimization, for example through linear programming techniques. Operating Regions for the BAL are developed to represent a parameter space within which a design is viable. To do this a model of oxygen transport within a diffusion-limited HFBR is developed and subsequently solved. The main innovation of this work relative to current literature is that a systematic attempt has been made to quantify the effects of BAL design and operating parameters in terms of producing viable designs. Other studies such as those carried out by Hay et al (2000) and Sullivan et al (2007) have tended to examine particular designs based on existing BALs and bioreactors and modify the operating parameters. The mathematical framework and techniques described here serve as a tool to understand the significance of these parameters and guide improvement in BAL design.

3.2 Theoretical Aspects

3.2.1 Development of an oxygen transport model

As described in Section 2.3.1 and Figure 2.10, Krogh cylinders (Krogh, 1919) are a common starting point in mathematical models of HFBRs (Brotherton and Chau, 1996, Piret and Cooney, 1991, Hay et al., 2000, Ye et al., 2006). This approach assumes a representative sub-unit of the hollow fibre bundle can be defined by assuming that each fibre is identical and arranged in a regular hexagonal pattern (Fig 2.10). The symmetry of the system allows the entire HFBR to be considered through a single Krogh cylinder sub-unit, considerably simplifying the computational effort required. While in real HFBRs the hollow fibres are not ideally arranged, this fact has not prevented the Krogh cylinder method being applied in the majority of work on hollow fibre modelling as few alternatives exist. Krogh cylinder models have also been validated against experimental results in

previous studies (Patzer, 2004, Sullivan et al., 2007), proving their suitability for this model.

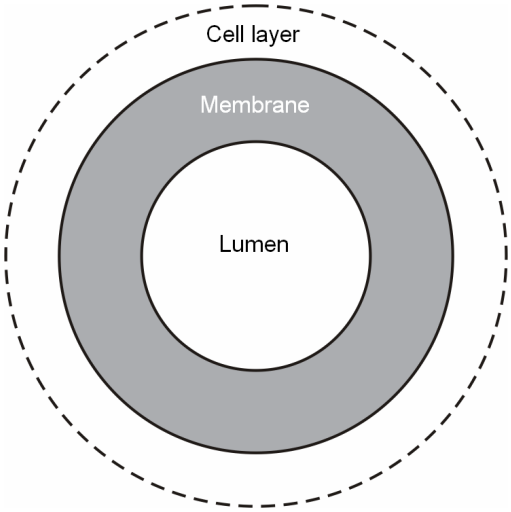

Figure 3.1: The use of Krogh cylinders in modelling a hollow fibre BAL. One fibre surrounded by a cell layer can describe the entire fibre bundle assuming interstitial spaces between the fibres can be ignored (Davidson et al., 2010).

Each sub-unit consists of three domains: the fibre lumen, fibre membrane and an annulus of extracapillary space (ECS). In this model of a BAL, the ECS domain is considered to consist of a monolayer of cells adherent to the fibre (Fig. 3.1). This is to reflect the arrangement of hepatocytes on sinusoids *in vivo*, as described in Section 2.1.3. A convection-diffusion equation is used to describe the steady-state transport of oxygen in the bioreactor (Eq. 3.1), where D is the isotropic diffusion coefficient of oxygen, c is the concentration, $\boldsymbol{u}$ is the fluid velocity and V represents the oxygen reaction rate. The equation will take different forms within each region of the sub-unit to represent the different mass transport mechanisms in each.

$$\nabla.(-D\nabla c) = \mathbf{u}.\nabla c - V \tag{3.1}$$

The convection-diffusion equation in the lumen domain is given by Equation 3.2. A cylindrical axisymmetric coordinate system is used, with radial coordinate r and axial coordinate z. The velocity of plasma flow within the lumen is assumed to adopt a Poiseuille profile as typically seen in pipe flow, with an average flow velocity defined by $\bar{u}$. (Fig. 2.11). The fibre lumen radius is represented by R_l. This is valid here as radial convection through the membrane can be assumed to be negligible, with no slip on the inner membrane surface (Kundu and Cohen, 2001). It can also be assumed that entrance effects are negligible and the flow is laminar and fully-developed due to typically low

Reynolds numbers and the high aspect ratio of the fibres (Brotherton and Chau, 1996). No oxygen generation or uptake takes place in the lumen and hence the reaction term is absent. In the following equations the concentration of oxygen is represented by a partial pressure pO_2 as is convention in the literature. The diffusion coefficient of oxygen in plasma is represented by D_{plasma}.

$$D_{plasma}\left(\frac{1}{r}\frac{\partial}{\partial r}\left(r\frac{\partial pO_2}{\partial r}\right)+\frac{\partial^2 pO_2}{\partial z^2}\right)=2\bar{u}\left(1-\left(\frac{r}{R_l}\right)^2\right)\frac{\partial pO_2}{\partial z} \tag{3.2}$$

Equation 3.3 describes the mass transport of oxygen within the fibre membrane. As stated above, the velocity term is absent as convection is assumed to be negligible in the membrane region. This is valid for membranes of low intrinsic permeability and molecular weight cut-offs less than 30 kDa (Brotherton and Chau, 1996) when the bioreactor is operated in a closed-shell mode. The cell layer on the fibre will also impede radial flow. These assumptions remove convective flow in the membrane and ECS and hence the BAL is diffusion-limited. Due to the relative sizes of pores to oxygen molecules, it has also been assumed that oxygen diffusion through the membrane is unrestricted and the diffusion coefficient is the same as in the free plasma (Sullivan et al., 2007).

$$D_{plasma}\left(\frac{1}{r}\frac{\partial}{\partial r}\left(r\frac{\partial pO_2}{\partial r}\right)+\frac{\partial^2 pO_2}{\partial z^2}\right)=0 \tag{3.3}$$

Equation 3.4 describes the mass transport of oxygen within the ECS/cell region. Again transport is solely by diffusion as there is no fluid flow, however in this case the diffusion coefficient represents diffusion through the cells as opposed to plasma (D_{hep}). The cells are assumed to consume oxygen according to a Michaelis-Menten kinetic relationship. As V_{max} values are often quoted in literature with units of mol/m^3/s, a solubility coefficient α is used to convert this into mmHg/s according to Henry's Law.

$$D_{hep}\left(\frac{1}{r}\frac{\partial}{\partial r}\left(r\frac{\partial pO_2}{\partial r}\right)+\frac{\partial^2 pO_2}{\partial z^2}\right)=-\frac{\alpha V_{\max} pO_2}{K_m+pO_2} \tag{3.4}$$

3.2.2 Boundary conditions

The inlet flow to the fibres is assumed to be plasma separated from venous blood that has passed through an oxygenator and contains oxygen at 90 mmHg partial pressure,

represented by *$pO_2(in)$ in Equation 3.5.*. This value is representative of normal arterial oxygen tension.

$$pO_2(r,0) = pO_2(in) \text{ for } 0 \le r < R_l \tag{3.5}$$

Zero axial diffusion can also be assumed at both the fibre inlet and outlet. The symmetry at the lumen centre-line can also be represented by a zero-flux condition. The length of the fibre is represented by *L*.

$$\frac{\partial}{\partial z}\left(pO_2(r,0)\right) = \frac{\partial}{\partial z}\left(pO_2(r,L)\right) = 0 \text{ for } 0 \le r < R_l \tag{3.6}$$

$$\frac{\partial}{\partial r} pO_2(0,z) = 0 \tag{3.7}$$

The following conditions represent continuity of flux and concentration at the inner and outer membrane surfaces respectively. It is assumed that no partitioning occurs between any of the Krogh cylinder regions. In addition, there is a zero axial flux condition at each end of the membrane. The radial positions of the membrane outer surface and Krogh cylinder boundary are given by R_m and R_e respectively.

$$\frac{\partial}{\partial r} pO_2(R_l,z) = \frac{\partial}{\partial r} pO_2(R_m,z) \tag{3.8}$$

$$pO_2(R_l,z) = pO_2(R_m,z) \tag{3.9}$$

$$D_{plasma} \frac{\partial}{\partial r} pO_2(R_m,z) = D_{hep} \frac{\partial}{\partial r} pO_2(R_e,z) \tag{3.10}$$

$$pO_2(R_m,z) = pO_2(R_e,z) \tag{3.11}$$

$$\frac{\partial}{\partial z}\left(pO_2(r,0)\right) = \frac{\partial}{\partial z}\left(pO_2(r,L)\right) = 0 \text{ for } R_l \le r < R_m \tag{3.12}$$

The remaining boundary conditions represent symmetry at the outer surface of the Krogh cylinder and zero flux through the ends of the cartridge in the ECS/cell layer.

$$\frac{\partial}{\partial r} pO_2(R_e,z) = 0 \tag{3.13}$$

$$\frac{\partial pO_2}{\partial z}(r,0) = \frac{\partial pO_2}{\partial z}(r,L) = 0 \text{ for } R_m \le r < R_e \tag{3.14}$$

3.2.3 Modelling parameter values

Table 3.1 lists the various parameters and corresponding values employed in the BAL model. These parameters have been chosen to mimic the physiological and physical characteristics of the system as much as possible.

Table 3.1: A list of published parameters used in calculations and modelling (Davidson et al., 2010)

Parameter	Value	Reference
D_{plasma}, oxygen diffusion coefficient in plasma	3 x 10^{-9} m^2/s	(Piret and Cooney, 1991)
D_{hep}, oxygen diffusion coefficient in hepatocytes	2 x 10^{-9} m^2/s	(Piret and Cooney, 1991)
d_{cell}, approximate cell thickness	25 μm	(Sullivan et al., 2007) (McCuskey, 2008)
V_{max}, maximum uptake rate of oxygen by hepatocytes	5.87 x 10^{-3} $mol/m^3/s$	(Sullivan et al., 2007) (Nyberg et al., 1994)
K_m, Michaelis-Menten constant	3 mmHg	(Sullivan et al., 2007) (Hay et al., 2001)
$pO_2(in)$, inlet oxygen partial pressure of plasma	90 mmHg	(Sullivan et al., 2007)
α, solubility coefficient for oxygen at 37 °C	481 mmHg/mol/m^3	(Sander, 2007)
ρ_{area}, surface density of hepatocyte monolayer on fibres	3 x 10^9 cells/m^2	(Sauer et al., 2003)
Hypoxic limit of oxygen partial pressure	2 mmHg	(De Groot et al., 1988)

The diffusion coefficient for oxygen in plasma is assumed to be equal to that commonly assumed for cell culture medium (Piret and Cooney, 1991). Parameters corresponding to primary rat hepatocytes have been used to describe the oxygen consumption characteristics of the cells, i.e. V_{max} and K_m. The maximal oxygen uptake rate, V_{max}, is described per unit volume of cells under the assumption that the volume fraction of cells in the cell layer is unity. The cell layer thickness is chosen to be equivalent to the width of one cell. The

anoxic limit is considered to be 2 mmHg as hepatocyte respiration is impaired below this oxygen tension (De Groot et al., 1988).

3.2.4 Modelling strategy

The convection-diffusion equation is modelled in a single representative sub-unit of the hollow fibre bundle to produce oxygen tension profiles for the BAL. An axially symmetric 2-dimensional coordinate system is used to represent the fibre (Fig. 3.2). This model is used to determine where the anoxia constraint (pO_2 > 2 mmHg) will lie on a chart of fibre number N versus lumen radius R_l. At this point it is also useful to define R_m as the sum of the lumen radius R_l and the membrane thickness w. R_e is then found by further addition of the cell layer thickness d_{cell}.

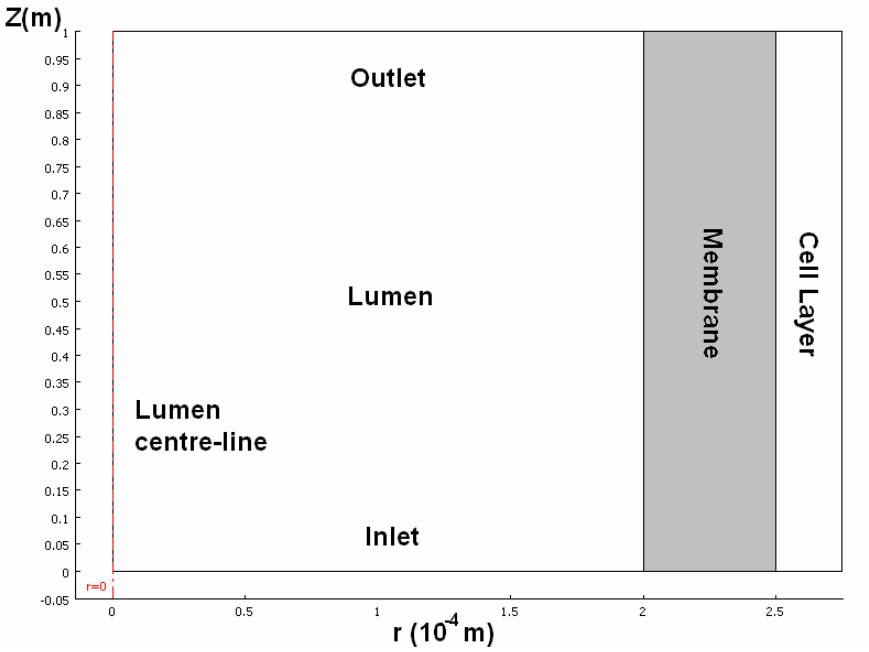

Figure 3.2: Krogh cylinder model as represented within COMSOL (Davidson et al., 2010).

The position of the anoxic zone is defined by the axial distance from the fibre inlet to the point where oxygen tension first falls to 2 mmHg. Based on intuition and initial modelling results, it can be assumed this point will fall on the outer boundary of the ECS/cell layer (Fig. 3.3). Cells beyond this point are assumed to experiencing anoxia. This axial distance, here named L_{hyp}, is a function of hollow fibre geometry and operating parameters such as plasma flow rate. When all other variables are constant, L_{hyp} is a function of the average

plasma flow velocity $\bar{u}$. On this basis the anoxia constraint can be defined as seen in Equation 3.18.

In order to solve the above equations, the modelling software COMSOL 3.5a was employed. This software allows systems of equations representing different physical phenomena to be solved simultaneously, based on finite element methods. In this case a steady-state Convection and Diffusion physics mode is chosen to solve the model equations. The domain of interest (Fig. 3.2) is discretized into a mapped mesh consisting of approximately 4000 elements. This is sufficient to ensure that further element refinement does not affect the modelling results within 3 significant figures. A mapped mesh of rectangular elements is used over a triangular free mesh as the small aspect ratio of the fibre causes issues in the free-meshing process. A UMFPACK solver with an increased tolerance setting of 10^{-8} to reflect the non-linearity of the equations is chosen. This algorithm tends to perform well over other built-in COMSOL solvers in this case, as the iterative solver can often converge to a solution.

3.3 Results

3.3.1 Model validation and initial results

To show that the model described previously can produce sensible results, it was validated against an alternative analytical approach to solving of the model equations. This process is outlined in detail in the work by Shipley et al (2010). The modelling equations were solved analytically by initially making a number of simplifying assumptions, such as zero-order oxygen consumption and a small aspect ratio of order 10^{-3}. Kummer functions were then used to define analytical expressions for radial concentration profiles at various axial positions along the fibre. When these concentration profiles were plotted alongside corresponding profiles produced through the modelling procedure described here, very strong agreement was found where concentrations were relatively high. Where concentration were relatively low, i.e. the distal end of the fibre, a percentage error of 3.39% was found between the concentration profiles. It is hypothesized the error largely arises due to the Michaelis-Menten constant K_m, ignored in the analytical model, becoming significant at low oxygen concentrations. These results indicate that the model used in this

work is consistent with an analytical approach. The model could be further validated through comparison with experimental results.

An example of a model solution produced by COMSOL can be seen below (Fig. 3.3). The colour map is a representation of the oxygen tension profile in the Krogh cylinder model of the BAL. The flow and transport regimes in the cylinder can be characterized by pertinent dimensionless numbers. A Reynolds number can be calculated by the expression $\frac{2\rho\bar{u}R_l}{\mu}$, where the characteristic length is fibre lumen diameter. Assuming a fluid density ρ of 1000 kg/m^3 and a dynamic viscosity μ of 10^{-3} Pa.s, Reynolds numbers for the system vary between 0.2 and 6, indicating the flow is well within the laminar regime. Axial Peclet numbers, given by $\frac{\bar{u}R_l^2}{D_{plasma}L}$, range between 10^{-2} and 2, indicating that axial diffusion can be significant in oxygen transport along the fibre. In a related study (Shipley et al., 2011), a dimensionless parameter representing the balance of oxygen consumption versus diffusion in the ECS was defined as $\frac{R_l^2\alpha V_m}{D_{hep}pO_2(in)}$. In this case it varies between approximately 10^{-1} and 1, indicating the process is not controlled by reaction rate.

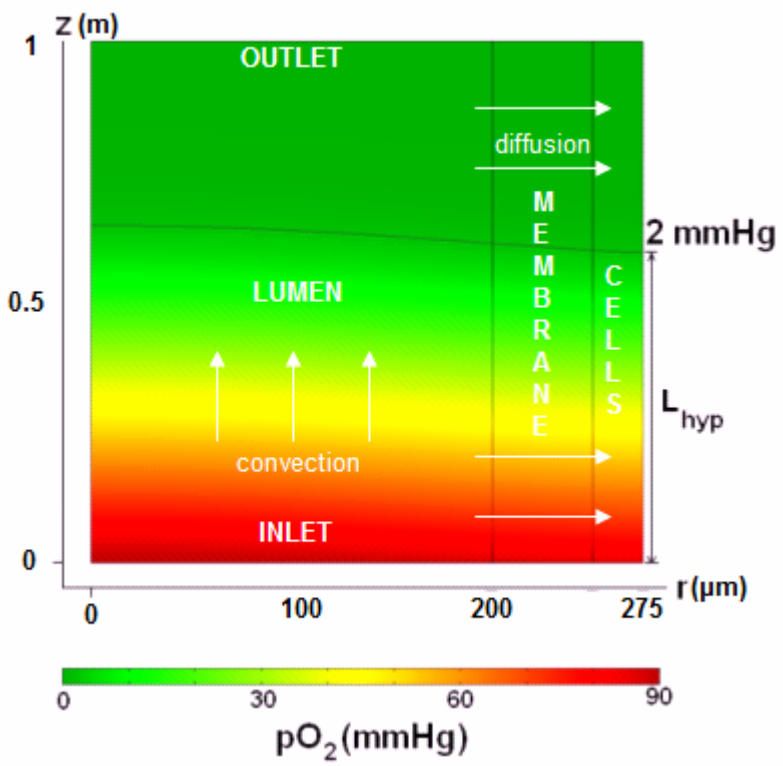

Figure 3.3: Modelling results are used to determine the position of the anoxic zone in the BAL. The colour map represents the profile of oxygen partial pressure in the Krogh cylinder. The modelling subdomains are labelled and arrows indicate the directions of oxygen convection and diffusion. The axial distance L_{hyp} indicates the position of the anoxic zone (Davidson et al., 2010).

3.3.2 Relationship between anoxic zone position and flow velocity

Initial modelling results make it clear that for a fibre of specified geometry, i.e. fixed lumen radius, membrane and cell layer thickness, L_{hyp} is directly proportional to average flow velocity $\bar{u}$. This can be seen below in Figure 3.4. The corresponding constant of proportionality is named k_{hyp} (Eq. 3.15). This finding matches those evident in the concentration profiles derived by Willaert et al (1999).

$$L_{hyp} = k_{hyp}\bar{u} \tag{3.15}$$

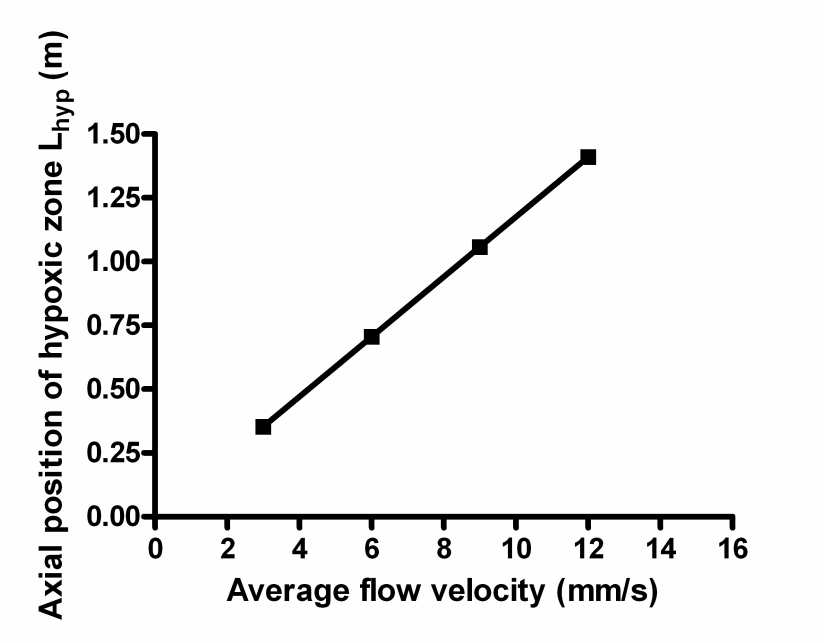

Figure 3.4: An example of the linear relationship between the axial position of the anoxic zone L_{hyp} and average flow velocity $\bar{u}$. These results were obtained for a lumen radius of 200 μm and membrane thickness of 50 μm. The R^2 value indicates a perfect fit (Davidson et al., 2010).

3.3.3 Operating constraints

Anoxia constraint

Given a total flow rate Q of plasma through the device, average flow velocity $\bar{u}$ will be inversely proportional to the number of hollow fibres in the bundle as shown below in Equation 3.16.

$$\bar{u} = \frac{Q}{N.\pi R_l^2} \tag{3.16}$$

Here N is number of fibres and R_l is the fibre lumen radius. Hence L_{hyp} is also inversely proportional to fibre number (Eq. 3.17).

$$L_{hyp} = \frac{k_{hyp} Q}{N.\pi R_l^2} \tag{3.17}$$

In order that the hepatocytes are not exposed to anoxic conditions, this length L_{hyp} must be greater or equal to the length of HFBR, L. The point at which it equals L represents a constraint on the maximum number of fibres in the hollow fibre bundle i.e. the flow rate is

only just keeping the cell layer surrounding each fibre above anoxic levels. This constraint is described by the equation below (Eq. 3.18):

$$\bar{u}_{\min} = \frac{Q}{N_{\max}.\pi R_l^2}$$

$$\therefore N_{\max} = \frac{k_{hyp} Q}{\pi R_l^2 . L} \tag{3.18}$$

The value of k_{hyp} is observed from modelling results and is only applicable to a particular geometry of hollow fibre (fixed R_l, w). Given the vast array of combinations of fibre geometrical parameters, it is impractical to obtain k_{hyp} for each permutation. Instead, an empirical relationship between k_{hyp} and R_l can be established from modelling results in the case of fixed membrane thickness, circumventing this issue. This relationship appears as a linear one in the form seen below in Equation 3.19 and Figure 3.5.

$$k_{hyp} = B_1 R_l + B_2 \tag{3.19}$$

Here B_1 and B_2 are empirical constants whose value depends on the membrane thickness w being considered. The R^2 value for this relationship is greater than 0.99 within the range of interest of lumen radius R_l (100-300 μm). As a result, the anoxia constraint to be plotted as a function of lumen radius with fixed membrane thickness w and plasma flow rate Q (Eq. 3.20).

$$N_{\max} = \frac{(B_1 R_l + B_2) Q}{\pi R_l^2 L} \tag{3.20}$$

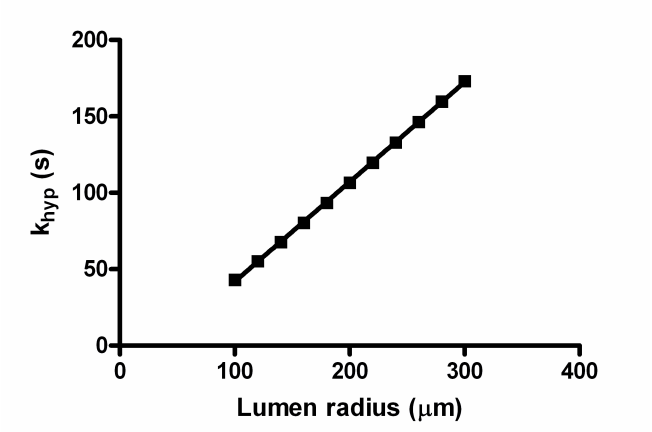

Figure 3.5: The relationship between k_{hyp} and R_l when all other parameters are constant. There is a clear linear trend (with non-zero intercept) with an R^2 value greater than 0.99. This observation allows values of B_1 and B_2 to be found (Davidson et al., 2010).

Cell number constraint

A second constraint on the BAL is defined by the cell population housed in the HFBR – the design must support an adequate population of cells in order for the BAL to function adequately. As the model assumes that the hepatocytes form a confluent monolayer on each fibre, there must be a minimum amount of fibre surface area to support the desired number of cells N_{cell} with cell density ρ_{cell} in the bioreactor. For a given fibre design the minimum number of fibres is therefore constrained by Equation 3.21.

$$N_{\min} = \frac{N_{cell}}{\rho_{cell}(2\pi(R_l + w).L)} \tag{3.21}$$

Each of the above constraints can be plotted on the same graph of fibre number N versus lumen radius R_l to define an 'Operating Region' bounded by the curves. By changing parameters such as plasma flow rate Q, membrane thickness w and fibre length L, the significance of each parameter in determining the size and position Operating Region can be determined.

3.3.4 Operating Region charts

An example of an Operating Region is depicted below (Fig. 3.6), derived from parameter values chosen so as to represent a typical design, i.e. a fibre length of 25 cm, membrane thickness of 50 μm and plasma flowrate of 200 ml/min. A range of fibre lumen radii from 100 to 300 μm is considered with a cell number of 10 billion, as this is considered to be the minimum required to support liver function. The chart in Figure 3.6 is used for comparison with those created with different parameter values. The size of each Operating Region is found through numerical integration and presented in terms of area relative to the 'standard' Operating Region in Figure 3.6. Larger Operating Regions indicate a wider range of viable designs and increased margin for error within the model.

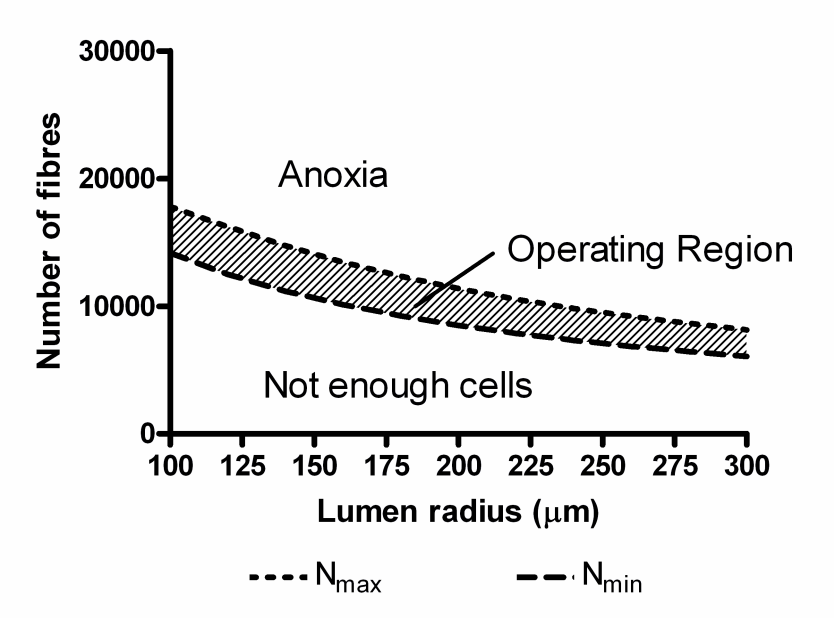

Figure 3.6: An Operating Region chart constructed from the following parameter values: L = 25 cm, w = 50 μm, Q = 200 ml/min, N_{cell} = 1.0 x 10^{10} cells. The Operating Region is denoted by the shaded region. The top curve, representing N_{max}, is due to the anoxia constraint within the BAL and the bottom curve, representing N_{min}, is due to the minimum cell number constraint (Davidson et al., 2010).

As fibre length increases the constraint on cell number relaxes while the anoxia constraint becomes more restrictive (Fig. 3.7). Fewer fibres are needed to provide an adequate surface area for the cell population to adhere to and hence the Operating Region shifts downwards. However, cells at the distal end of longer fibres become more likely to experience anoxic conditions. The Operating Region hence becomes smaller with increasing length: the relative sizes are 1.67 and 0.71 for fibre lengths of 15 cm and 35 cm respectively, compared to the Operating Region area of Figure 3.6 (where fibre length is 25 cm).

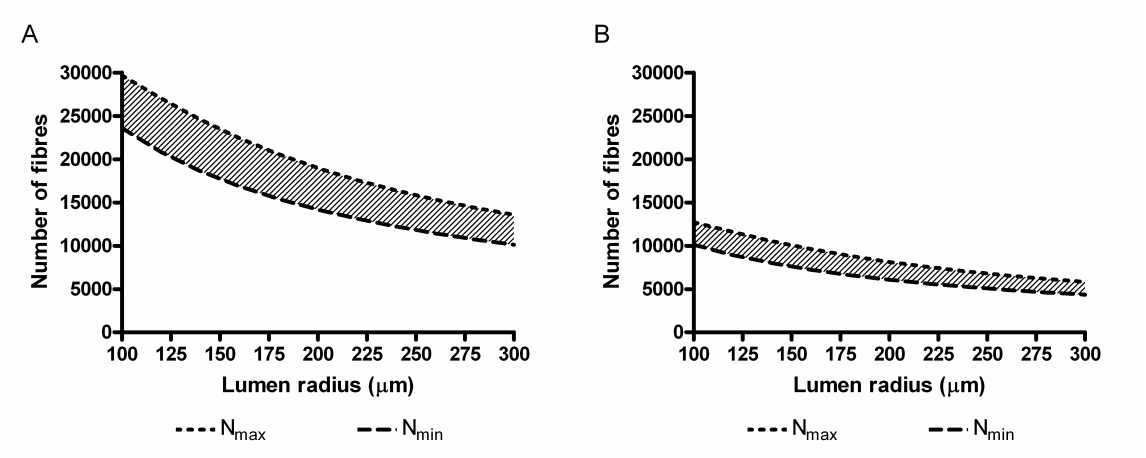

Figure 3.7: Operating regions for a BAL with 2 different fibre lengths: (A) L = 15 cm, (B) L = 35 cm. The other parameters are N_{cell} = 1.0 x 10^{10} cells, Q = 200 ml/min, w = 50 μm (Davidson et al., 2010).

Figure 3.8 shows that the cell number constraint is unaffected by the plasma flow rate as it depends solely on the available fibre surface area. It is clear however that increasing the flow rate causes the anoxia constraint to relax and hence the region becomes larger for greater Q, with a relative area of 3.04 for a flow rate of 300 ml/min, the technical upper limit (Fig. 3.8B). A flow rate of 100 ml/min is insufficient to allow a viable Operating Region to be defined, as not enough oxygen can be supplied to all the cells i.e. the N_{min} curve lies above N_{max}.

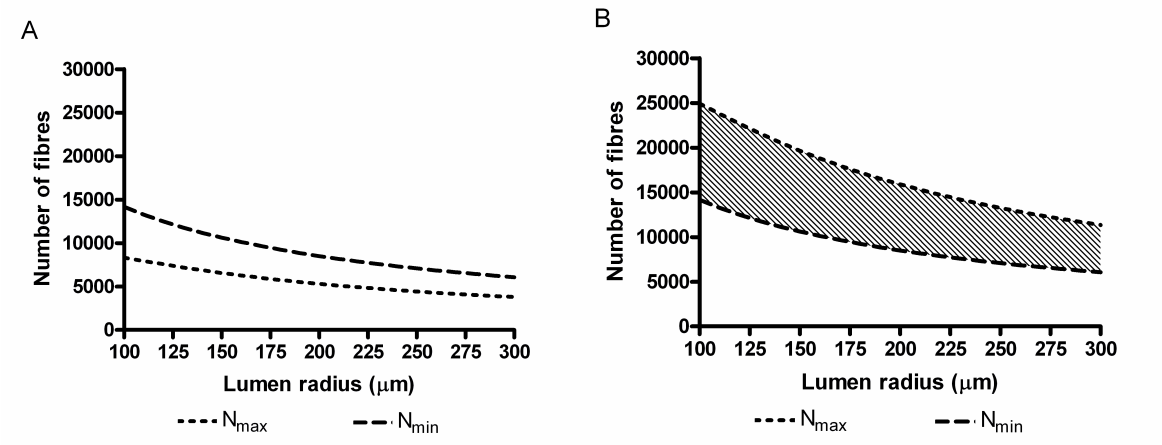

Figure 3.8: Operating regions with varying plasma flow rate: (A) Q = 100 ml/min (B) Q = 300 ml/min. The other parameters are N_{cell} = 1.0 x 10^{10} cells, L = 25 cm, w = 50 μm (Davidson et al., 2010).

Figure 3.9 illustrates the fact that the number of cells in the device is only significant in the cell number constraint and has no impact on the anoxia constraint. For a given fibre geometry the minimum fibre number N_{min} is proportional to cell number N_{cell} and the cell

number constraint becomes more restrictive as more cells are loaded into the device. In this case the lower cell number of 5 billion results in an Operating Region 1.26 times bigger than the standard Operating Region (10 billion cells). For a cell number of 15 billion, no viable designs exist as it is impossible to provide enough oxygen to the cells at the distal end of the HFBR at the flow rate considered (Davidson et al., 2010).

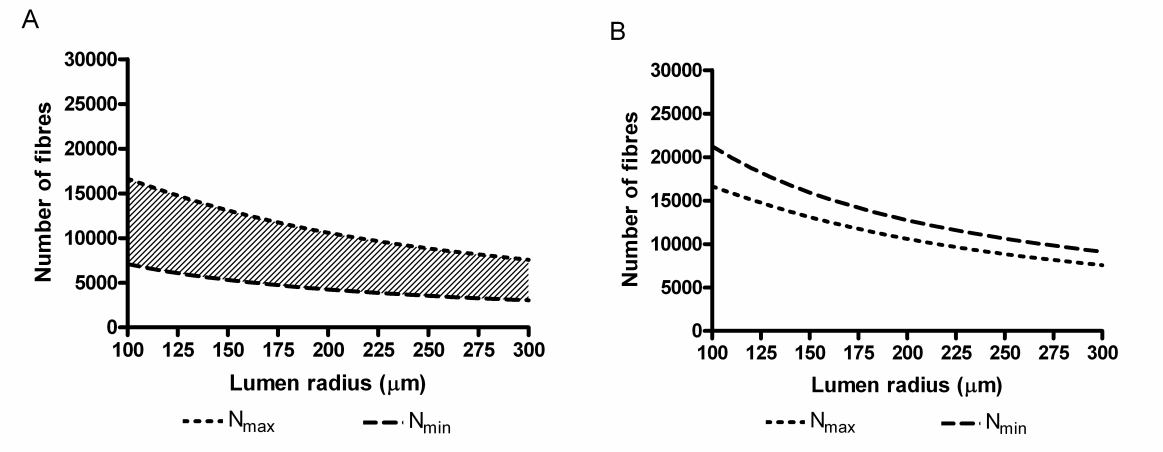

Figure 3.9: Operating regions with varying cell number: (A) N_{cell} = 5.0 x 10^9 (B) N_{cell} = 15.0 x 10^9. The other parameters are Q = 200 ml/min, L = 25 cm, w = 50 μm (Davidson et al., 2010).

Over the range considered of membrane thicknesses considered, the value appears to have a small impact upon the Operating Region. The relative areas are 0.96 and 1.04 for thicknesses of 40 and 60 μm respectively (Fig. 3.10). Increasing the thickness restricts oxygen delivery to the cells, but also increases the available surface area per fibre for cell adhesion. These effects combine to shift the Operating Region to a lower range of fibre number while marginally decreasing its size.

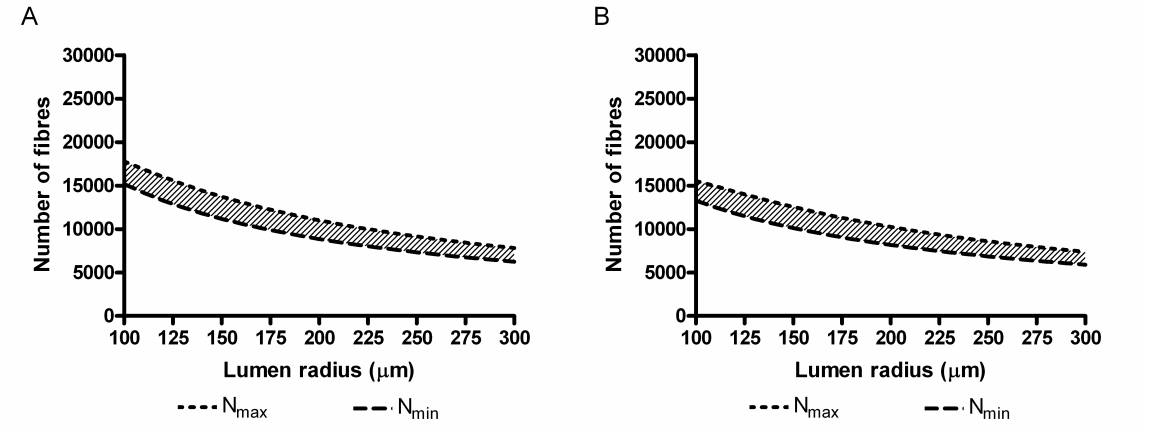

Figure 3.10: Operating regions with varying membrane thickness: (A) w = 40 μm (B) w = 60 μm. The other parameters are Q = 200 ml/min, L = 25 cm, N_{cell} = 10.0 x 10^9 (Davidson et al., 2010).

3.3.5 Minimum flow rate and maximum cell number

For a given fibre geometry, the point at which the anoxia and cell number constraints overlap (i.e. $N_{min} = N_{max}$) can be used to make some important definitions. For a given cell number N_{cell}, the value of Q at this point is the minimum flowrate needed to support the cells. For a given Q, N_{cell} is the maximum number of cells that can be seeded in the BAL. Equations 3.22 and 3.23 describe these relationships below:

$$Q_{\min} = \frac{N_{cell} R_l^2}{2\rho_{cell}(R_l + w)(B_1 R_l + B_2)} \tag{3.22}$$

$$N_{cell(\max)} = \frac{2Q\rho_{cell}(B_1 R_l + B_2)(R_l + w)}{R_l^2} \tag{3.23}$$

Interestingly, both of these expressions are independent of the fibre length L. It may be counter-intuitive that the maximum number of cells that can be held in the device is independent of the fibre (and hence HFBR) length. However, the increase in length (cells per fibre) is offset by the reduction in number of fibres as the flow rate per fibre must increase to supply sufficient oxygen to cells at the distal end of the fibres. Hence the total number of cells in the BAL is constant for given fibre geometry.

The above expression for $N_{cell(max)}$ can be differentiated using the quotient rule with respect to R_l in order to calculate the value of R_l that maximizes the number of cells in the device (Eq. 3.24).

$$R_l = \frac{-2B_2 w}{B_1 w + B_2} \tag{3.24}$$

The corresponding value of $N_{cell(max)}$ can then be found with this value of R_l. Differentiation of Equation 3.22 also results in the same value for lumen radius that will minimize the plasma flow required to the device.

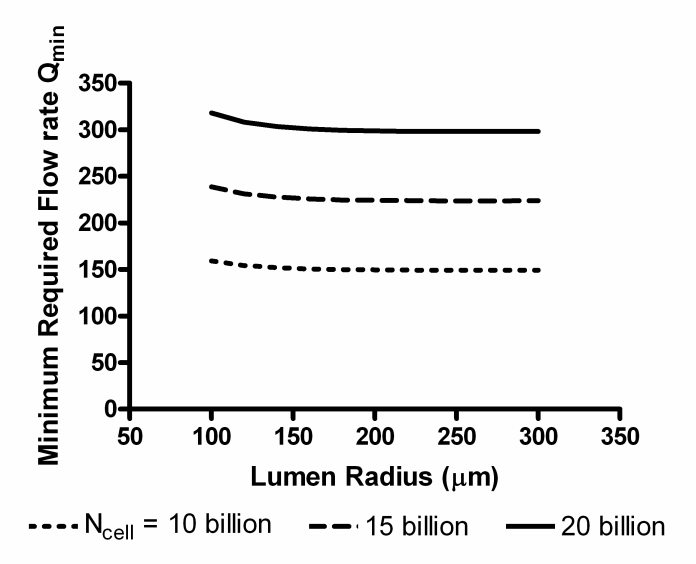

Figure 3.11: Minimum flow rate Q_{min} plotted as a function of lumen radius R_l for three cell populations.

The minimum flow rate required is plotted as a function of lumen radius in Figure 3.11, for three different cell populations in the device. The values in Table 3.1 are used for modelling parameters not otherwise indicated. In each case, a lumen radius of 251 μm results in the minimum value of Q_{min}. The Q_{min} values are 149, 224 and 298 ml/min for cell numbers of 10, 15 and 20 billion respectively.

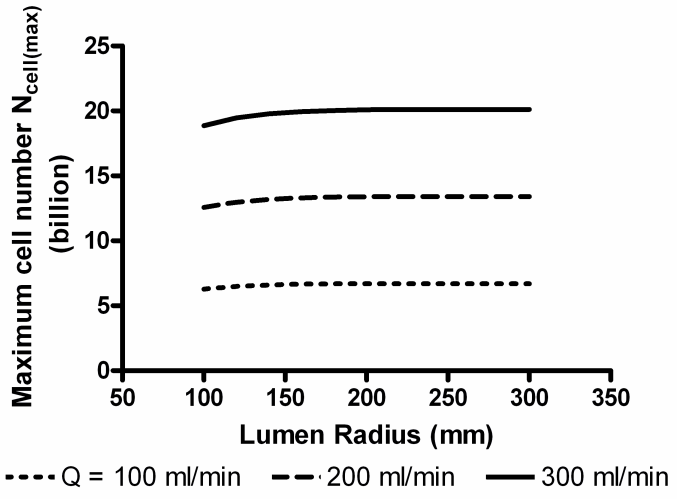

Figure 3.12: Maximum cell number $N_{cell(max)}$ plotted as a function of lumen radius R_l for 3 flow rates.

Figure 3.12 displays the maximum cell number $N_{cell(max)}$ as a function of lumen radius for three plasma flow rates. $N_{cell(max)}$ is maximized for a fibre radius of 251 μm. For this

radius the BAL can support cell numbers of up to 6.7, 13.4 and 20.1 billion at plasma flow rates of 100, 200 and 300 ml/min.

3.3.6 Priming volume

The priming volume of the HFBR is equal to the total intraluminal volume of the fibres. As this represents the volume of plasma that is removed from the patient there are benefits to safety in restricting its size. It has been reported that the priming volume for a BAL should not exceed 1 litre (Chan et al., 2004). The maximum priming volume in the HFBR for a given fibre geometry can be found by considering the number of fibres to be equal to N_{max}. The priming volume can then be found by the following expression:

$$V_p = N_{\max} . \pi R_l^2 L \tag{3.25}$$

By using the definition of N_{max} from Equation (18), the priming volume is given by:

$$V_p = Q\left(B_1 R_l + B_2\right) \tag{3.26}$$

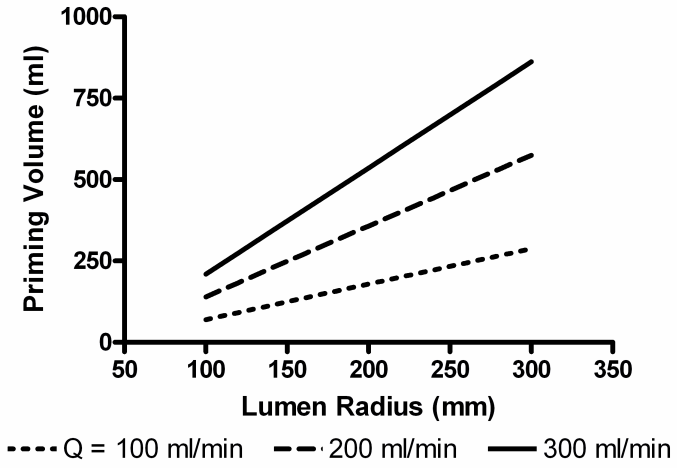

Figure 3.13: BAL priming volume V_p as a function of lumen radius R_l, for three plasma flow rates.

As can be seen above, priming volume V_p increases linearly with fibre lumen radius R_l as expected from Equation 3.26. Increasing the plasma flow rate Q also causes V_p to increase though over the range of Q and R_l modelled, V_p remains below the suggested one litre design constraint of the system.

3.4 Discussion

Using a 2D Krogh cylinder model it was possible to quantify the constraint that conditions in the hollow fibre bioreactor must not become anoxic. By plotting this constraint alongside the constraint for minimum cell number, Operating Regions for the HFBR were established.

The length of hollow fibre was varied from 15-35 cm to cover the range of sizes of hollow fibre cartridges in haemodialysis. With longer fibres, the increased surface area allows more cell attachment and subsequently fewer fibres are required to meet the cell number constraint. However, the cells at the distal end of the longer fibres are more likely to become exposed to anoxic conditions and require a greater flow rate of oxygen-carrying plasma, leading to a more restrictive anoxia constraint. As a result, the Operating Region occupies a lower range of fibre number. The anoxia constraint tightens faster than the cell number constraint relaxes, leading to a contraction in the Operating Region for larger fibre length. This indicates that BALs with shorter fibres are 'safer' in that errors in the model are less likely to result in anoxic conditions.

It is essential to supply enough oxygen to ensure the hepatocytes' viability in the BAL, however it has been reported that blood plasma flow rates are limited to 100-300 ml/min in BAL applications (Pless and Sauer, 2005). At the lower end of the scale it becomes impossible to support a population of 10 billion hepatocytes while avoiding anoxia. The situation is improved with increasing flowrate. For more cells, it would be expected that flow rates close to the maximum will be necessary to provide sufficient oxygen. Calculations show that the theoretical maximum cell number that can be supported with a flow rate of 300 ml/min is approximately 20 billion cells, or 20% of the cell mass of a human adult liver. This number is found by setting N_{min} equal to N_{max} and rearranging the equation to solve for N_{cell}.

It has been assumed that the BAL should support 10^{10} cells as this is often regarded as a minimum number of cells that a BAL should contain to be effective (Diekmann et al., 2006, Strain and Neuberger, 2002). It is possible however for the BAL to support a range of cell numbers, the impact of which on the Operating Region was determined. The results

are fairly intuitive, with the cell number constraint steadily becoming more restrictive until the design becomes unfeasible. The anoxia constraint is unaffected by the total cell number. This is a result of the Krogh cylinder method where modelling considers only a single fibre. Each fibre is treated as being covered in a monolayer of cells, regardless of total cell or fibre number in the device.

Finally, the effect of membrane thickness upon the Operating Regions was determined. Thicker membranes allowed a greater surface area for cell attachment per fibre, but also resulted in greater mass transfer restrictions. In this model, diffusion through the membrane is assumed to occur at an equal rate as in plasma. This effect would be exacerbated should oxygen diffusion become restricted through the membrane. The Operating Region shifts to occupy a lower range of fibre number and contracts slightly for greater membrane thickness, suggesting thinner membranes allow a greater range of viable BAL designs. Thinner membranes also provide greater surface area to volume ratios, allowing BALs to contain greater cell numbers per unit volume. Ultimately the minimum membrane thickness will be constrained by practical and mechanical considerations.

In general, most of the Operating Regions are wider at lower fibre lumen radii. This indicates that employing numerous, smaller bore fibres is more likely to result in a viable BAL design than fewer, larger diameter fibres. Small fibre diameters also reduce the priming volume of the BAL, requiring less blood to be taken from the patient. The Operating Regions indicate that viable designs often require in excess of approximately 10,000 fibres for intermediate fibre lengths and lumen radii. The upper limit of fibre number is more difficult to ascertain and depends in large part upon the device plasma flow rate and fibre length. The charts of minimum flow rate Q_{min} and maximum cell number $N_{cell(max)}$ suggest that cell populations of over 20 billion can be supported in the device for flow rates around the technical limit of 300 ml/min. This cell number is relatively large compared to some existing BAL designs and suggests that effective BAL designs may be possible.

Work undertaken by Hay et al. (Hay et al., 2000, Hay et al., 2001) sought to utilize mathematical modelling to determine the efficacy of the ELAD and HepatAssist designs of the time. For the ELAD it was concluded that while it may be possible to support liver cell lines of low oxygen demand in the system, the hollow fibre design was insufficient to

support more metabolically active cell lines such as human primary hepatocytes. The mathematical model used is broadly similar to the one presented in this work, though the authors consider maximal oxygen consumption rates (V_{max}) of a magnitude greater than seen here. The highest V_{max} corresponded to results from a rat hepatocyte monolayer. 2D cultures of hepatocytes however are known to have oxygen demands an order of magnitude higher than 3D cultures, possibly due to 2D cultures being unnatural and causing stress to the cells (Patzer, 2004). Whole blood was also considered to be the perfusate of the system and hence the oxygen-carrying characteristics of haemoglobin were also modelled. This should allow greater oxygenation, though as the blood was considered to be venous and not oxygenated prior to entering the hollow fibres, the inlet partial pressure of oxygen was only 40 mmHg. This possibly negated any benefit of including the haemoglobin in the model and resulted in poor oxygenation, a view echoed by Moussy (Moussy, 2003). The ELAD design being modelled was considered to contain 20 billion C3A cells (an immortalized human cell line derived from HepG2 cells) but was only supplied with a flow rate of approximately 170 ml/min. From the results presented here, it is clear that this flow rate, coupled with the low inlet pO_2, would not be enough to support such a large cell population. Hay et al's conclusions support the findings in this Chapter, while also illustrating a useful feature of the Operating Region concept; it allows deficiencies in BAL design to be readily identified.

This work has considered that plasma is used to perfuse the BAL and hence no haemoglobin is present. It can be seen that viable BAL designs could be found in this way. Other models consider that either whole blood perfuses the BAL or some concentration of haemoglobin-based oxygen carriers (HBOCs) are circulating in the media. Extensive work in this area was carried out by a group led by Andre F. Palmer of the Univerisity of Ohio (formerly Notre Dame). One study sought to model oxygen delivery within a HFBR perfused with media containing various different HBOCs (Sullivan and Palmer, 2006). The values for inlet oxygen tensions, flow rates and HBOC concentration were varied and it was concluded that using oxygen carriers and well oxygenated media would optimally oxygenate the bioreactor. However, that model considered a cell layer approximately three times thicker per fibre than seen in this study, and also a higher value for V_{max}. In this case each fibre would have to provide oxygen to three times the number of cells and hence hypoxia becomes more restrictive. This would explain the need for oxygen carriers in that case, despite similar fibre geometry and flow rates per fibre to this study.

The mathematical model presented here is similar to that developed by Sullivan et al. (Sullivan et al., 2007), including a number of the parameter values. Sullivan et al. found that HBOCs were necessary in order to provide ideal oxygenation to a HF-BAL. However, as in the last example the cell layer per fibre is approximately 3 times thicker than in this work. By controlling inter-fibre distance, the fibres can be arranged to prevent any more than a monolayer of cells attaching to each fibre. This is similar to the situation *in vivo* where normally a single layer of hepatocytes borders each sinusoid (Telford and Bridgman, 1995). This also reduces the oxygen delivering 'duty' of each fibre and eases hypoxia restrictions.

This work has sought to define a rationale for HF-BAL design, whether it is the HFBR dimensions or BAL operating parameters. To this point there has been little in existing literature that makes an argument for using a particular set of design parameters. From this work, the use of Operating Region charts allows us to determine the relative importance of each geometric and operating variable. Thus viable BAL designs could be produced by controlling the operating parameters and hollow fibre characteristics of the device. It is difficult to make direct comparisons between our work and actual BAL designs, as the model here may not represent them accurately. For instance, most designs have a greater inter-fibre distance so that more than one layer of cells will surround each fibre. However, the qualitative trends seen here allow some meaningful comparisons to be made. In the next Chapter and beyond, the relevance of the Operating Region concept can be increased through considerations of liver physiology and differing designs of existing, commercialized designs of BALs.

3.5 Conclusions

This work has approached design of a BAL in a novel, systematic manner, to ascertain how various design parameters can impact upon device viability. Whereas studies typically focus on existing designs and specifications, ranges of possible designs have been considered here to produce a graphical method that allows a prediction over whether a BAL design will be functional. The results also indicate general trends that should be followed such as using more fibres of shorter length and smaller diameter which leads to

larger Operating Regions. The model suggests that a cell mass equivalent to approximately 10-20% of the adult liver can be supported through judicious choices regarding the hollow fibre characteristics and BAL operating conditions.

Chapter 4: A Theoretical Approach to Zonation in a Bioartificial Liver

4.1 Introduction

In a review of the existing state of BALs in Section 2.2, it became clear that device design needs to be improved in order to progress to positive results and clinical acceptance. Chapter 3 outlines the concept of Operating Regions, a graphical method to identify viable BAL designs and discern favourable design trends. It was seen that under the right conditions, BALs containing therapeutically relevant cell numbers would be viable. However, one aspect that has not been considered fully in BAL designs to date and also the Operating Region concept is the phenomenon of liver zonation, an important facet of liver physiology.

As blood travels through the liver microcirculatory system, or sinusoids, the concentration of substrates such as oxygen or hormones will change, causing the signals received by the hepatocytes in different regions of the lobule to also differ (Fig. 4.1). As a result hepatocyte metabolism and gene expression becomes dependent on the cell's position along the liver lobule. This concept was introduced previously in Section 2.1.4. Liver zonation is defined by the heterogeneity in cell function according to position. The cells in the periportal zone, the region close to branches of the portal vein and hepatic artery, differ from those in the perivenous zone, which is the region close to the central vein. Heterogeneity exists in the presence of enzymes and receptors within the cells (Kietzmann and Jungermann, 1996). Jungermann and Kietzmann (2000) explain the various functional differences between the periportal and perivenous zones. As an example, processes such as bile formation and urea synthesis are more prevalent in the periportal zone whereas glutamine formation and xenobiotic metabolism take precedence in the perivenous zone.

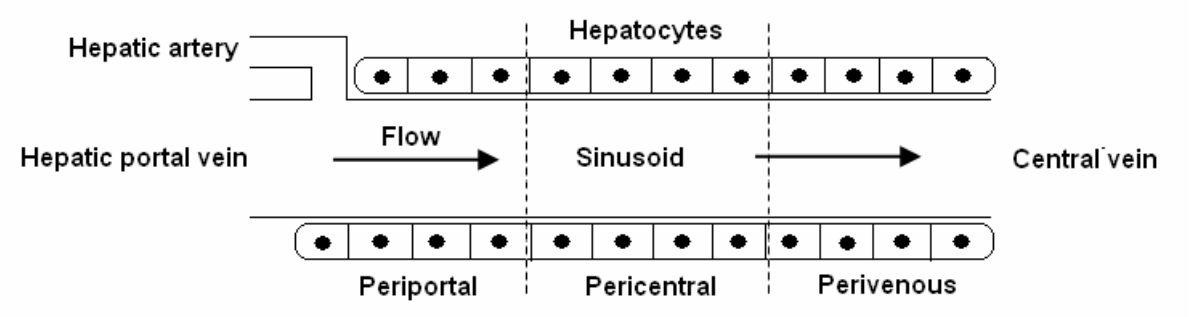

Figure 4.1: Schematic of liver microcirculation and zonation. The gradient of oxygen tension along the sinusoid is a primary modulator of liver function and delineates the three metabolic zones (Davidson et al., 2010).

Liver zonation is very important in the coordination of liver function. A good illustration of this is the liver's control of blood sugar levels. In times between meals when blood glucose is reduced, periportal hepatocytes begin to release glucose from glycogen which in turn is metabolized to lactate in the perivenous cells. As lactate enters the circulation and reaches the periportal zone, enzymes involved in gluconeogenesis are upregulated to convert it to glycogen. When blood sugar levels are high after meals, glucose passes by the periportal zone and travels directly to the perivenous hepatocytes where insulin allows it to be converted to glycogen for storage (Jungermann and Kietzmann, 2000, Allen and Bhatia, 2003, Yu et al., 2009).

Zonation in the liver is generally thought to be primarily modulated by gradients of oxygen, hormones and extracellular matrix components in the liver lobule. In particular, oxygen is found to be a modulator of both short-term metabolism and long-term gene expression in vivo (Jungermann and Kietzmann, 2000, Kietzmann and Jungermann, 1996, Gebhardt, 1992, Lindros, 1997). In one study it has been found that a physiological-like oxygen gradient in a flat-plate bioreactor containing rat hepatocytes contributed to heterogenous distribution of phosphoeonolpyruvate carboxykinase (PEPCK) and cytochrome P450 2B (CYP 2B). The spatial patterning of these proteins in the bioreactor was similar to the patterns normally observed *in vivo* (Allen and Bhatia, 2003). In a subsequent article, rat hepatocytes were co-cultured with non-parenchymal cells in a flat-plate bioreactor under a physiological oxygen gradient. The spatial induction of CYP 2B and CYP 3A was examined and found to mimic *in vivo* zonation patterns (Allen et al., 2005). These results confirm that oxygen is a primary modulator of liver zonation both *in vivo* and *in vitro*.

Within a bioreactor, oxygen gradients will be determined by aspects such as cellular uptake, operating conditions and bioreactor geometry. In this chapter, it has been hypothesized that if bioreactor conditions can be manipulated to produce a physiological oxygen gradient, the liver cells will exhibit similar behaviour as *in vivo*. The Operating Region concept and BAL model of Chapter 3 is hence expanded to include definitions of distinct liver zones as defined by local oxygen tensions. The size of each zone will vary according to the range of viable operating parameters and fibre geometry as defined by the Operating Region. The results show that while the size of each metabolic zone can vary over a large range, the distribution of the three metabolic zones could be controlled to an extent through BAL design parameters. In particular cases all of the zones can be made to occupy the same volume of the BAL. In addition, unexpected negative consequences arising from over-oxygenation of the cell mass are revealed.

4.2 Theoretical Aspects

The mathematical model employed here to describe oxygen mass transport in the BAL is essentially the same as that one outlined in Chapter 3; that is a system of convection-diffusion equations are solved within a Krogh cylinder representation of a BAL. Again, the finite element-based software COMSOL 3.5a is used to perform the modelling and obtain results. However as the Krogh cylinder is of a very high aspect ratio, meshing of the structure proved to be problematic in some cases for the work of Chapter 3. To remedy this, it was decided to scale the axial coordinates of the model, in this case by a factor of 100. This scaling requires adjustments to be made to the governing equations of the system – the diffusion coefficient becomes anisotropic, 10^4 times smaller in the axial direction, and the axial flow velocity is scaled 10^2 times smaller. The different scaling of these parameters results from the power of the length exponent in their units. This procedure does not affect the results produced. COMSOL is then able to solve the equations numerically to produce oxygen concentration profiles in the Krogh cylinder (Fig. 4.2). The dimensionless parameters used to define mass transport characteristics in Section 3.3.1 take the same values here.

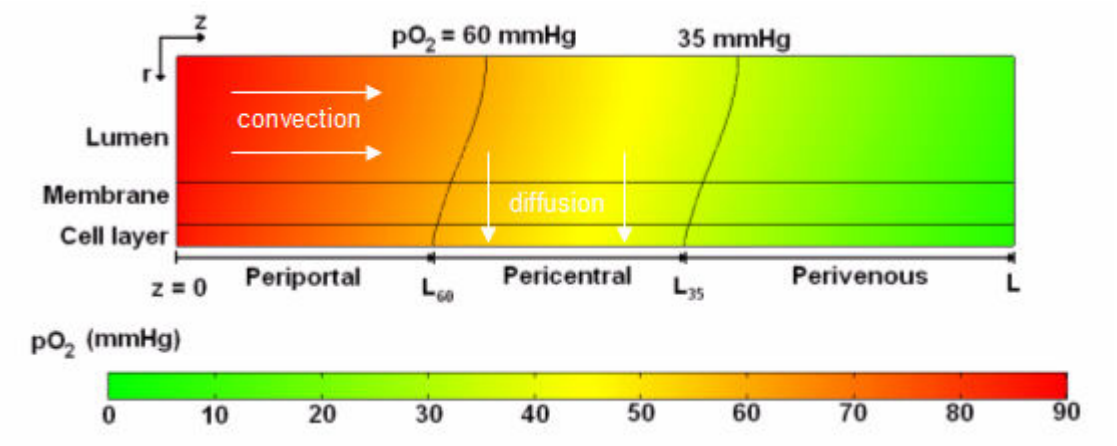

Figure 4.2: An example of a model solution found using COMSOL. The colour map defines the local oxygen tension and arrows indicate the direction of convective and diffusive flux. The definitions of the three metabolic zones have been added to the illustration.

A further enhancement to the modelling procedure outlined to the previous chapter was made. In order to efficiently produce large sets of data where the geometry and operating parameters of the BAL are varied, the COMSOL model file is converted to a MATLAB function. This is achievable as COMSOL has built-in MATLAB integration. The inputs of the function are the inlet partial pressure of oxygen $pO_2(in)$, the maximum oxygen uptake rate V_{max}, the number of cell layers per fibre C_L and the thickness of the fibre membrane w. The MATLAB function solves the model over a range of fibre lumen radii and average flow velocities using built-in COMSOL algorithms. The outputs of the function are the axial positions of the metabolic zone boundaries L_x as can be seen in Figure 4.2, where the subscript x denotes the relevant oxygen tension. The data produced is arranged so that zone boundary axial positions are given as a function of average flow velocity $\bar{u}$, for each different value for lumen radius R_l. As in Chapter 3, the empirical relationships found allow the boundary position of each metabolic zone to be expressed as a function of fibre lumen radius R_l, when all other parameters are held constant.

Again, as in the previous chapter this allows an operating constraint to be defined for the BAL; oxygen levels should not fall below 2 mmHg as this would lead to cell necrosis (De Groot et al., 1988). This constraint results in a definition of the maximum allowable number of hollow fibres in the BAL N_{max} as a function of fibre geometry and a given device plasma flow rate Q (Eq. 4.1).

$$N_{\max} = \frac{(M_2 R_1 + C_2)Q}{\pi R_1^2 . L} \tag{4.1}$$

In Equation 4.1, M_2 and C_2 are empirical constants obtained from the modelling results, relating position of the hypoxic zone to fibre lumen radius. These parameter names replace B_1 and B_2 of Chapter 3 to allow consistency with the zonation equations below. The subscript denotes the partial pressure of oxygen being referred to, in this case 2 mmHg to represent anoxic conditions. In addition to the oxygen-related constraint, a minimum number of hepatocytes are required to achieve the desired device functionality. Hepatocytes depend on anchorage to a substrate for maintenance of their function and phenotype (Morelli et al., 2007, Lee et al., 2008). This gives rise to a requirement for minimum fibre surface area in the device and hence minimum fibre number N_{min}. This constraint can be represented by Equation 4.2.

$$N_{\min} = \frac{N_{cell}}{2\pi\rho_{cell} C_L (R_1 + wL)} \tag{4.2}$$

Equation 4.2 differs from the definition of N_{min} in Equation 3.21 with the addition of the cell layer number parameter C_L. This reflects the possibility that more than one layer of cells can be adherent to each hollow fibre. As in Chapter 3, the number of hollow fibres required to produce a viable design is defined by the range between N_{min} and N_{max}.

4.2.1 Zonation equations

As oxygen is a primary modulator of liver zonation, the position of the periportal (proximal to branches of the hepatic artery and portal vein), pericentral (central portion of the liver lobule) and perivenous (proximal the central vein) zones can be defined by the local oxygen tensions. *In vivo*, blood enters the liver lobule with an oxygen tension of 60-65 mmHg which falls to 30-35 mmHg in the perivenous zone (Jungermann and Kietzmann, 2000). This is difficult to replicate, especially when using fractionated blood plasma which does not contain haemoglobin and hence has a reduced oxygen-carrying capacity. As a result of this, oxygen levels tend to be higher at the inlet and lower at the outlet of the bioreactor than in the liver lobule. This wider oxygen range still tends to produce in vitro zonation similar to the native liver lobule (Allen et al., 2005, Allen and

Bhatia, 2003). The periportal zone has been defined to exist where oxygen tensions are above 60 mmHg, the pericentral zone occupies the range from 35 to 60 mmHg and the perivenous zone experiences oxygen tensions below 35 mmHg (Chen and Palmer, 2009, Sullivan and Palmer, 2006, Sullivan et al., 2007). The same definitions will be applied here and can be seen in Figure 4.2.

In Chapter 3, the position along the hollow fibre that marked the onset of anoxia was related to plasma flow rate by a proportionality coefficient *k*. The position of the boundaries of each metabolic zone can be found in the same way. For a viable design that satisfies the constraints of Equations 4.1 and 4.2, the approximate fractional size of each metabolic zone is given below in Equations 4.3 to 4.7. The fractional size of each zone is assumed to be equal to the proportion of the axial distance between its boundaries to the total fibre length (Fig. 4.2).

Periportal zone size

$$f_{PP} = \frac{L_{60}}{L} = \frac{k_{60}\bar{u}}{L} = \frac{k_{60}.Q}{N\pi R_l^2 L} = \frac{(M_{60}R_l + C_{60})Q}{N\pi R_l^2 L} \tag{4.3}$$

In Equation 4.3, f_{pp} is the fractional size of the periportal zone, L_{60} is the axial distance along the fibre to the boundary of the periportal zone (60 corresponding to 60 mmHg oxygen tension) and L is the length of the fibre. The zone boundaries in the model will be curved, and hence the calculation here that uses the proportion of L_{60} to L will be an approximation. The axial distance to the zone boundary is proportional to the flow velocity $\bar{u}$. The proportionality coefficient k_{60} can be represented as a linear function of fibre lumen radius R_l with a slope of M_{60} and an intercept of C_{60}. This relationship was established in Chapter 3 in finding the position of the anoxic zone in the fibre (Fig. 3.5). The number of fibres in the bundle is given by N, which can vary between the maximum and minimum constraints (Eqs. 4.1 and 4.2). The principle used here to define the periportal zone size in Equation 4.3 is also applied to define the pericentral and perivenous fractional zone sizes in Equations 4.4 - 4.8.

Pericentral zone

If the exit oxygen partial pressure is less than 35 mmHg, the perivenous zone will exist in the BAL. In this case the pericentral zone size is given by Equation 4.4:

$$f_{PC} = \frac{L_{35} - L_{60}}{L} = \frac{((M_{35} - M_{60})R_l + (C_{35} - C_{60}))Q}{N\pi R_l^2 L} \tag{4.4}$$

If this is not the case then Equation 4.5 is used:

$$f_{PC} = 1 - \frac{L_{60}}{L} \tag{4.5}$$

Perivenous zone

If the exit pO_2 is less than 35 mmHg and the perivenous zone exists, its size is given by Equation 4.6:

$$f_{PV} = \frac{L - L_{35}}{L} = 1 - \frac{(M_{35}R_l + C_{35})Q}{N\pi R_l^2 L} \tag{4.6}$$

Conversely if the exit oxygen partial pressure is above 35 mmHg, the perivenous zone size is absent (Eq. 4.7):

$$f_{PV} = 0 \tag{4.7}$$

From the definition of the zone sizes in Equations 4.3 – 4.7, it is possible to find the device flow rate Q or fibre number N that results in the periportal and perivenous zones occupying the same volume. These parameters are named Q_{eq} and N_{eq} respectively as they represent a configuration where periportal and pericentral hepatic functions have equal prevalence. Whether this is actually an optimal situation for the BAL is a point discussed later. By rearranging Equations 4.3 and 4.6 such that the periportal and perivenous fractional zone sizes are equal, the equation can be solved for Q_{eq} and N_{eq} (Eqs. 4.8 and 4.9):

$$Q_{eq} = \frac{N\pi R_l^2 L}{(M_{35} + M_{60})R_l + C_{35} + C_{60}} \tag{4.8}$$

$$N_{eq} = \frac{Q((M_{35} + M_{60})R_l + C_{35} + C_{60})}{\pi R_l^2 L} \tag{4.9}$$

If Q_{eq} is below 300 ml/min i.e. the technical upper limit of plasma flow rate in BAL applications (Pless and Sauer, 2005), or N_{eq} is within the confines of the Operating region

then a BAL can designed where the periportal and pericentral metabolic zones occupy an equal amount of the cell volume.

4.2.2 Parameter values

As in Chapter 3, modelling parameter values were chosen so as to represent typical hollow fibre BAL systems. The ranges of fibre lumen radius R_l and length L are representative of common hollow fibre geometries. The range of plasma flow rate Q was determined by two factors; the maximum flow rate due to technical reasons (300 ml/min) and the minimum flow rate (200 ml/min) that can produce adequately sized Operating Regions as observed in the previous chapter. A range of cell numbers N_{cell} was chosen around an intermediate value of 10 billion cells, this number is generally considered the minimum required for a functional BAL (Sullivan et al., 2007, Allen et al., 2001). The inlet partial pressure of oxygen $pO_2(in)$ was varied between 70 and 110 mmHg. The lower end of the scale is similar to physiological arterial oxygen tension while the upper end approximately represents maximum oxygen solubility in plasma at 37° C. The value for maximal oxygen uptake rate V_{max} was equal to a value reported for hepatocytes in a similar system (Nyberg et al., 1994). This value falls within the range of oxygen consumption rates (OCR) reported for 3D hepatocyte cultures and summarized by Patzer (2004). The range for V_{max} reported by Patzer was replicated in this study. The oxygen consumption rates in units of mol/cell/s were converted by assuming that each cell had the same volume as a sphere of 25 μm diameter. At the lower end of the scale V_{max} was equal to 2.93 μM/s and at the upper limit was equal to 11.25 μM/s. As hepatocytes form a layer one or two cells thick around each sinusoid (Telford and Bridgman, 1995), the effect of having a double cell layer ($C_L = 2$) around each hollow fibre was studied.

Table 4.1: Parameter values considered in the model, with references for the ranges

Parameter	Studied range	Standard Value	References
Fibre lumen radius R_l	100 – 300 μm	200 μm	(Hay et al., 2000, Sullivan et al., 2007, Hay et al., 2001)
Fibre length L	15 – 35 cm	25 cm	(Moussy, 2003, Hay et al., 2000)
Plasma flow rate Q	200 – 300 ml/min	250 ml/min	(Pless and Sauer, 2005)
Inlet partial pressure of oxygen $pO_2(in)$	70 – 110 mmHg	90 mmHg	(Sullivan et al., 2007)
Maximal oxygen uptake rate V_{max}	2.93 – 11.25 μM/s	5.87 μM/s	(Sullivan et al., 2007, Patzer, 2004)
BAL cell population N_{cell}	7.5 – 12.5 billion	10 billion	(Allen et al., 2001)
Cell layer number C_L	1-2	1	(Saxena et al., 2003)

4.3 Results

To illustrate how zonation profiles can be incorporated into the concept of Operating Regions, the standard design parameters of Table 4.1 were used to construct an Operating Region chart (Fig. 4.3). In Figure 4.3A, the maximum fibre number N_{max} limit defines how many fibres can be contained within the BAL while maintaining adequate hepatocyte oxygenation. The minimum fibre number N_{min} limit defines the minimum number of fibres required to provide the BAL with an adequate cell population. Figure 4.3B illustrates how the zones are distributed in a BAL being operated under the same conditions for a fibre lumen radius of 200μm. The chart shows the fractional zone sizes at the limits of fibre number (N_{min} and N_{max}) and hence the possible extremes of zonal distribution while staying within the Operating Region. The effects of varying the operating and design parameters on the zone distributions are explored in the Section 4.3.1. In addition, values of plasma flow rate Q_{eq} that minimize the difference in size of the periportal and perivenous zones

(Eq. 4.8) are plotted where possible. The value of fibre number that gives an equal distribution of the periportal and perivenous zones, N_{eq} is also shown (Eq. 4.9). This is done by adding an extra line to the Operating Region charts in each case.

Reynolds and Peclet numbers can be calculated to describe the characteristics of mass transport in the model. Reynolds number, when calculated as described in Section 3.3.1, ranges approximately between 0.2 and 6. This is confirmation that plasma flow in the fibre is laminar. Peclet number again varies between approximately 10^{-2} and 2, showing that axial diffusion of oxygen in the lumen can become significant. A parameter relating oxygen consumption to diffusion in the cell layer, defined as $\frac{R_l^2 \alpha V_m}{D_{hep} pO_2(in)}$, varies approximately between 0.1 and 1, showing that neither diffusion or reaction mechanisms are particularly dominant.

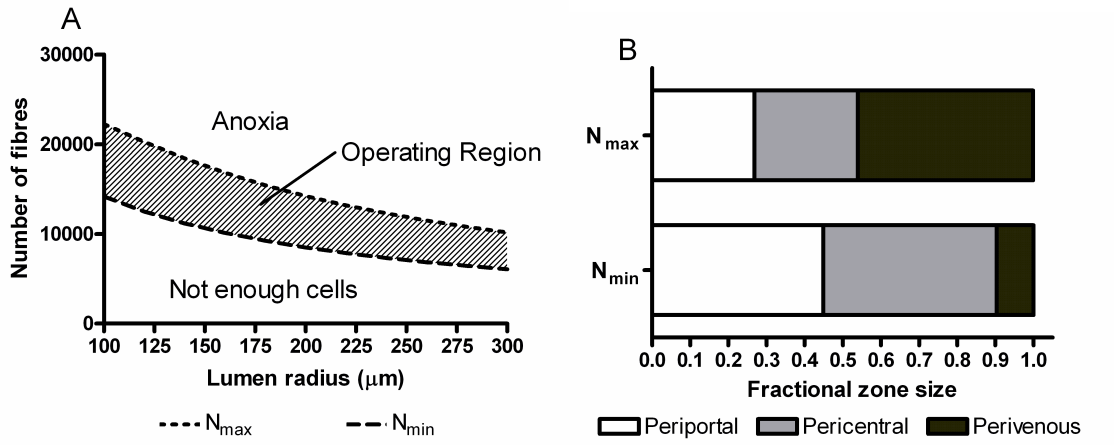

Figure 4.3: (A) Operating region chart produced using the parameters of Table 4.1 (B) The distribution of the metabolic zones at both extremes of the Operating Region, for a fibre radius of 200 μm.

4.3.1 Zonation profiles for varying fibre geometry

The significance of the hollow fibre lumen radius to the zone distribution in the BAL can be observed in Figure 4.4. The influence appears to be minimal with the distribution changing little over the range of fibre radii considered (Fig. 4.4A). When operating with the plasma flow rate Q_{eq} (Fig. 4.4B), the periportal and perivenous zones each occupy 34.1,

33.2 and 32.9% of the cell volume for lumen radii of 100, 200 and 300 μm respectively. The Operating Region for various lumen radii can be redrawn using the standard parameters of Table 4.1 with an added line to represent the fibre number that gives rise to an equal distribution of the periportal and perivenous zones (Fig 4.4C). The N_{eq} line passes approximately through the centre of the Operating Region.

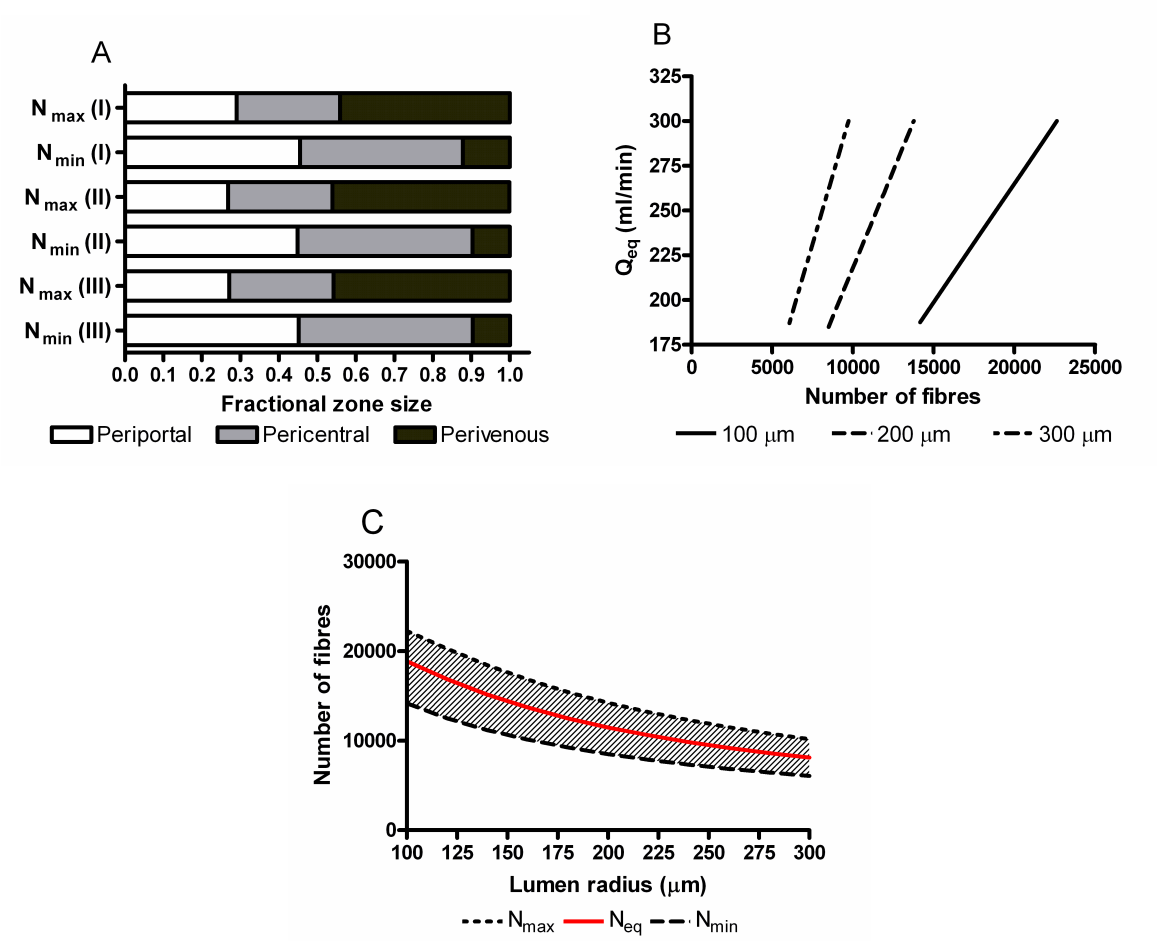

Figure 4.4: Charts describing the influence of varying lumen radius on zonation profiles. (A) Distribution of metabolic zones in the case of (I) R_l = 100 μm, (II) R_l = 200 μm and (III) R_l = 300 μm (B) The flow rate required to produced balanced periportal and perivenous zones Q_{eq} is shown as a function of fibre number (C) The Operating Region with an additional N_{eq} line to represent the design configuration where the periportal and perivenous zones occupy equal portions of the cell mass.

Fibre length does not have any influence upon zone distribution and hence the zone distribution chart is not shown. While this may seem counterintuitive, changes to fibre length are offset by the corresponding changes in N_{min} and N_{max} such that the effect is cancelled out. However, fibre length does have an influence on the plasma flow rate needed to balance the metabolic zone distribution (Fig. 4.5A). In each case of fibre length, a minimum flow rate of 132 ml/min will cause the periportal and perivenous zones to each

occupy 33.2% of the cell volume. An Operating Region can also be constructed to show how N_{eq} varies as a function of fibre length. The value of N_{eq} is approximately half way between the fibre number constraints N_{min} and N_{max}.

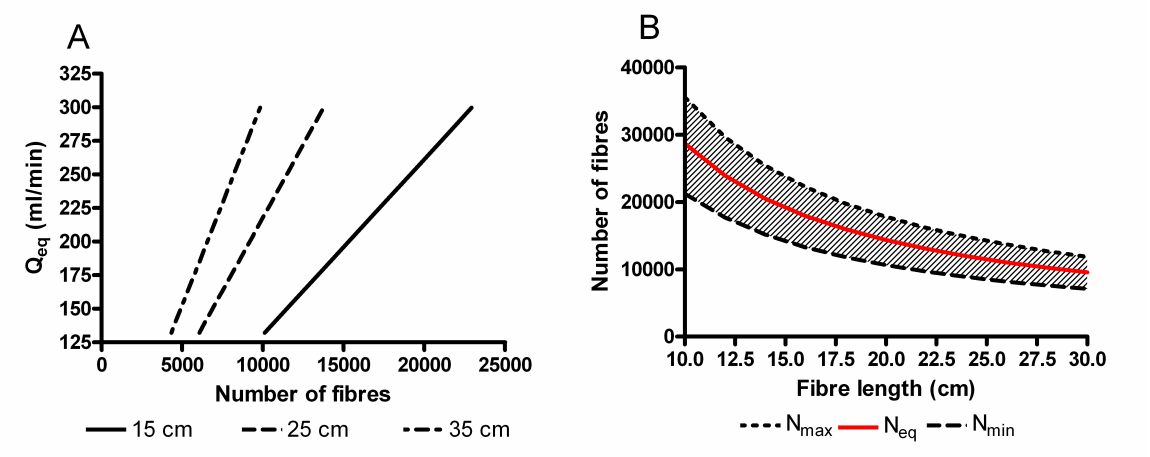

Figure 4.5: Charts describing the influence of varying fibre length on zonation profiles. (A) The Q_{eq} plot for 3 values of fibre length L: 15, 25 and 35 cm. As the fibre length does not affect the distribution of zones at the N_{min} and N_{max} design limits that chart is not shown. (B) The Operating Region, redrawn to show the fibre number constraints and N_{eq} line as a function of fibre length using a fibre lumen radius of 200 µm

4.3.2 Zonation profiles for varying plasma flow rates

Figure 4.6A shows how varying plasma flow rates in the BAL affect the relative size of each metabolic zone. The zone distribution is unaffected if the BAL is operated on the upper limit constraint i.e. the number of fibres N is equal to N_{max} and oxygen levels are just barely sufficient. In this case the periportal, pericentral and perivenous zones occupy 26.8, 27.1 and 46.0% of the cell volume respectively. At the other extreme where $N = N_{min}$, increasing flow rate tends to increase the relative sizes of the periportal and pericentral zones. The periportal zone occupies a maximum of 53.8% of the BAL for the highest flow rate while the perivenous zone disappears entirely in this case. Operating Regions were drawn for the cases where the plasma flow is 200 or 300 ml/min (Fig. 4.6B and 4.6C). The relative position of the N_{eq} line within the Operating Region changes in each case, initially lying close to the N_{min} constraint for Q = 200 ml/min and then moving towards the N_{max} constraint at the higher flow rate.

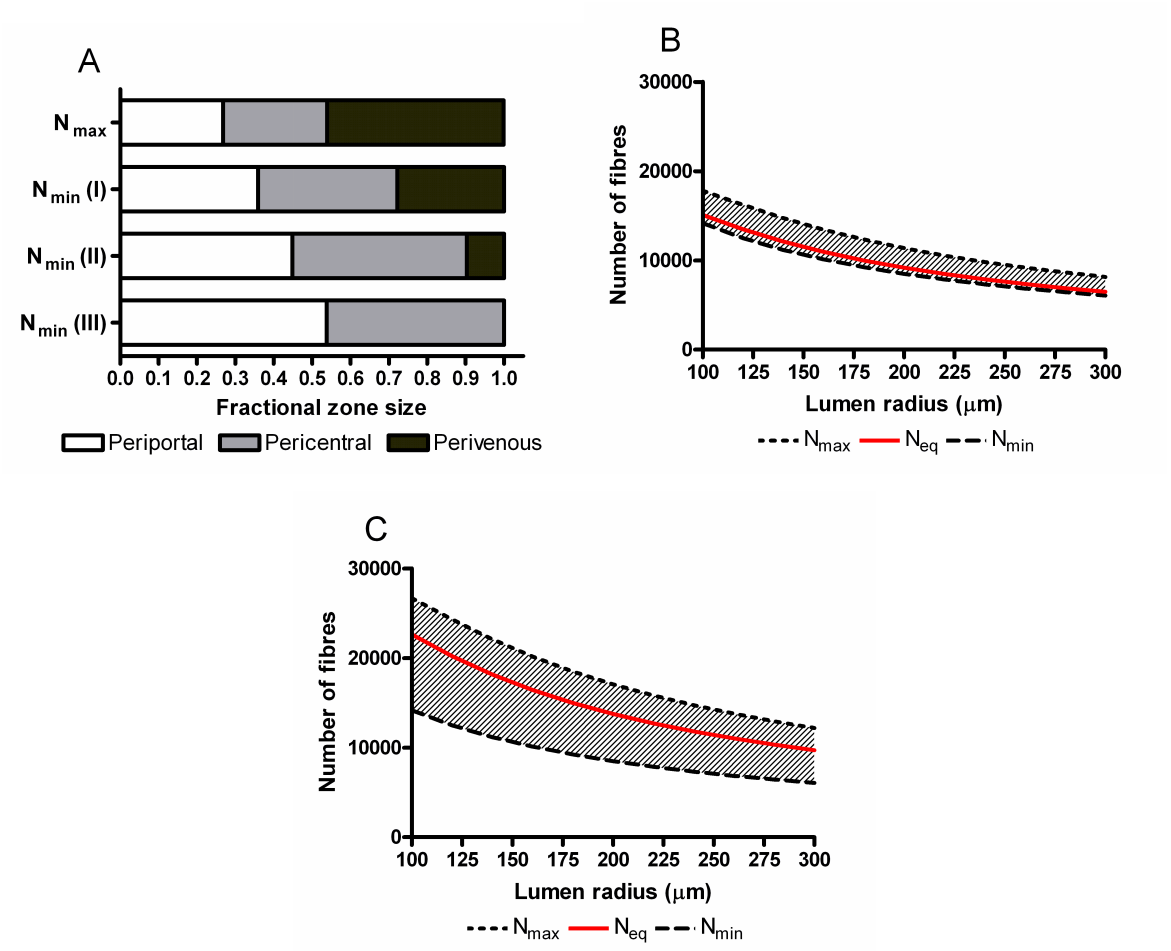

Figure 4.6: Visualization of the influence of plasma flow rate on zonation profiles. (A) Distribution of metabolic zones in the case of (I) Q = 200 ml/min, (II) Q = 250 ml/min and (III) Q = 300 ml/min. The zone distribution is unaffected by Q when operating on the N_{max} limit and hence the bar is drawn only once. (B) The Operating Regions when Q = 200 ml/min and (C) 300 ml/min is drawn with the N_{eq} line added.

4.3.3 Zonation profiles for varying inlet oxygen tension

The distribution of each metabolic zone under differing inlet oxygen tensions can be seen in Figure 4.7A. At a lower level of 70 mmHg the perivenous zone is largest, occupying between 44.8 - 58.3% of the cell volume depending on the number of fibres. When a higher oxygen tension of 110 mmHg is employed, the perivenous zone shrinks in size and when the fibre number is minimum it disappears entirely. The periportal zone dominates in this situation, occupying 80.0% of the cell volume. When using an inlet oxygen partial pressure of 70 mmHg the flow rate required to produce equal periportal and perivenous zones is above 300 ml/min within the fibre number constraints and therefore it is impossible to achieve an equal zone distribution in the BAL for this partial pressure. For a

given number of fibres in the BAL, a higher partial pressure of oxygen allows equal zones to be achieved (33.2% each for 90 mmHg, 38.9% each for 110 mmHg) with a lower device flow rate (Fig. 4.7B). A minimum flow rate of 122 ml/min can create an equal zone distribution in the case of $pO_2(in)$ = 110 mmHg. Figures 4.7C and 4.7D show how the inlet oxygen tension affects the position of the equal zones fibre number N_{eq} within the Operating Region charts. With inlet oxygen tension set to 70 mmHg, the N_{eq} line lies below the Operating Region whereas for 110 mmHg oxygen tension it is above the Operating Region. In each of these cases it is hence impossible to obtain equal periportal and perivenous zones while satisfying the operating constraints of the BAL.

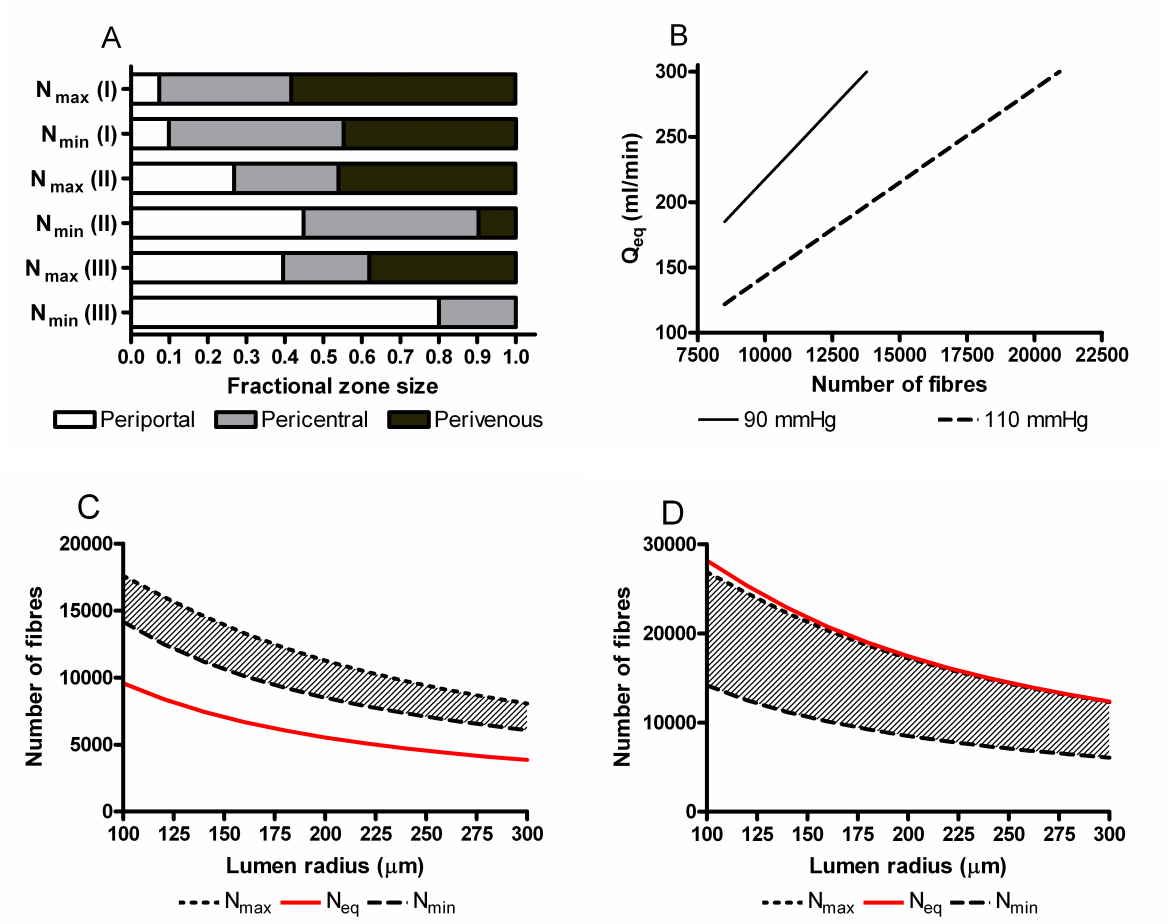

Figure 4.7: The effects of varying inlet oxygen partial pressure on zonation. (A) Distribution of metabolic zones in the case of (I) $pO_2(in)$ = 70 mmHg, (II) $pO_2(in)$ = 90 mmHg and (III) $pO_2(in)$ = 110 mmHg. (B) In the Q_{eq} plot, a $pO_2(in)$ value of 70 mmHg required a Q value greater than 300 ml/min to produce equal periportal and pericentral zones and hence this was not included in the chart. (C and D) The Operating Regions constructed for values of $pO_2(in)$ = 70 mmHg and 110 mmHg respectively, with an added line to represent N_{eq}.

4.3.4 Zonation profiles for varying cell number

As was the case for flow rate, the cell number N_{cell} does not affect the distribution of zone sizes when the BAL is operated on the N_{max} constraint (Fig. 4.8A). However, when the BAL is operated with the minimum allowable number of fibres, the perivenous zone increases from 0 to 27.8% of the cell volume when the highest cell number is inoculated. To produce a zone distribution where the periportal and perivenous zones both occupy 33.2% of the cell volume each, the BAL should be operated with a plasma flow rate Q_{eq}, given in the chart as a function of fibre number (Fig. 4.8B). The contour is unaffected by the cell population size, though the lower limit of fibre number N_{min} will change. In Figures 4.8C and 4.8D the positions of the N_{max} and N_{eq} lines are unchanged in the Operating Regions for either of the cell numbers N_{cell} considered, 7.5 and 12.5 billion respectively.

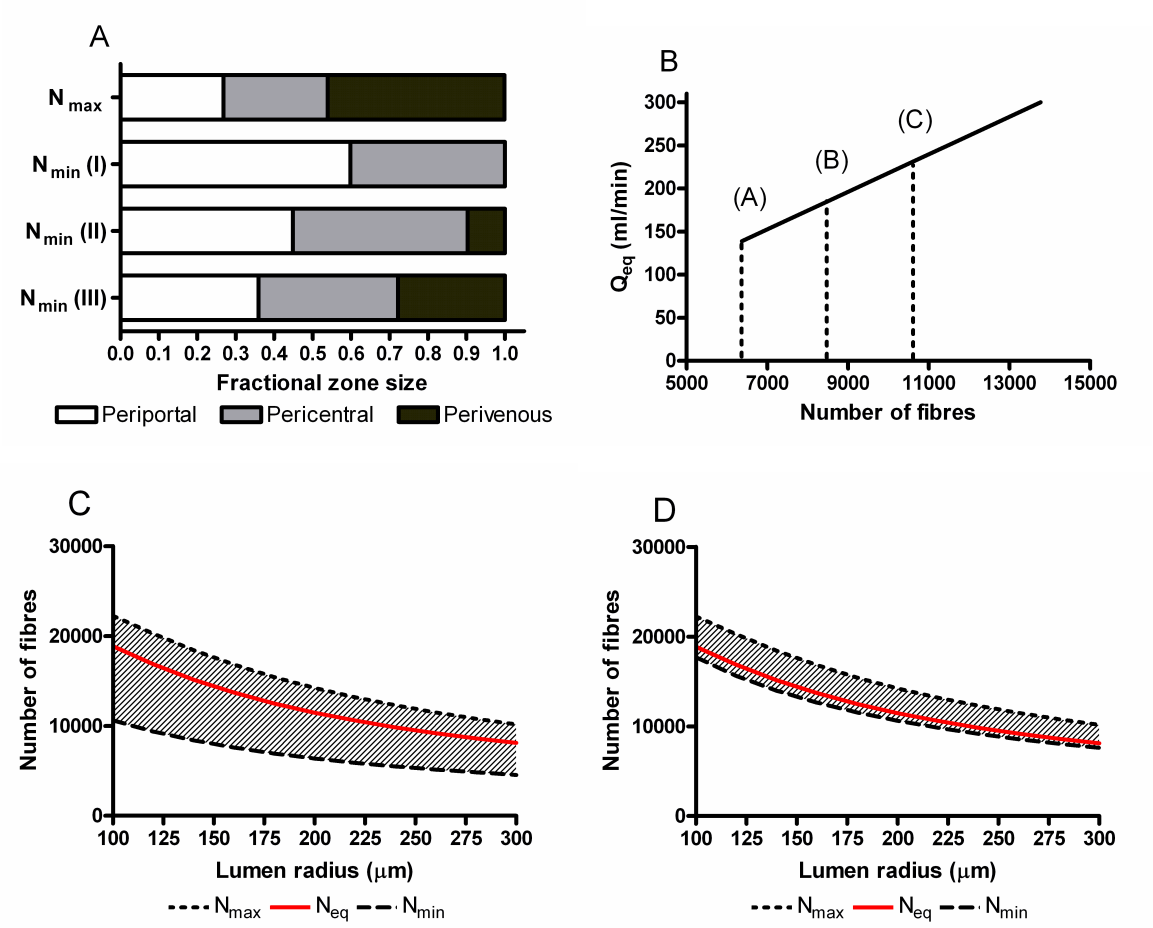

Figure 4.8: Charts describing the influence of cell number on zonation. (A) Distribution of metabolic zones in the case of (I) N_{cell} = 7.5 billion, (II) N_{cell} = 10 billion and (III) N_{cell} = 12.5 billion cells. (B) Q_{eq} is plotted up to a limit of 300 ml/min for each of these N_{cell} values and the lines produced are co-incident. The vertical dash lines indicate the position of N_{min} for each of the three cases. (C and D) Operating Regions are plotted for cell populations of 7.5 and 12.5 billion cells respectively with an additional line describing N_{eq}.

4.3.5 Zonation profiles for varying maximum oxygen uptake rate

Various values of maximum oxygen uptake rate V_{max} have been reported for hepatocytes so the significance of this parameter was examined in Figure 4.9. A valid Operating Region could not be produced for a V_{max} value of 11.25 μM/s for the standard plasma flow rate value in Table 2.1 (250 ml/min), so a Q value of 300 ml/min was considered instead. When using the lowest V_{max} value of 2.93 μM/s, the entire BAL consists of periportal hepatocytes when operating on the N_{min} limit. When V_{max} is equal to 11.25 μM/s the perivenous zone is the largest in the BAL, occupying 47.9 – 49.9% of the cell volume depending on the fibre number (Fig. 4.9A). For this reason it was impossible to produce an

equal zone distribution for the upper limit V_{max} value with a Q_{eq} value of less than 300 ml/min. A lower V_{max} value allows equal zone distribution to be achieved with a lower plasma flow rate. In the case of V_{max} equal to 2.93 μM/s, a minimum flow of 87 ml/min could produce periportal and pericentral zones each occupying 34.2% of the cell volume. Operating Region charts were constructed for each of the extreme V_{max} values, though it was necessary to use a flow rate of 300 ml/min in order to produce a valid Operating Region for the higher oxygen uptake rate. For the smaller maximal uptake rate of 2.93 μM/s (Fig. 4.9C) there is a large Operating Region where the N_{eq} line lies in the upper part of the region. In contrast, for a higher uptake rate of 11.25 μM/s the Operating Region is vanishingly small (Fig. 4.9D) and it is impossible to achieve and equal distribution of zones within it.

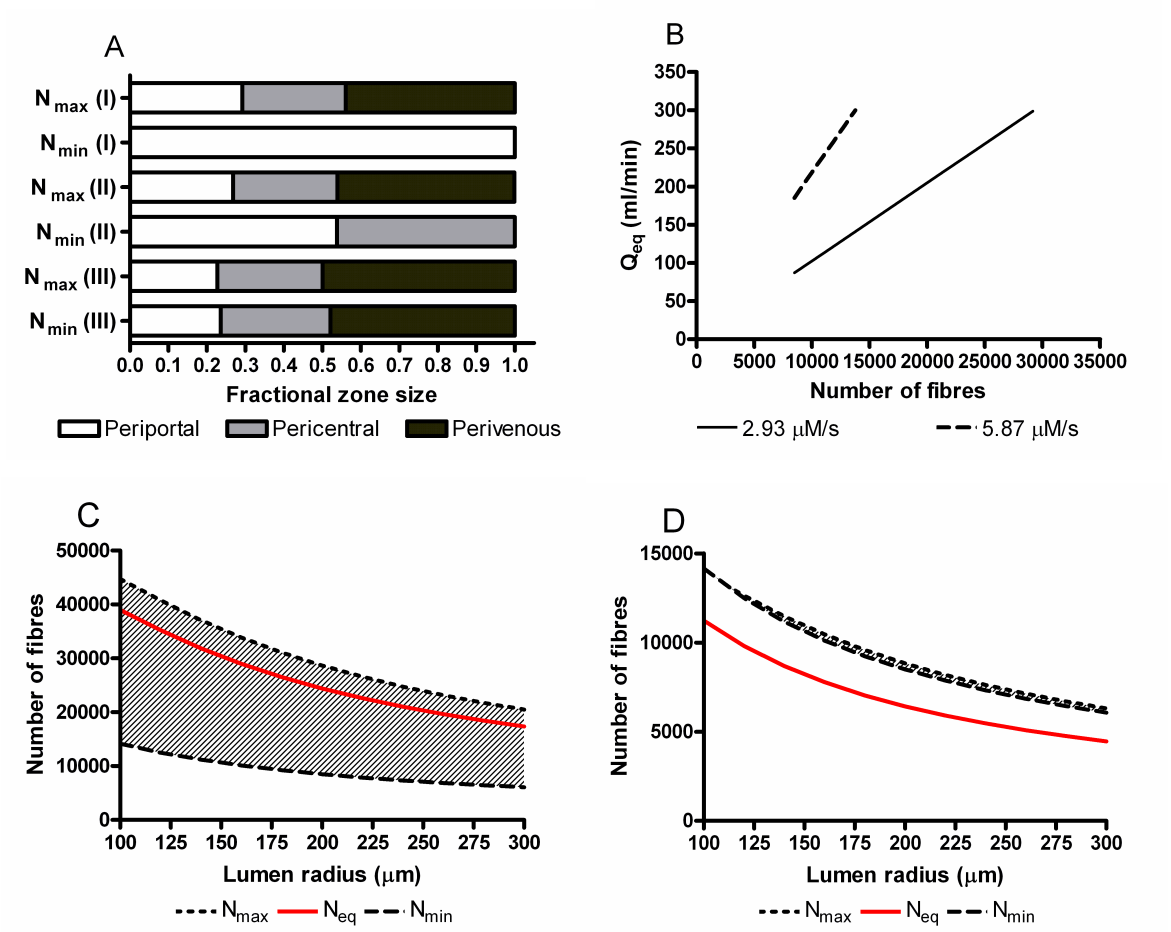

Figure 4.9: Visualization of the impact of varying oxygen uptake rates on zonation. (A) Distribution of metabolic zones in the case of (I) V_{max} = 2.93 μM/s, (II) V_{max} = 5.87 μM/s and (III) V_{max} = 11.25 μM/s. (B) For a V_{max} value of 11.25 μM/s, it was not possible to create an equal zone distribution for a Q value of less than 300 ml/min and hence that line is not included on the Q_{eq} chart. (C and D) The Operating Regions are plotted for V_{max} values of 2.93 and 11.25 μM/s respectively. It was necessary to use a plasma flow rate of 300 ml/min in each of these charts in order to produce a valid Operating Region for the higher oxygen uptake rate.

4.3.6 Influence of single or double cell layer on zonation profile

Hepatocytes can be cultured as either a single or double layer on each hollow fibre, and the effect on the zone distribution can be seen in Figure 4.10A. The addition of an extra cell layer per fibre causes a gradual reduction in the size of the periportal and pericentral zones, accompanied by a corresponding increase in the perivenous zone size. The periportal zone fractional size at the N_{max} limit reduces from 26.8% for a cell monolayer to 22.1% for a double layer, or from 44.9% to 33.1% at the N_{min} limit. Conversely, the perivenous zone size increases from 46.0% to 51.2% of the cell volume at the N_{max} limit or from 9.7% to

23.1% at the N_{min} limit. For a monolayer system, operating at Q_{eq} (Fig. 4.10B) will produce periportal and perivenous zones of 33.2% fractional volume whereas they will each occupy 30.1% in the double layer system.

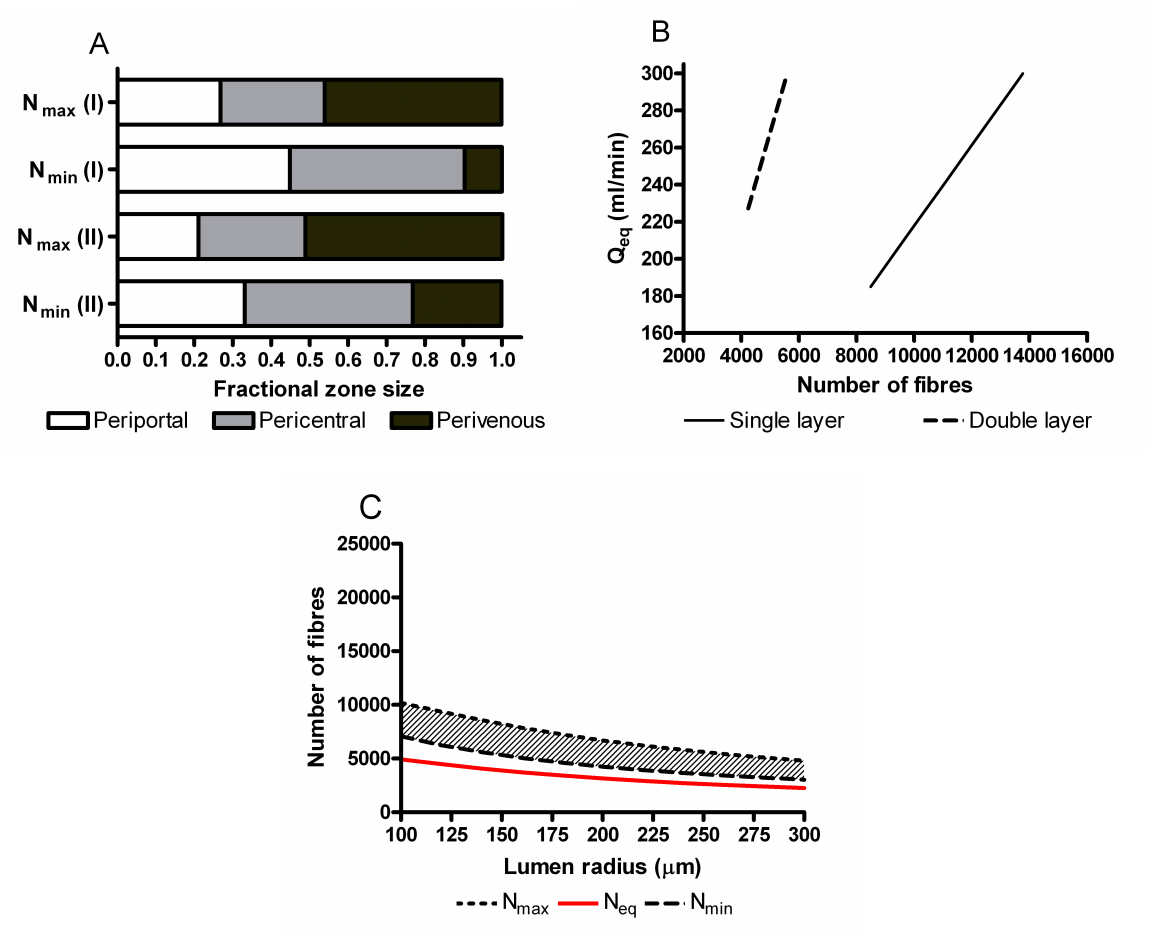

Figure 4.10: Impact of single or double layers of cells on zonation profiles. (A) Distribution of metabolic zones in the case of (I) a single cell layer and (II) a double cell layer model. (B) The Q_{eq} plot for each case is also shown. (C) An Operating Region for the case of a double cell layer is shown. The N_{eq} line lies outside of the region indicating it is impossible to obtain equal periportal and perivenous zones

4.4 Discussion

As in Chapter 3, a mathematical model of oxygen transport within a bioartificial liver was set up and solved using finite element software. The procedure was enhanced through the use of axial scaling of the modelling equations and the use of MATLAB script. Once again, the results of the simulations were used to define Operating Regions within which the BAL could adequately oxygenate a defined cell population. It was explained how

oxygen tensions within the bioreactor delineate three metabolic zones as seen in the liver *in vivo*. This chapter describes how altering the design parameters of the BAL affect the distribution of these zones while remaining in the Operating Region.

The effects of hollow fibre radius and length were illustrated in Figures 4.4 and 4.5. It can be seen that lumen radius has very little effect on zonal distribution while fibre length has no influence. These parameters are important, however, in forming the Operating Regions and hence determining the values of N_{min} and N_{max}. In Chapter 3 it was concluded that it was preferable to use numerous, shorter and thinner hollow fibres as opposed to fewer larger and longer fibres as this tended to produce wider Operating Regions and hence offer greater design flexibility and margin for error in the model. Over the ranges considered, it appears that fibre length or radius do not affect the ability to equally distribute the periportal and perivenous zones. Values of Q_{eq} can be found within an acceptable range (< 300 ml/min) and the fibre number N_{eq} occupies roughly the centre of the Operating Region. As such fibre geometry is not a key factor in the distribution of the metabolic zones.

A key parameter in the design of a BAL is the flow rate of plasma from the patient to the device. As expected, increasing the flow rate of oxygen-carrying plasma into the BAL will increase the proportion of periportal hepatocytes. However, a risk arises as a result of using high flow rates; the perivenous zone can become very small or disappear entirely. Hepatocytes in the perivenous zone play roles in the liver glucostat function and xenobiotic metabolism through expression of the relevant proteins. If the BAL is over-oxygenated, these functions could be impaired or entirely absent from the system. This situation highlights the need to mimic the *in vivo* oxygen gradient as closely as practically possible. The Operating Region charts clearly show that increased flow rates results in larger regions and hence offer more design flexibility. Also it can be seen that the position of the N_{eq} line changes in each case as does its relative position with respect to the operating constraint lines. It can be concluded that plasma flow rate is an important consideration with regards to desired zone distribution.

The inlet oxygen tension to the BAL was previously chosen to be 90 mmHg as this is approximately equal to arterial oxygen levels and as seen in Chapter 3 was able to adequately oxygenate the BAL in most cases. *In vivo* however the liver has a dual blood supply from the hepatic portal vein and hepatic artery. Around two-thirds of the blood

supply is venous and hence hepatocytes actually experience oxygen tensions between 60-65 mmHg, some way below 90 mmHg (Jungermann and Kietzmann, 2000). The presence of haemoglobin as an oxygen-carrier ensures the lower inlet oxygen tension does not lead to cell necrosis due to anoxia. As haemoglobin is assumed to have been separated from the blood plasma in the model presented here, it is necessary to operate with higher-than-physiological oxygen tensions. The periportal zone is restricted to a small volume in the case of 70 mmHg inlet oxygen tension whereas it dominates the cell volume when the plasma is oxygenated to 110 mmHg. It can be concluded that 70 mmHg is too low to operate the BAL and hope to achieve equal zone distributions as flow rates above the technical limit of 300 ml/min would be required. On the other hand, maximizing the oxygen content of the plasma appears to offer more flexibility in controlling the size of the metabolic zones. A minimum flow rate of 122 ml/min is required to balance the zones in the case of inlet oxygen tension being 110 mmHg if the BAL is operated with the parameters of Table 2.1. The duty of the plasma pump in the BAL can be reduced through use of higher oxygen tensions, though whether the hepatocytes will function to the same degree at non-physiological oxygen tensions is another question. There is some evidence suggesting that hyperoxic environments can damage hepatocytes (Miyazaki et al., 1991). The Operating Region charts indicate that for the conditions considered, it is not possible to equally distribute the zones and remain within the Operating Region for each of the inlet oxygen tensions considered (70 and 110 mmHg). Under a moderate oxygen tension however, this is possible as seen for example in Figure 4.4C where the same conditions are used but the inlet oxygen tension is 90 mmHg.

The number of cells required in the BAL is subject to debate, with the patient's residual liver function being a factor. Generally it is regarded that the minimum number of hepatocytes should be 10% of the cell mass in the liver, corresponding to approximately 10 billion cells (Allen et al., 2001, Sullivan et al., 2007, Morsiani et al., 2002). A range of cell numbers around this figure was examined to see how this parameter affected the zone distribution. Operating with a smaller number of cells corresponds to a lower required fibre number N_{min} and hence the Operating Region widened. This results in a greater degree of choice in regards to zonal distribution. For the higher cell number of 12.5 billion the Operating Region is significantly constricted. As a result less control exists over the distribution of the metabolic zones though according to the chart for Q_{eq} a plasma flow rate from 230 – 300 ml/min will cause each of the metabolic zones to occupy approximately

one-third of the cell volume, depending on the fibre number. The Operating Region charts also indicate that equal zone distributions can be found within them. This would indicate that a greater number of cells could reside in the BAL while still maintaining equal zone distribution. According to our calculations (not presented), up to 16.2 billion cells could be supported in the device while maintaining equal zone distribution with a maximum plasma flow rate Q of 300 ml/min. The parameters of Table 4.1 were used to calculate this value.

In modelling oxygen uptake by hepatocytes, one parameter that is difficult to accurately identify is the maximum rate of oxygen uptake V_{max}. The parameter is very sensitive to culture conditions and a range of values have been reported in the literature, from 24 to 900 amol/cell/s (Patzer, 2004). For the upper limit value studied here (11.25 μM/s) it was found that viable Operating Regions could only be defined when the maximum flow rate of 300 ml/min was used. For a low V_{max} (2.93 μM/s) it is possible that the entire BAL can be occupied by periportal hepatocytes, an undesirable situation which would unbalance the functions of the BAL. However, a lot of control does exist over the zone distribution due to the wide Operating Region and a lower inlet flow rate or oxygen tension could compensate for the lower oxygen demand. On the other hand, if the hepatocytes have a high oxygen demand there is almost no control over the zone distribution. It would be necessary to increase the plasma oxygen content or reduce the number of cells inoculated in the BAL in order to more evenly distribute the zones. Under the standard conditions of Table 2.1 and an increased flow rate of 300 ml/min, it is impossible to achieve equal zone distribution within the Operating Region for the upper value of V_{max}. In a real system it is likely that the oxygen demand will vary transiently, beginning high and then decreasing as the cells adapt to their new environment (Patzer, 2004).

The mathematical model from the previous chapter was modified to account for cells being arranged as a double layer on each fibre as opposed to solely being monolayers. By increasing the number of cells surrounding each fibre, fewer fibres are required in the BAL which is beneficial from a manufacturing point of view. However, it can be seen in the results above that a double hepatocyte layer around each hollow fibre causes the relative size of the perivenous zone to increase over the monolayer model. The periportal zone shrinks while the pericentral zone remains relatively unchanged in size. As a result, the minimum flow rate required to achieve equal zone distribution is greater in the double

layer system, 227 ml/min opposed to 185 ml/min in the monolayer model. With a flow rate of 250 ml/min as in the standard parameters of Table 4.1, it is impossible to achieve equal zone distribution within the Operating Region when considering a double cell layer system.

It has been assumed that an equal distribution of the periportal, pericentral and perivenous zones would be optimal with respect to BAL functionality. For this reason, charts were produced that give values of plasma flow rate and fibre number that will cause the periportal and perivenous zones to occupy the same proportion of the cell volume. However, perhaps the relative importance of each of the liver functions should be established before making this conclusion. For example, ammonia clearance takes place primarily in periportal hepatocytes whereas xenobiotic metabolism is typically seen in the perivenous zone. If ammonia clearance could be achieved through artificial means such as adsorption or filtration in series with the BAL as seen in several hybrid devices such as the HepaMate or TECA-HALSS (Xue et al., 2001, Gerlach et al., 1994, Rozga et al., 1992), then perhaps it would be beneficial to increase the proportion of perivenous hepatocytes that detoxify drug molecules. Further experimental and anecdotal evidence is required to establish this hypothesis.

4.5 Conclusions

Oxygen is a primary regulator of liver cell heterogeneity and hence is key in the coordination of various liver functions. In order to design a BAL that can function in a similar manner to the *in vivo* organ, physiological gradients of oxygen tension should be replicated as closely as possible within the extracorporeal device. Using a mathematical model and operating parameters that satisfy both oxygenation and cell number constraints, it was possible to see how each parameter was significant in controlling the distribution of the metabolic zones. As expected, increasing oxygenation of the BAL through higher flow rates and inlet oxygen tensions allows a greater range of zone sizes. However, it is possible to over-oxygenate the hepatocytes in a way that the perivenous zone is either small or absent entirely, potentially impairing the functionality of the BAL. Conversely, when using higher cell loadings or cells with higher oxygen demands the periportal zone can be reduced in size. This study shows how it is possible to control the distribution of the liver

metabolic zones, while remaining within the operating limits of the BAL design. By making these considerations, the efficacy of BAL designs should improve and take a further step towards clinical use.

Chapter 5: Modelling and Optimization of Commerical Bioartificial Liver Systems

5.1 Introduction

In the previous chapters, a mathematical modelling approach to studying oxygen mass transport and its ramifications in BALs has been developed. The results allowed comparisons to be made between various BAL designs in terms of their likely viability or effectiveness in terms of replicating the three metabolic zones present in the liver. In this chapter, the concepts outlined previously are expanded and applied specifically to existing commercial BAL designs: the HepaMate, Bioartificial Liver Support System (BLSS) and Extracorporeal Liver Assist Device (ELAD). These devices represent the BALs that have undergone the most extensive clinical trials and are closest to clinical application.

5.1.1 Bioartificial liver background

HepaMate

Currently owned by HepaLife Biosystems, Inc., the HepaMate (Fig. 5.1) was previously known as the HepatAssist. This BAL was first developed by a group at the Cedars-Sinai Medical Centre in Los Angeles, California (Rozga et al., 1992) and was involved in the largest single clinical trial of all BALs to date. This model housed approximately 5 billion cryopreserved porcine hepatocytes co-cultured with cellulose microcarriers. Its safety was demonstrated in a Phase I multicentre trial where 32 of 39 acute liver failure patients were bridged to transplantation, with 6 recovering spontaneously (Mullon and Pitkin, 1999). A Phase II/III clinical trial was then initiated where 171 patients with acute liver failure or nonfunction after transplant were enrolled, with 86 receiving treatment from a BAL and the rest forming a control group (Demetriou et al., 2003). It was found that the BAL group had an increased survival rate, but only in a patient subgroup and the treatment has not yet obtained FDA approval (Pryor and Vacanti, 2008). Currently there is no information to suggest clinical trials are ongoing.

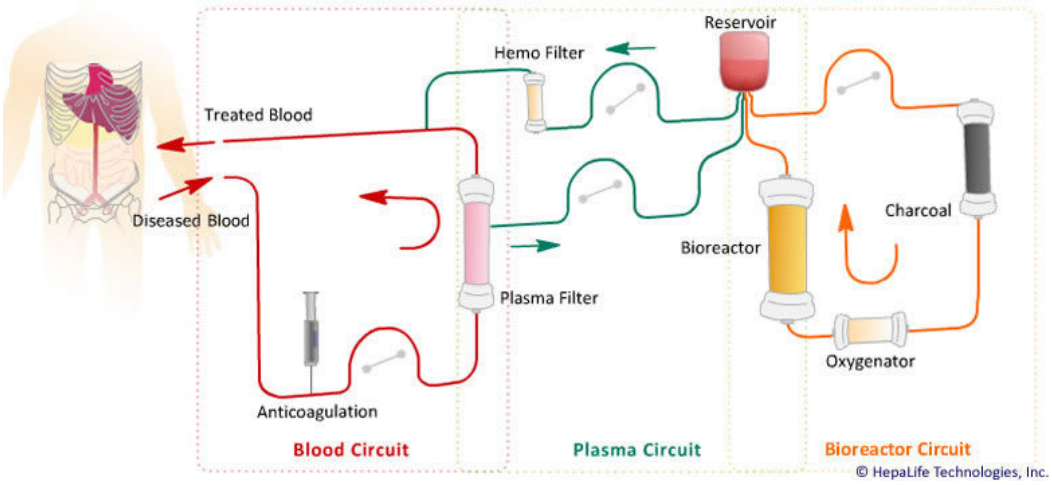

Figure 5.1: A schematic of the HepaMate BAL, from HepaLife™ website (2011)

Extracorporeal Liver Assist Device (ELAD)

Originally developed by a group at the Baylor College of Medicine in Houston, Texas, (Sussman et al., 1991) the ELAD is now being developed and marketed by Vital Therapies, Inc. of San Diego, California. The design of the bioreactor has changed significantly (Fig. 2.7), originally consisting of a single hollow fibre cartridge perfused by whole blood to now perfusing separated plasma through four parallel hollow fibre bioreactors (Brotherton et al., 2007). A contentious issue surrounding the ELAD is the use of an immortalized human cell line, C3A cells. The use of tumour-derived cells raises some questions of safety (Rozga et al., 1992). There is also a suggestion that C3A cells do not perform certain liver functions as well as primary hepatocytes (Nyberg et al., 1994). The design does incorporate a cell filter after the bioreactor stage in order to prevent foreign cells reaching the patient and to date there have been no reported issues related to the cell type in patients treated with the ELAD. The ELAD has completed 6 clinical trials to date, including a randomized controlled study at King's College Hospital, London (Ellis et al., 1996). An abnormally high survival rate in the control patient group (75% when 50% was expected) confounded any observable benefit of ELAD treatment in terms of survival rates. More recently a Phase II multicentre trial in China consisting of 17 patients was carried out where 90 day survival rates appeared to improve over controls (39% versus 25%) and the device was well tolerated (Hillebrand et al., 2010). According to the company's website, clinical trials are ongoing in several countries and producing positive results.

Bioartificial Liver Support System (BLSS)

The BLSS is owned by Excorp Medical, Inc. a company based in Minnesota, USA with operations also in China. Unique to this BAL compared to the previous two is the use of whole blood rather than separated plasma in the hollow fibre bioreactor stage of the BAL (Fig. 5.2). Patzer et al have suggested this improves mass transfer over using fractionated plasma (Patzer et al., 2002a). Like the HepaMate, porcine hepatocytes are used, and the system was used to test whether the transfer of porcine endogenous retrovirus (PERV) was an issue (Kuddus et al., 2002). The results suggested that PERV transmission did not occur under standard conditions and that the BLSS was safe. Pre-clinical studies have been completed (Patzer et al., 2002b, Patzer et al., 1999) but there has been limited experience with the BLSS in human patients with a study of one individual (Mazariegos et al., 2002) and a Phase I trial involving four patients (Mazariegos et al., 2001). Phase I/II clinical trials in the USA and China are currently being planned according to the company website.

The BALs described above are in various stages of development and clinical trials. By using available literature data on each of the designs, they can be incorporated into updated versions of the mathematical models described in the previous chapters. The resulting oxygen tension and zonation profiles can then be assessed and in turn improved by modifying each of the designs in some way. This is achieved by defining two optimization protocols that are incorporated into the mathematical model to return optimal configurations for each of the BALs.

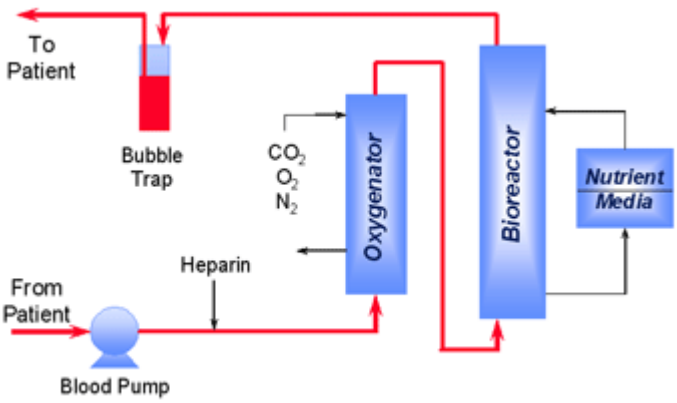

Figure 5.2: A schematic of the BLSS, from the Excorp Medical, Inc. website (2011)

5.2 Theoretical Aspects

5.2.1 Mass transport equations

The system of modelling equations employed in this study is based on that described in previous chapters, with some modifications to describe the unique features of each BAL. Also, the definition of the metabolic zones is updated to allow better comparison with *in vivo* oxygen tension gradients. In each case the convection-diffusion equation (Eq. 3.1) is solved to obtain the oxygen tension profiles, where D is the diffusion coefficient, c is the species concentration and V is the reaction term:

$$\nabla(-D\nabla c) = \mathbf{u}.\nabla c - V \tag{3.1}$$

As in Chapters 3 and 4 the Krogh cylinder model is used to describe each BAL where the form of the convection-diffusion differs between the lumen, membrane and ECS subdomains. The system of equations employed for each BAL is outlined below.

HepaMate and ELAD model equations

The HepaMate and ELAD designs are very similar to the BAL models solved in previous chapters, with one significant difference – the cells do not form a layer on the membrane in the ECS but instead are suspended in a gel matrix. The only practical difference this makes to Equation 3.4 is an additional cell volume fraction, ε, which is added to the transport equation in the ECS (Eq. 5.1). All other equations and boundary conditions stated in Chapter 3 are unchanged.

$$D_{hep}.\left(\frac{1}{r}\frac{\partial}{\partial r}\left(r\frac{\partial pO_2}{\partial r}\right)+\frac{\partial^2 pO_2}{\partial z^2}\right) = -\frac{\varepsilon\alpha V_{\max} pO_2}{K_m + pO_2} \tag{5.1}$$

BLSS model equations

The BLSS is distinct from the other two BAL designs in two important ways. First of all, whole blood is used to perfuse the bioreactor rather than fractionated plasma. This is important as the presence of haemoglobin in the red blood cells significantly affects

oxygen transport and must be accounted for in the model equations. The association of oxygen and haemoglobin in the blood stream necessitates an extra equation system in the fibre lumen. The reaction term V_{Hb} is added to the oxygen transport equation in the lumen to represent the rate of dissociation of oxygen from haemoglobin (Eq. 5.2). Here, blood is assumed to be a Newtonian fluid. This is not true in practice as blood exhibits shear-thinning behaviour and hence the velocity profile will not be a typical Poseuille flow. In addition, the added blood components may affect oxygen diffusivity. Here the flow and diffusion coefficient are assumed to be equal to those in plasma, in order to simplify the model.

$$D_{plasma}\cdot\left(\frac{1}{r}\frac{\partial}{\partial r}\left(r\frac{\partial pO_2}{\partial r}\right)+\frac{\partial^2 pO_2}{\partial z^2}\right)=2\bar{u}\left(1-\left(\frac{r}{R_l}\right)^2\right)\cdot\frac{\partial pO_2}{\partial z}+V_{Hb} \tag{5.2}$$

In order to define the rate of oxygen dissociation, an approach developed by Moll (1968) and subsequently used by Sullivan et al (2007, 2008) is employed. Here the binding/release of oxygen from haemoglobin is considered a single-step reversible reaction. V_{Hb} can be considered to be the rate of the binding minus the rate of release of oxygen to produce Equation 5.3, where k_{O2} is the rate constant for oxygen release, Hb is the concentration of haemoglobin in the blood and S is the fractional saturation of haemoglobin.

$$V_{Hb}=k_{O2}Hb\left(\left(\frac{S_{eq}}{1-S_{eq}}\right)(1-S)-S\right) \tag{5.3}$$

S_{eq} in the above equation is the haemoglobin saturation when blood is in equilibrium with the gas phase and is a function of local oxygen tension. In this case the Margaria equation is chosen to describe the relationship (Margaria, 1963). This equation is a simplification of the earlier Adair equation and is based on the observation that the affinity for the fourth and final oxygenation of the haemoglobin molecule is 125 times greater than the previous three steps. The form of the Margaria equation is given below (Eq. 5.5). Here K and m are constants calculated from curve-fitting experimental oxygen dissociation curves.

$$S_{eq}=\frac{\left(\frac{1+KpO_2}{KpO_2}\right)^3+m-1}{\left(\frac{1+KpO_2}{KpO_2}\right)^4+m-1} \tag{5.4}$$

In order to calculate the oxygen tension profile in the lumen, a second convection-diffusion equation representing the haemoglobin-bound oxygen must be solved simultaneously (Eq.

5.5). In this equation the reaction term V_{Hb} is present but opposite in sign relative to the transport equation for unbound oxygen (Eq. 5.2). The diffusion coefficient for haemoglobin in the blood is represented by D_{Hb}.

$$HbD_{Hb}.\left(\frac{1}{r}\frac{\partial}{\partial r}\left(r\frac{\partial S}{\partial r}\right)+\frac{\partial^2 S}{\partial z^2}\right)=2Hb\bar{u}\left(1-\left(\frac{r}{R_l}\right)^2\right).\frac{\partial S}{\partial z}-V_{Hb} \tag{5.5}$$

This equation for haemoglobin saturation S also has its own associated boundary conditions. At the inlet, the blood is considered to be in equilibrium with the gas phase (Eq. 5.6). Red blood cells do not pass through the fibre membrane and so there are no flux boundary conditions at both the lumen centre-line (due to symmetry) and membrane surface (Eq. 5.7). A zero diffusive flux boundary condition is assumed at the lumen outlet (Eq. 5.8).

$$S(r,0)=S_{eq} \tag{5.6}$$

$$\frac{\partial}{\partial r}S(0,z)=\frac{\partial}{\partial r}S(R_l,z)=0 \tag{5.7}$$

$$\frac{\partial}{\partial z}S(r,L)=0 \tag{5.8}$$

In addition to whole blood being used, the ECS ports of the BLSS bioreactor are opened and cell medium is circulated to remove any substances harmful to the cells (Patzer et al., 2002b). However, the ECS flow rate is only 0.25% of that compared to the flow through the fibres however and was found to be negligible in terms of affecting oxygen profiles in the BLSS Krogh cylinder model (data not shown). However, the open ECS port acts as another source of oxygen for the cells and the boundary conditions must reflect this. It is unclear what this secondary inlet oxygen tension is so in this model it is assumed to be equal to the lumen inlet oxygen tension (Eq. 5.9).

$$pO_2(r,0)=pO_2(in) \text{ for } 0\le r<R_l \text{ and } Rm\le r<R_e \tag{5.9}$$

Similar to the HepaMate and ELAD, the porcine hepatocytes used in the BLSS are suspended in a collagen gel in the ECS and don't form layers on the fibre. Hence Equation 5.1 also applies to the ECS oxygen transport equation in the BLSS model.

5.2.2 Metabolic zone definitions

As in the Chapter 4, the size of each metabolic zone can be estimated from the modelling results. In this work, the definitions are updated in order to improve comparisons between the BALs and the *in vivo* oxygen tension profiles. In the previous chapter, all hepatocytes experiencing oxygen tensions above 60 mmHg were defined as being periportal. *In vivo* however, the maximum oxygen tension in the liver sinusoids is approximately 70 mmHg (Allen and Bhatia, 2003). Hence all cells experiencing higher oxygen tensions are now assigned to a 'hyperoxic' zone to reflect the non-physiological conditions. It is unclear what effect if any the higher oxygen tensions will have on cell function compared to normal periportal hepatocytes, but it is useful when comparing the zonation distribution profiles the *in vivo* oxygen spectrum. By the same logic, hepatocytes that experience oxygen tensions lower than 25 mmHg are no longer considered to be within the perivenous zone but in a new 'hypoxic' zone. An 'anoxic' zone is defined for hepatocytes where the local oxygen tension is less than 10 mmHg as these cells are vulnerable to necrosis (Consolo et al., 2009). In previous chapters a value of 2 mmHg was to describe the anoxic limit (De Groot et al., 1988), the new higher value represents a higher safety factor in BAL designs. Table 5.1 summarizes how each zone is defined.

Table 5.1: The range of oxygen tensions that defines each of the metabolic zones

Zone	Oxygen Tension Range (mmHg)
Hyperoxic	> 70
Periportal	60 – 70
Pericentral	35 – 60
Perivenous	25 – 35
Hypoxic	10 – 25
Anoxic	< 10

5.2.3 BAL optimization protocols

Once zonation profiles have been established for the BALs under their standard operating conditions as defined in literature, the main objective in this chapter is to ascertain whether operating conditions could be changed to create more evenly distributed profiles. The approach taken here is to identify what plasma/blood rate will result in the ideal zonation profile. However, there is a question over how to define an 'evenly distributed profile'. In this work, two optimization protocols are followed. The first, Optimization Protocol I, seeks to equalize the combined size of the hyperoxic and periportal zones and the combined size of the perivenous and hypoxic zones i.e. Optimization Protocol I returns a flow rate that minimizes the difference in the size of the high and low oxygen tension zones. The second protocol, Optimization Protocol II, seeks to equalize the size of the periportal and perivenous zones specifically. This protocol does not consider hepatocytes outside of the physiological range of oxygen tension as their functionality is unknown. For both protocols, there is also a condition that no cells in the BAL are exposed to an anoxic environment. Figure 5.3 illustrates how the Optimization Protocols are defined.

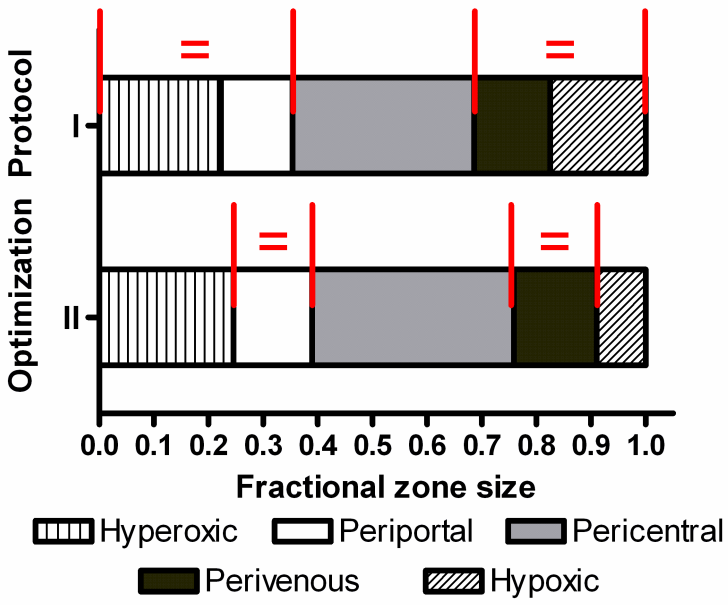

Figure 5.3: The zone distribution charts for each Optimization Protocol. The = sign shows the relevant metabolic zones for each case. Protocol I seeks to match the combined high oxygen zone size with the low oxygen zone size. Protocol II only considers the size of the periportal and perivenous zones.

5.2.4 Modelling parameter values

To model each of the BALs described above parameter values must be found which describe the uniqueness of each system. A literature search was performed to identify as many as possible of the parameter values needed to accurately simulate each BAL. Table 5.2 details the modelling parameters that were common to each BAL model whereas Table 5.3 outlines the values unique to each BAL. In some cases it was necessary to estimate likely values as some information has not been reported elsewhere to the author's knowledge.

Table 5.2: A list of the common parameters in each BAL model

	Parameter Value	Reference
D_{plasma} (m^2/s)	3 x 10^{-9}	(Piret and Cooney, 1991)
D_{hep} (m^2/s)	2.5 x 10^{-9}	Calculated
K_m (mmHg)	3	(Sullivan et al., 2007)

A number of the parameters listed in Tables 5.2 and 5.3 were not directly taken from literature sources but calculated or estimated. For example, literature values for the Krogh cylinder outer radius R_e are difficult to find for the specific BALs being considered here. In order to estimate this parameter, the assumption was made that the cell volume fraction in the ECS of each bioreactor was 0.5. This is based on the knowledge that an interstitial space volume fraction of 0.4 – 0.55 was reported for hepatomas (Gullino et al., 1965, Moussy, 2003). Assuming that HepG2/C3A cells and porcine hepatocytes have diameters of 16 μm (Hay et al., 2000) and 25 μm (Sullivan et al., 2007) respectively and knowing how many hollow fibres and total cell number are in each BAL, the value of R_e can be calculated by Equation 5.10 where d_{cell} represents the cell diameter. Table 5.3 contains the calculated values for R_e for each BAL.

$$R_e = \sqrt{\frac{\frac{N_{cell}}{\varepsilon N_f}\left(\frac{2}{3}\pi d_{cell}^3\right) - \pi R_m^2 L}{\pi L}} \tag{5.10}$$

A fibre number N of 870 was assigned to the HepaMate model in Table 5.3. This figure was calculated on the basis of previous literature values. Hay et al. (2001) reported N to be 670 and R_e to be 576 μm but at that time the HepaMate (in it's previous incarnation, the

HepatAssist) housed only 5 billion cells. Today the HepaMate is known to contain 14 billion cells. An increase of fibre number N to 870, assuming an unchanged cell density in the ECS, reflects the increased cell number while maintaining the previous value of R_e.

The maximal oxygen uptake rate V_{max} values were also indirectly obtained from literature. These values were calculated through data supplied by Nyberg et al (1994) for rat hepatocytes and HepG2 cells in a 3D gel entrapment bioreactor. In this study the oxygen consumption rates were measured on a per cell basis i.e. mol/cell/s. In order to convert them to volumetric oxygen uptake rates, the values are divided by the volume of an individual cell assuming they are spherical with diameters as reported above. As a result a value of 5.87×10^{-3} mol/m^3/s was assigned to the HepaMate and BLSS models which both use primary porcine hepatocytes. Though the animal is different this value was chosen to be representative of mammalian primary hepatocytes. The V_{max} value for the ELAD model was calculated to be 11.2×10^{-3} mol/m^3/s.

Oxygen diffusion rates through the membrane were calculated using an equation derived by Renkin (1954) to describe restricted diffusion through membrane pores. Using the Einstein-Stokes equation to estimate the radius of an oxygen molecule, it was found by the Renkin equation that for typical membrane pore sizes oxygen diffusion was not significantly restricted. As a result the same diffusion coefficient D_{plasma} for oxygen is applied to both the lumen and membrane subdomains in the Krogh cylinder model. The oxygen diffusion coefficient in the ECS D_{hep} was calculated as the mean of D_{plasma} and the diffusion coefficient of oxygen in tissue which has been given as 2×10^{-9} m^2/s (Piret and Cooney, 1991). This assumes the cells volume fraction ε was 0.5 as stated above.

Table 5.3: A list of each of the unique parameters used in the models for each of the BALs

	HepaMate	Reference	ELAD	Reference	BLSS	Reference
R_l (μm)	320	(Hay et al., 2001)	100	(Moussy, 2003)	100	J. Patzer*
R_m (μm)	380	(Hay et al., 2001)	130	(Moussy, 2003)	120	J. Patzer*
R_e (μm)	575	Calculated	158	Calculated	140	Calculated
L (cm)	45	(Hay et al., 2001)	23.4	(Moussy, 2003)	17.7	J. Patzer*
Q (ml/min)	200-400	(Hay et al., 2001)	500	(Millis et al., 2002)	200-250	J. Patzer*
N_{cell} (x10^9 cells)	14	HepaLife website	11	(Millis et al., 2002)	10	(Mazariegos et al., 2002)
N	870	Calculated	8000	Vital Therapies website	13500	J. Patzer*
V_{max} (mol/m^3/s)	5.87 x 10^{-3}	Calculated	11.2 x 10^{-3}	Calculated	5.87 x 10^{-3}	Calculated

* Parameter values were disclosed in an email from Professor Jack Patzer (University of Pittsburgh) following a request to Excorp Medical, Inc.

Extra parameters are also needed to describe the oxygen and haemoglobin binding/release kinetics in the BLSS model. The values used are shown below in Table 5.4.

Table 5.4: The values for the parameters required to model whole blood in the BLSS model

	Value	Reference
Hb	8.8 mol/m^3	(Chen and Palmer, 2009)
D_{Hb}	6.8 x 10^{-15} m^2/s	(Sullivan et al., 2007)
k_{O2}	33.5 s^{-1}	(Chen and Palmer, 2009)
K	0.01278 mmHg^{-1}	(Hay et al., 2000)
m	125	(Margaria, 1963)

5.2.5 Modelling strategy

As in previous chapters the finite element multiphysics software package COMSOL 3.5a is used to solve the modelling equations. The Krogh cylinder is constructed and the subdomain and boundary condition equations are input. As in the previous chapter, as the Krogh cylinder models are of a very high aspect ratio the geometry is scaled in both axial and radial directions. This avoids problems in the COMSOL solver algorithms and allows high-quality finite-elements. As a result all of the model equations must be scaled appropriately to reflect the new coordinate system. MATLAB scripting is used to build each model rather than the COMSOL GUI as this allows more efficient optimization of the plasma/blood flow rates. Essentially, the MATLAB script allows each BAL model to be solved for a range of flow rates and assess the zonation pattern produced for each one. The value of Q to the nearest 5 ml/min is returned when the ideal zonation pattern is found for each of the optimization protocols. While it is possible to be more specific with regards to the optimized flow rates, the assumptions made in the model mean that the increased accuracy would not justify the extra computational effort required.

5.3 Results

5.3.1 HepaMate standard and optimized models

Standard HepaMate model

Figure 5.4 is a representation of the oxygen profile in a Krogh cylinder sub-unit representing the HepaMate design under standard operating conditions. Reynolds and Peclet numbers can be calculated as described in Section 3.3.1. Under the standard operating conditions of the HepaMate as seen in Table 5.3, Reynolds number varies between 7.6 and 15.2 and hence the flow is laminar. Peclet number will vary between 0.9 and 1.8 indicating neither convection nor diffusion dominates in the fibre lumen. A parameter to describe the balance of oxygen diffusion and consumption in the cell region, as described in Section 3.3.1 and in work by Shipley et al. (2010), is of order 1. From this it can be concluded diffusion and reaction mechanisms will both be significant in the cell region. Figure 5.5 displays the corresponding metabolic zone distribution profile. As the standard plasma flow rate is not known for the HepaMate, a range of values was examined in this figure. For flow rates of 200 and 300 ml/min, which are typical of this application, there are significant regions of anoxia and hence probable cell necrosis. For a flow rate of 400 ml/min, the zone distribution is skewed towards the low oxygen zones over the higher oxygen environment zones. The periportal zone only occupies 2.5% in this instance.

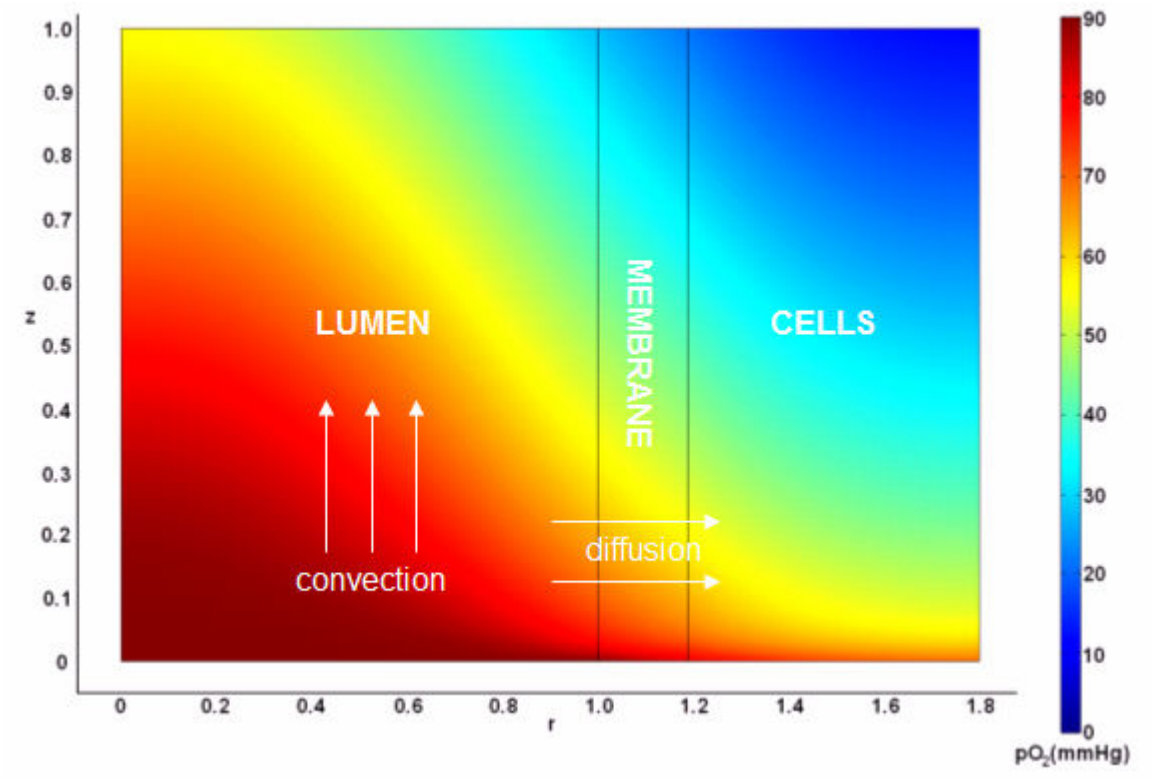

Figure 5.4: The oxygen profile for the HepaMate model under standard conditions. The minimum oxygen partial pressure is 12.1 mmHg when operating with a plasma flow rate of 400 ml/min. A dimensionless coordinate system is used.

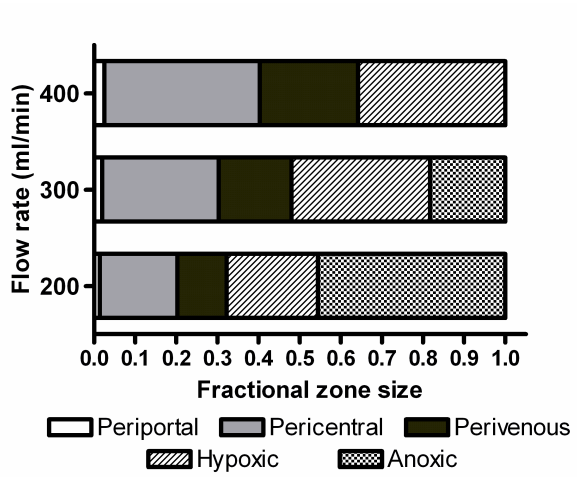

Figure 5.5: The standard zonation profile in the HepaMate under standard conditions. As the flow rate is not known, three representative values are studied; 200, 300 and 400 ml/min.

Optimized HepaMate Modelling

In Figure 5.6A, the existing HepaMate model is optimized with respect to plasma flow rate. For the first optimization protocol, which seeks to equalize the high and low oxygen environment zones, a flow rate of 400 ml/min (the maximum considered allowable)

produced a profile where the periportal zone only occupied 2.5% of the cell volume whereas the perivenous and hypoxic regions jointly occupied 59.6% of the cell volume. A similar picture emerges for Optimization Protocol II where a flow rate of 375 ml/min produced the distribution. The periportal zone makes up 2.2% of the cell volume while the perivenous zone occupies 22.2%. Clearly the optimization protocol has failed to produce well-balanced zones in this case.

For Figure 5.6B, the design of the hollow fibre module was changed. This was done to produce more evenly distributed zone profiles. The reasons for this are explained further in the discussion. Table 5.5 shows the original and modified hollow fibre parameters. For optimization protocol I, a flow rate of 315 ml/min caused the high oxygen zones (i.e. the hyperoxic and periportal zones) to occupy 28.3% of the cell volume and the low oxygen zones to occupy 27.8%. For Optimization Protocol II, a flow rate of 355 ml/min induced the periportal zone and perivenous zones to occupy 19.1% and 18.4% of the cell volumes respectively.

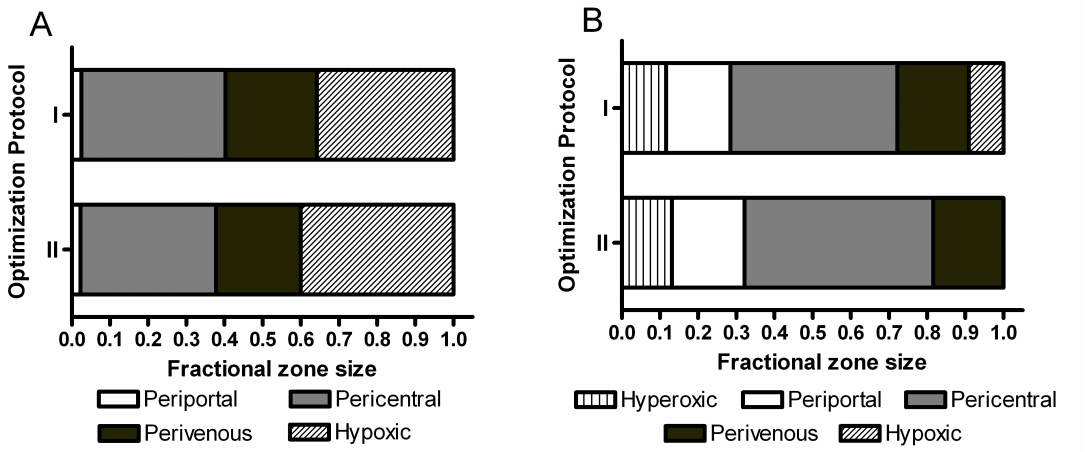

Figure 5.6: Optimized zonation profiles for the HepaMate. (A) The flow rate of the HepaMate is optimized for two situations. Q = 400 ml/min for the first optimization protocol and Q = 375 ml/min for the second optimization protocol. (B) The HepaMate hollow fibre design is changed (Table 5.5) and the optimal flow rates are recalculated. Q = 315 ml/min for the first protocol and Q = 355 ml/min for the second optimization protocol.

Table 5.5: The old and new hollow fibre parameters for the optimization of the HepaMate

	Old Parameters	New parameters for optimization
Lumen radius R_l (μm)	320	160
Outer fibre radius R_m (μm)	380	190
Fibre length L (cm)	45	25
Fibre number N	870	4800
Krogh cylinder radius R_e (μm)	576	576

5.3.2 BLSS standard and optimized models

Standard BLSS model

Figure 5.7 shows the oxygen profile for the BLSS under standard operating conditions with a normal human hematocrit when modelled using COMSOL and the relevant equations above. The minimum oxygen partial pressure in the Krogh cylinder is 77.1 mmHg. The corresponding zonation profile can be seen in Figure 5.8, where two inlet oxygen tensions were considered. In the former case, all hepatocytes are within a hyperoxic environment whereas in the latter the majority (82.8%) are within the periportal zone. Reynolds number for the standard flow conditions in the BLSS takes a value of approximately 1.5-2 and Peclet number is approximately 0.1. This indicates blood flow is laminar and diffusive transport in the lumen is significant. The dimensionless parameter characterizing diffusion/reaction balance in the cell region varies between approximately 0.1 – 1, showing both mechanisms are significant.

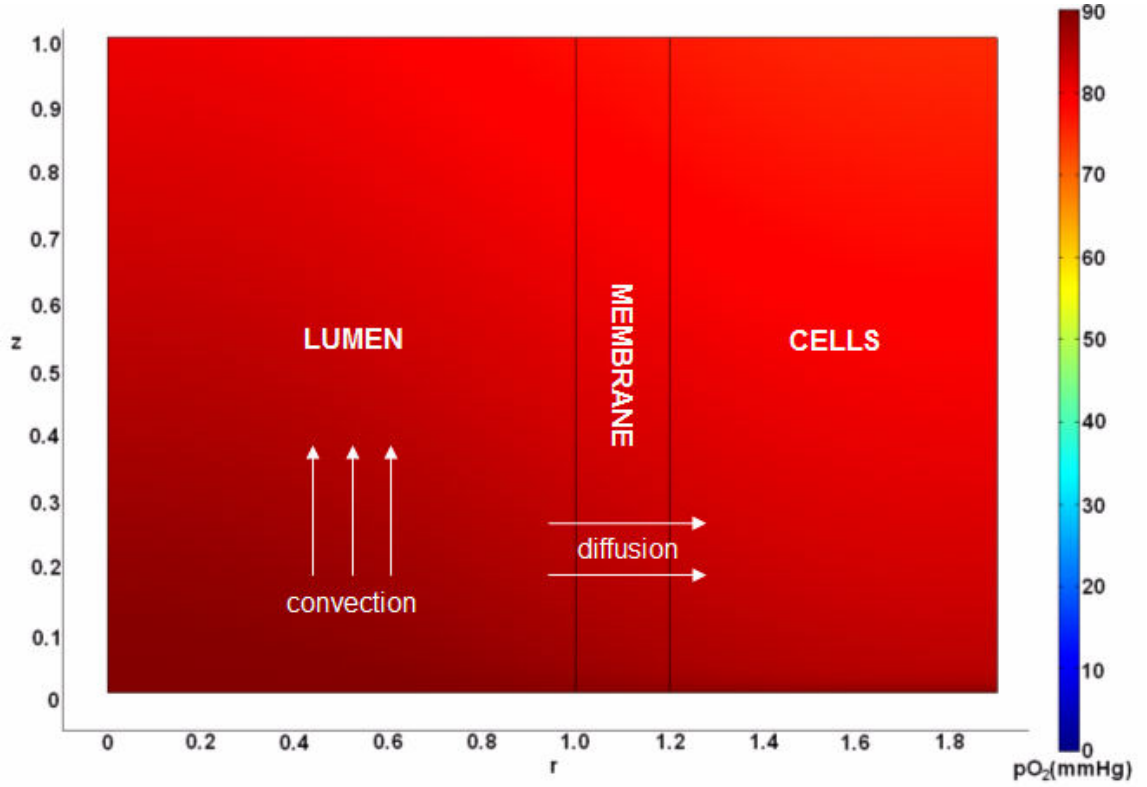

Figure 5.7: The oxygen profile in the standard model of the BLSS, with a full haematocrit and a blood flow rate of 200 ml/min. The minimum oxygen tension in the model is 75.3 mmHg.

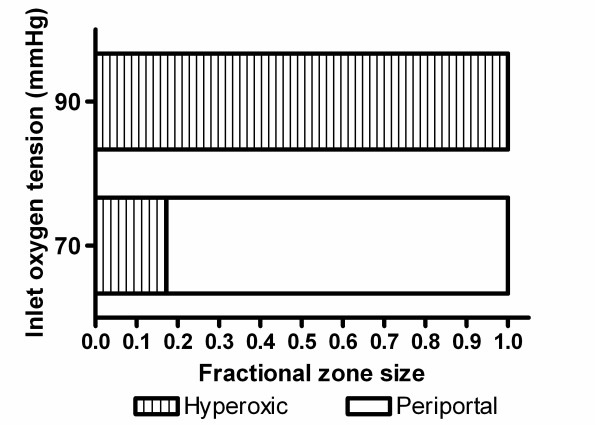

Figure 5.8: The zone distribution in the BLSS under the standard operating parameters and a blood flow rate of 200 ml/min. Each bar represents a different inlet partial pressure of oxygen.

Optimized BLSS model

Initially the optimal flow rates were found based on the standard BLSS design, i.e. using whole blood. The optimized zone distribution can be seen in Figure 5.9A. An inlet partial pressure of 70 mmHg was used in order to mimic in vivo oxygen conditions. However, the optimization protocols fail in this instance as the periportal and perivenous zone occupy

8.2% and 5.2% of the cell volume respectively with the remainder residing in the pericentral zone. The pericentral zone is dominant and the zonation profile is unbalanced. This occurs at a blood flow rate of 15 ml/min for both optimization protocols.

In Figure 5.9B, the red blood cells are removed from the model and the inlet oxygen concentration raised to 90 mmHg. This was done to widen and reposition the oxygen tension spectrum in the BAL. For optimization protocol I the high oxygen zones make up 35.6% of the cell volume, while the low oxygen zones occupy 28.4%. This occurs when a plasma flow rate of 200 ml/min. The periportal and perivenous zones occupy 16.3% and 16.8% of the cell volume respectively for optimization protocol II, with a flow rate of 225 ml/min.

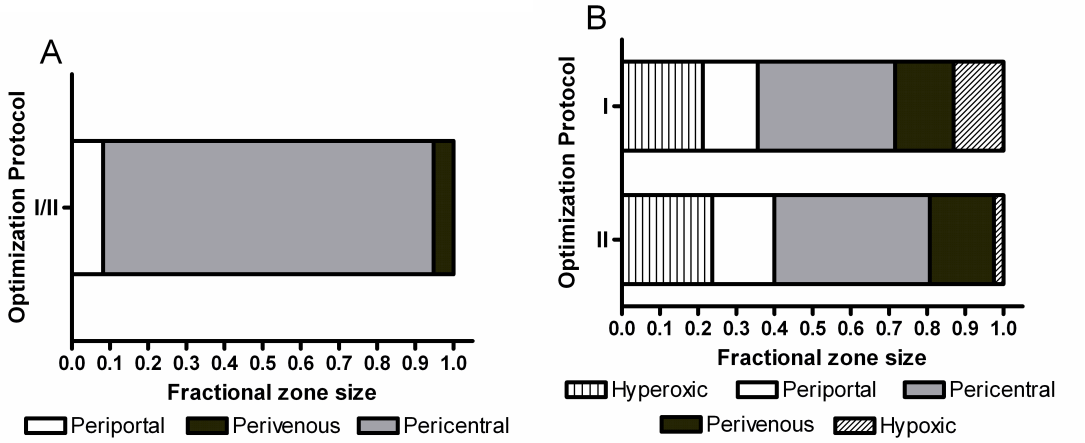

Figure 5.9: Optimized zone distributions for the BLSS. (A) The optimal zone distribution in the case of a full hematocrit and an inlet oxygen tension of 70 mmHg. The optimal flow rate is 15 ml/min for both optimization protocols is the same and hence only one bar is present. (B) By removing the red blood cells and increasing the inlet oxygen tension to 90 mmHg, the above optimal zone patterns are achieved. The flow rate for protocol I is 200 ml/min and for protocol II it is 225 ml/min.

5.3.3 ELAD standard and optimized models

Standard ELAD Model

Using the available literature values for the ELAD design parameters, an oxygen tension profile in the corresponding Krogh cylinder sub-unit can be produced as seen below in Figure 5.10. The zonation profile for the standard ELAD set-up is in Figure 5.11, where two inlet partial pressures are tested. In either case the range of oxygen tension is too high for low oxygen zones to appear, especially with a 90 mmHg inlet oxygen tension where the

whole cell volume falls into the hyperoxic zone. Reynolds number under standard operating conditions is approximately 6.6 and Peclet number is calculated as 0.5. These conditions are consistent with the other models studied so far, where flow is laminar and convection and diffusion are both significant. A value of 0.2 for the diffusion/reaction parameter in the cell region shows that diffusion is relatively more significant.

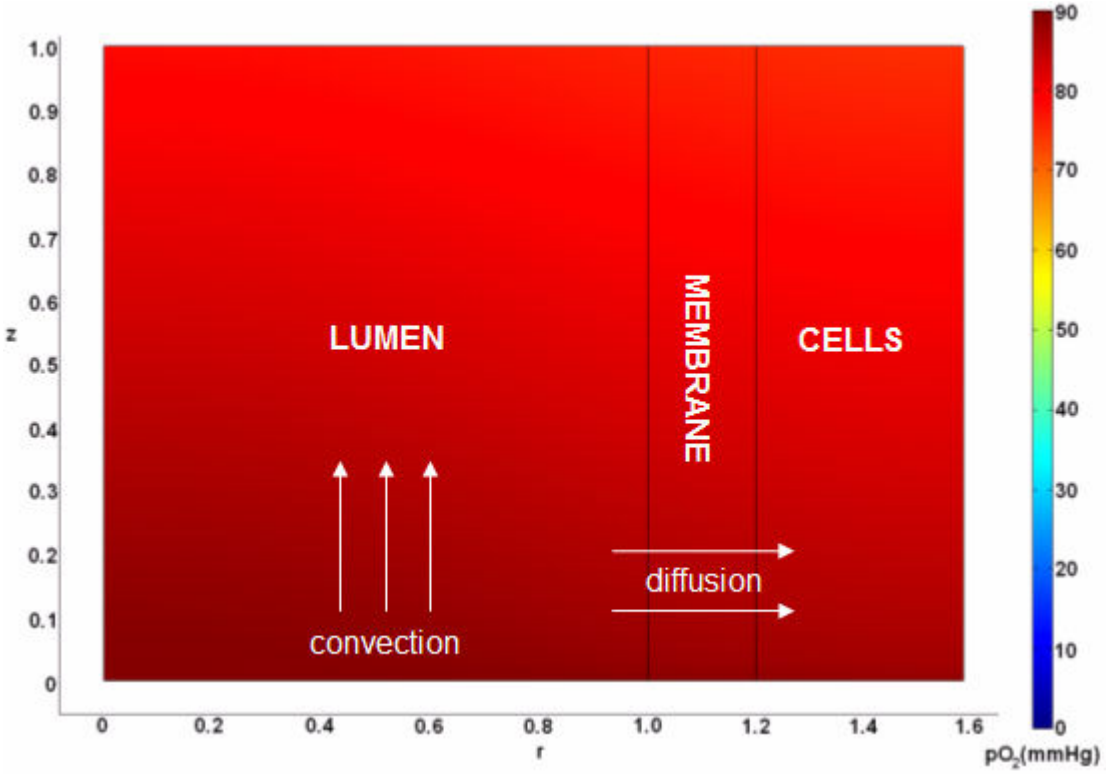

Figure 5.10: The oxygen profile in the standard model of the ELAD. The minimum oxygen tension in the model is 74.8 mmHg when inlet oxygen tension is set to 90 mmHg.

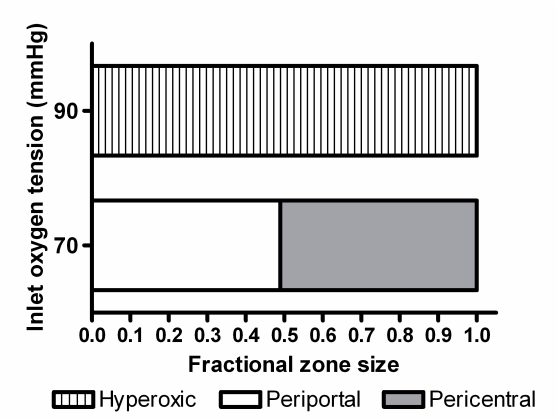

Figure 5.11: The zonation profile in the ELAD under standard conditions, for two inlet oxygen partial pressures. When the inlet oxygen partial pressure is 90 mmHg, all zones bar the hyperoxic zone are absent. For the lower inlet tension, the cells are approximately equally divided between the periportal and pericentral zones.

Optimized ELAD model

Figure 5.12A shows the optimal zonation profile with an inlet oxygen tension of 70 mmHg. In this case both optimization protocols produce the same result; a profile where the periportal and perivenous zones occupy 18.3% and 17.0% of the cell volume respectively. This occurs when a plasma flow rate Q of 185 ml/min is employed. For Figure 5.12B, the inlet oxygen tension is raised to 90 mmHg. When the plasma flow rate is optimized to 90 ml/min by protocol I, the high oxygen and low oxygen zones occupy 35.4% and 31.3% of the cell volume respectively. Optimization protocol II results in a flow rate of 105 ml/min and the periportal and perivenous zones occupy 14.4% and 15.1% of the cell volume respectively.

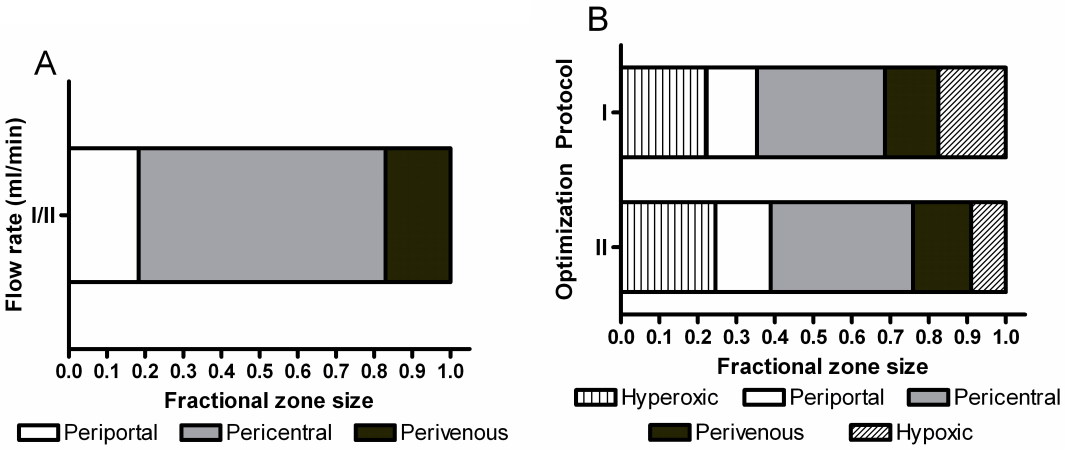

Figure 5.12: The optimized zone profiles for the ELAD with varying inlet oxygen tension. (A) With an inlet tension of 70 mmHg the plasma flowrate for both optimization protocols is 185 ml/min. (B) An inlet oxygen tension of 90 mmHg was employed. The plasma flow rate for protocol I was 90 ml/min and for protocol II was 105 ml/min.

5.4 Discussion

In this chapter, the techniques and findings from previous chapters were applied to existing privately-owned BAL designs that are currently undergoing clinical trials. This involved looking at the existing BAL designs and operating parameters and then applying the mathematical model developed previously to them. The concepts of the Operating Region

and zonation analysis could then be utilized. As mentioned in the discussion of Chapter 4, liver zonation is a physiological feature that doesn't appear to be fully considered in existing BAL designs. This view is supported by the modelling results for each of the BALs operating under standard conditions where the zone distribution profiles appear to be skewed towards either high or low oxygen environments. The plasma/blood flow rates were also optimized for each design to improve the distribution of the metabolic zones. Two different protocols for optimization were defined, the first matching the combined sizes of the high and low oxygen zones and the second that matches the size of the periportal and perivenous zones specifically. For the HepaMate and BLSS however it was found that a fundamental change to the BAL design, a change in fibre number and size for the former and the removal of red blood cells in the latter, was necessary in order for the optimization protocols to produce well balanced zone distributions.

In the case of the HepaMate it was unclear from literature what plasma flow rate is used for clinical applications. Hence in the standard parameter model a range of flow rates from 200 – 400 ml/min was examined. This corresponded with the range of flow rates modelled by Hay et al (2001), though their upper limit value of 600 ml/min was ignored as it is not clear whether this flow rate can be achieved in a clinical setting. This is based on the assumption of previous chapters that the plasma flow rate was limited to approximately 300 ml/min due to technical and rheological constraints (Pless and Sauer, 2005). In any case, the modelling results revealed that oxygen deficiency could be problematic in the HepaMate as anoxic zones were present for flow rates up to 300 ml/min. Even in the case of the maximum flow rate of 400 ml/min, the zone distribution was still skewed towards the low oxygen metabolic zones with the periportal hepatocytes occupying only a very small fraction of the cell volume. In light of this, a means to more evenly distribute the metabolic zones should be found.

For the first attempt at optimizing the plasma flow rate, it is clear that whatever flow rate is employed the periportal zone becomes exceedingly small. Clearly some other aspect of the HepaMate design must be addressed before a substantial improvement can be made. Several options are available: increase the inlet oxygen tension to the device; reduce the number of hepatocytes within the ECS; increase the flow rate even further or somehow change the hollow fibre bundle design. It is undesirable to reduce the cell population within the BAL device as this may have implications for the BAL's functionality. Also,

increasing the inlet oxygen tension would further distance the cell environment from their *in vivo* state where the maximum oxygen tension is typically 70-90 mmHg. Increasing plasma flow rate is also technically difficult and ineffective as can be seen in the relatively unchanged size of the periportal zone for flow rates of 200-400 ml/min. A further option may be to use whole blood to increase oxygen delivery to the cell mass, though this may bring issues relating to blood clotting and fibre blocking and hence is not ideal. All that remains is the latter option, to alter the hollow fibre design.

In Chapter 3, it was concluded that short, small-bore and numerous fibres tended to produce wider Operating Regions. Larger Operating Regions also allow a greater range of zone distribution as seen in Chapter 4. In the HepaMate design, literature values indicate that the hollow fibres have a relatively large lumen radius of 320 μm and a length of 45 cm. In addition, there are only 870 fibres in the entire bundle when the fibre number is updated to take account of the increased cell population. The resulting interfibre distance is approximately 392 μm. This is a large distance for oxygen to diffuse through tissue, as in the body the maximum diffusion distance is approximately 200 μm (Palsson, 2004). By increasing the fibre number and making them shorter, it should allow greater control over the range of possible zone distributions. As an example to illustrate this, new fibre design parameters were used for the optimization protocols (Table 5.5). This allows for a much more even distribution of the zones with balance between the high and low oxygen metabolic zones.

The modelling results for the BLSS operating under standard conditions revealed that in contrast to the HepaMate, oxygen supply was not limited. However, the model suggests that the oxygen tensions in the BLSS occupy too high a range. Two inlet oxygen tensions were considered, 90 mmHg as this figure was used in previous chapters and is approximately equivalent to arterial blood and 70 mmHg as this corresponds to physiological oxygen tension in the liver. In both cases the perivenous zone is completely absent from the zonation profile and as a result it may be inferred that some liver functions in the BLSS may be compromised.

In attempting to optimize the blood flow rate in the BLSS under standard conditions, it was found that a very low flow rate of 15 ml/min produced a pattern that still appeared very unbalanced with the pericentral zone occupying almost all of the cell volume. It is clear

that while the presence of red blood cells and their haemoglobin ensures that the cells will not be starved of oxygen, the resulting spectrums of oxygen tension are not physiologically relevant. It isn't feasible to further reduce the blood flow rate as this will likely cause other nutrients e.g. glucose to become limiting. It was decided to model the BLSS in the absence of red blood cells, i.e. to remove the effect of haemoglobin on the oxygen transport equations. The resulting optimized zone profiles are significantly more balanced. Though it may seem counter-intuitive to remove the red blood cells and hence make the BLSS less biomimetic, in this case it improved the functionality of the device. Use of whole blood in these devices can also be associated with problems due to leukocyte activation and cell damage (Allen et al., 2001). An alternative to removing the red blood cells may be to increase the hepatocyte number and hence oxygen consumption in the device. This may necessitate redesigning of the hollow fibre bundle but may improve the efficacy of the device.

The ELAD was also modelled using standard parameter values found in the literature. An issue that must be addressed surrounding the C3A cell type is whether they exhibit the same response in terms of oxygen modulation as compared to primary hepatocytes, i.e. whether the zonation definitions above apply to them. There is evidence that oxygen tension is a modulator of their expression of cytochrome P450 (Camp and Capitano, 2007). On this basis it is assumed here that the zonation profiles presented here are relevant to the C3A cell type but further research on the topic is necessary.

Similar to the BLSS, the range of oxygen tensions under standard operating conditions in the ELAD appeared to be too high despite no red blood cells being present. This was the case even when using a lower inlet oxygen tension of 70 mmHg and is likely a result of the very high plasma flow rate being employed (500 ml/min) and the relatively short inter-fibre distance of less than 50 μm. The procedure for optimizing the plasma flow rate in the ELAD was simpler than that for the previous two BALs. The obvious step to take was to look at zonation profiles at a lower range of flow rate as the standard flow rate of 500 ml/min was significantly greater than that seen previously in BAL applications. Inlet oxygen tensions were set to either 70 or 90 mmHg as the available literature values did not make this value clear. In both cases, moderate plasma flow rates were found to produce evenly distributed zonation profiles. Similar to the BLSS, an alternative solution may be to increase the cell loading in the device to increase oxygen consumption in the device with

the added benefit of potentially greater efficacy. Also, it may be possible to partially fractionate the blood, i.e. use a proportion of the red blood cells to carry oxygen to the BAL rather than removing them entirely.

In modelling the BALs described above, a number of assumptions had to be made over parameter values that have not been disclosed through recent literature or company websites. As such there is some uncertainty over how accurately the BALs have been portrayed here, for example the hollow fibre design in the HepaMate may be different to what has been assumed in this chapter. However, the broad characteristics of each system have been captured, for instance through the number and type of liver cells employed in each BAL. Should more detailed information become available for each BAL, it would only require a small effort to update the models described here to reflect the new design parameters. The utility of the mathematical framework developed over previous chapters has been illustrated here through application to specific BALs. Should the design of these BALs be different in reality, it would not diminish the ability of the framework to describe those same systems.

5.5 Conclusions

In previous chapters, a framework was established and developed to examine oxygen mass transport within hollow fibre-based BALs. The implications of oxygenation on metabolic zonation and hence device functionality of the BAL were also established. The lessons and techniques of these previous chapters have been taken and applied to three distinct privately-owned BAL designs that are currently progressing through various stages of clinical trials. In each case, modelling results for each of the BALs have suggested that under current operating and design conditions oxygenation to the cells is in someway inadequate or non-ideal. In the HepaMate it was concluded that the hollow fibre design was inappropriate and by changing it according to the lessons of Chapter 3 (i.e. a greater number of shorter, thinner fibres), oxygenation could be improved and well-balanced zonation profiles could be established. For the BLSS, it was deemed that by operating the device with patient plasma rather than whole blood allowed the zonation profiles to become balanced. In the ELAD, simply reducing the plasma flow rate through the hollow fibre cartridges would be enough to improve the zone distribution. These findings suggest

that in each of the BALs, consideration of the modelling results and the zonation physiological phenomenon can lead to more efficient and effective BALs.

Chapter 6: Discussion and Conclusions

6.1 Discussion of findings

In this section, the overall impact of this work will be considered in the context of the literature at present. In Chapter 2, an extensive review of literature relevant to BALs and modelling of such HFBR systems was performed. The functions and physiology of the human liver were studied and summarized to provide a context for liver support therapies. As the liver is such an important organ, the consequences of liver failure are often fatal with death rates being as high as 90% (Mareels et al., 2006, de Rave et al., 2002). The shortage of donor organs for the treatment of liver failure has spurred the growth of the liver support field. This has encompassed devices such as the MARS and SPAD artificial livers (Stange et al., 1999, Peszynski et al., 2001) which each use albumin dialysis to detoxify blood, and BALs such as the BLSS and ELAD (Mazariegos et al., 2002, Sussman et al., 1991) which incorporate liver cells. As liver cells can potentially replace a wider range of liver functions and BALs have been more prevalent than their wholly artificial counterparts, it was decided to study these systems in particular. Much of the work on these systems in the past has been testing through pre-clinical (Patzer et al., 2002b) or small human trials (Ellis et al., 1996). Undoubtedly, this work is important as many issues still surround the practicalities of BAL design (Section 2.2.3). However, a mathematical modelling approach is more suitable to tackle fundamental issues over mass transport of nutrients to the cell population.

Modelling work has been performed on BAL systems previously and numerous examples have been described. For example, Hay et al modelled previous versions of the ELAD and HepatAssist and examined whether sufficient oxygen was being delivered (Hay et al., 2000, Hay et al., 2001). However, one feature of the literature that is apparent is the lack of consideration over how modelling results may actually improve BAL design. To date, modelling has generally been a tool for verification or otherwise of existing BAL or HFBR designs. There is apparently little thought given towards how trends that can be identified from modelling can inform better designs. As a result, particular HFBRs are being employed in BALs with little rationale behind their choice. This apparent gap in the

literature is what this work aims to address. This has been done primarily through the development of the Operating Region principle, where the results of a series of modelling simulations are collated and adapted to a graphical display. This method of data presentation allows quick visual verification of BAL designs and through comparison of various Operating Region charts, beneficial BAL design trends can be identified. For example, from looking at Operating Region charts constructed for hollow fibres of varying length, it became clear that the use of short fibres over fewer longer fibre resulted in a larger parameter space where the design constraints could be satisfied. As a result the BAL design has a greater protection against unforeseen deviations from the mathematical model. There has been no such claim in previous literature; rather the issue of hollow fibre geometry is largely ignored. The value of the Operating Region charts in identifying these trends is clear; BAL designers now have a clear rationale for choosing particular HFBR designs over others.

Another element of BAL design that is generally under-represented in the literature is the preservation of a physiological cell environment within the BAL. While hollow fibres do have characteristics in common with capillary networks in the body, there otherwise seems to be little regard for biomimetic features in the BAL. One aspect of liver physiology that can be carried over to BALs is that of zonation, where the gradient of oxygen tension along the liver sinusoids has a modulating effect on hepatocyte function. In order to represent the full spectrum of liver functions within the BAL, the spectrum of oxygen tension in the BAL should closely match that *in vivo*. This has been explored in some modelling work as described in Section 2.3.5, but not in the sense of controlling zone distribution to create a more effective BAL. For example, Sullivan et al have modelled oxygen mass transport and zonation in their own BAL design when the medium has been supplemented with oxygen carriers (Sullivan et al., 2007, Sullivan et al., 2008). However, current literature lacks any detail over how zonation profiles can be manipulated through HFBR design and operating parameters. In this work, the range of possible zone distributions while remaining within the bounds of the Operating Region was explored. It was found that zone profiles could be predicted and therefore controlled in BALs. In certain cases each metabolic zone could be made to occupy the same fraction of the cell mass. This presents the BAL designer with the potential to improve device functionality through maintenance of the correct oxygen gradients in the system.

This work has developed tools to improve and optimize the designs of BALs. Where the literature once was sparse on rationales for choosing particular HFBR designs and operating parameters, this report has filled the void. As an example of this potential, the principles of the Operating Region and zonation were applied to commercial BAL designs, each one currently in various stages of the clinical trial process. In each case, it was found that the designs could be improved and indeed optimized with regard to oxygen delivery. Surprisingly, it appeared that both the BLSS and the ELAD were over-oxygenating their respective cell masses in that the oxygen tensions were above *in vivo* levels. Literature has generally focussed on the limitations of hollow fibres in supplying oxygen; it was unexpected that in these cases too much oxygen was being delivered. This is a new discovery that has not yet been reported in literature, underlining how tangible and important benefits to BAL design can be gleaned through application of the methods developed here. Ultimately, adoption of these principles can hasten the transition of BAL technology from a concept to a real clinical device which can save the lives of many people.

6.2 Conclusions

This work has examined one of the major technical hurdles in BAL design, namely the mass transport of oxygen. Faced with this issue, the answer was to develop a framework to rationalize and optimize the choice of design parameters for BALs.

The first step taken towards this goal was to develop a mathematical model based to describe the mass transport of oxygen within a BAL, as seen in Chapter 3. The model assumed Krogh cylinder geometry, i.e. that through symmetry of a perfectly straight array of hollow fibres that do not interact, it is sufficient to model one representative sub-unit to describe the whole fibre bundle. The model also incorporates features typical in the field such as a Poisueille flow profile in the fibre lumen and Michaelis-Menten reaction kinetics to describe oxygen uptake by the cells. In order to solve the model equations, the finite element-based software COMSOL was employed. By using software, arrays of modelling solutions could be produced by sequentially varying parameter values, such as plasma flow rates or fibre length and radius.

In order to represent the modelling data in a meaningful way, a constraint representing the minimum required supply of oxygen was defined as a function of the model solutions. A further constraint representing the minimum required cell number was also identified and defined as a function of the HFBR design parameters. The definitions of each constraint allowed them to be represented graphically, hence producing the Operating Region chart. The Operating Region chart displays a parameter space where the BAL operating constraints can be satisfied simultaneously, allowing visual verification of particular BAL set-ups. In addition to this, through varying parameters such as fibre length and radius, plasma flow rate and cell number, beneficial design trends could be identified. Importantly, the results also showed that therapeutically relevant cell volumes of between 10-20% of the adult liver cell mass could be supported in the BAL.

To further develop the usefulness of the Operating Region principle, greater consideration of liver physiology was incorporated into the mathematical model in Chapter 4. In particular this concerned applying definitions of metabolic zonation to the BAL cell mass where local oxygen tensions delineate each zone. If the BAL is to function in a similar manner to the native liver, it was hypothesized that the range of oxygen tensions should closely match that seen *in vivo*. Modelling parameters were varied to ascertain their importance in influencing the distribution of the metabolic zones in the cell mass. It was found that fibre geometry did not have a strong influence over the distribution of the zones, whereas parameters such as inlet oxygen tension, plasma flow rate, cell number and maximal oxygen uptake rate were important factors. It was also found that a double cell layer model also made it more difficult to evenly distribute the zones compared to a single cell layer. Under certain conditions, e.g. where the cells have a relatively low oxygen uptake rate, it was shown that it is possible to over oxygenate the cells. In this situation the zonation profile is skewed towards the periportal zone, possible leading to reduced BAL functionality. This situation has to date not been examined in literature, where traditionally it has been assumed oxygen mass transport is limited in HFBR cell culture applications. In addition to examining the importance of the modelling parameters in determining the zone distribution profiles, the flow rates and cell numbers that would result in evenly distributed profiles were also ascertained. Although it cannot be confirmed that equal zone sizes represent the optimum situation in the BAL, Chapter 4 demonstrates that through careful choice of the design parameters it is possible to control zone sizes to particular

specifications. This has the potential to improve BAL efficacy through mimicry of the physiological cell environment.

Chapters 3 and 4 have established a framework for evaluating BALs in terms of oxygen supply and liver cell function for general designs, i.e. to first determine the parameter space where the operating constraints of BALs can be satisfied and then optimize the design through consideration of zonation profiles. These principles were applied to examples of existing BALs, through some modifications to the mathematical model. Initially, each of the example BALs operating under normal conditions were modelled using parameters obtained from literature or otherwise assumed. It was clear in each case that oxygenation was non-ideal; regions of anoxia were present in the HepaMate while the cell mass appeared to be over-oxygenated in the ELAD and BLSS. Unbalanced metabolic zones would result in each of these BALs as a consequence, potentially hampering their functionality. For each BAL, the optimal plasma or blood flow rate was found to balance the zones but this proved to be ineffective for the HepaMate and BLSS. In each of these cases the BAL design was altered to achieve balanced zonation profiles; the fibre design was modified for the former and the red blood cells separated from the plasma in the case of the latter. The work in Chapter 5 demonstrated the utility of the mathematical framework developed in the previous chapters by diagnosing mass transport issues in each of the BALs and in theory, being able to remedy them.

In this work, the fundamental issues regarding mass transport to the liver cells and their corresponding metabolic behaviour have been considered. HFBRs have been used extensively in BALs though have been hampered through deficient oxygen supply to the cell mass. The techniques and findings disseminated here have sought to link HFBR design and operating parameters to oxygen supply to aid BAL designers who previously had no rationale for choosing a bioreactor design. In the first instance, Operating Region charts can be constructed for various BAL configurations to allow rapid and simple verification. The design can then be optimized with regards to the desired zonation profile to maximize its therapeutic potency. It is hoped that through this work the next generation of BALs can successfully make the transition from a concept to a clinical reality, where countless lives can be saved.

6.3 Future Work

The work presented here is novel and important to the design of future generations of BALs. However, there are further steps that can be taken to build on this work and increase its relevance. The main component to be added is comprehensive physical, experimental data that can further validate the model employed to describe the BALs. In particular, the oxygen consumption rate is a vital parameter in determining the characteristics of the BAL (Catapano and DeBartolo, 1996). Identifying this parameter would involve seeding cells into the ECS of a hollow fibre bioreactor and measuring oxygen uptake under various conditions. A method based on the one outlined by Mishra and Starly (2009) could be employed, where fibre optic sensors are used to measure oxygen levels in real time within alginate matrices containing a liver cell line. Alternatively, magnetic resonance imaging techniques have been used to determine dissolved oxygen levels in hollow fibre bioreactors (Williams et al., 1997) and could be utilised here. Michaelis-Menten parameters could then be estimated by fitting the model solution to experimental data.

Additional features can be added to the modelling, for example the use of artificial oxygen carriers in the plasma stream. This would allow a greater amount of oxygen to be carried by the plasma and possibly improve the range of viable BAL designs while also offering greater flexibility over the metabolic zone distribution. The use of the oxygen carrier perfluorocarbon (PFC) in BALs has been studied by Kinasiewicz et al (2008b). They found that C3A cells had increased protein synthesis rates when the medium was supplemented with PFC. PFC has been used to deliver oxygen in other tissue engineering applications such as cardiac tissue engineering (Radisic et al., 2005).

An approach used extensively in this work and in hollow fibre modelling in general is the Krogh cylinder representation. It is favoured over other approaches as it transforms a fundamentally complicated system consisting of thousands of individual fibres into a relatively simple model. However, a number of the assumptions made to do this are not realistic. For example, the assumption that all the fibres are perfectly straight and arranged in a hexagonal pattern (Fig. 2.10) does not hold in practice. As a result the assumption that

the mass transport profiles of each fibre do not interact is also invalid. The Krogh cylinder approach is certainly useful and experimentally-validated models based on it do exist, however perhaps a future direction may be to examine other modelling strategies. One example may be the porous medium model developed by Labecki et al. (1995). This model treats the ECS and hollow fibres as interpenetrating porous regions which allows the interchange of fluid and solutes. This model removes the need to assume regularly spaced, identical fibres and has been used to describe protein transport in HFBRs (Labecki et al., 2004, Labecki et al., 1996). It does require modification to describe diffusive transport of small molecules such as oxygen however. An alternative modification to the Krogh cylinder model may be to employ techniques developed by Sardonini and DiBiasio (Sardonini and DiBiasio, 1992, Sardonini and DiBiasio, 1993). In this model, the position of the hollow fibres in the cartridge is randomly generated. Using numerical and statistical methods, the resulting cell density profiles could be found. This adds a layer of complexity to the model, but may be hard to scale-up to BALs containing thousands of fibres. Application of some of these principles may lead to interesting developments in BAL design.

Outside the scope of BALs, the techniques developed in this work can also be applied in other fields. Mass transport is a significant issue for any hollow fibre bioreactor application due to the membrane separation of cells and medium. Within tissue engineering, hollow fibre bioreactors are used to grow tissues such as bone (Morgan et al., 2007, Ellis and Chaudhuri, 2007, Ye et al., 2006) and or as the basis of a bioartificial pancreas (Dulong and Legallais, 2007, Pillarella and Zydney, 1990) or kidney (Saito, 2003). In each case it is feasible to employ the Operating Region approach to guide optimization of hollow fibre design. Outside of tissue engineering, biofilms are grown on hollow fibre surfaces for various applications such as nitric oxide removal from waste gases (Kumar et al., 2010) or treatment of wastewater (Beyenal and Tanyolac, 1994). The Operating Region concept could also be applied in these instances.

References

Abdullah, N. S. & Das, D. B. (2007) Modelling nutrient transport in hollow fibremembrane bioreactor for growing bone tissue with consideration of multi-component interactions. *Chemical Engineering Science,* 62**,** 5821-5839.

Abdullah, N. S., Das, D. B., Ye, H. & Cui, Z. F. (2006) 3D bone tissue growth in hollow fibre membrane bioreactor: implications of various process parameters on tissue nutrition. *International Journal of Artificial Organs,* 29**,** 841-851.

Allen, J. W. & Bhatia, S. N. (2003) Formation of steady-state oxygen gradients in vitro - Application to liver zonation. *Biotechnology and Bioengineering,* 82**,** 253-262.

Allen, J. W., Hassanein, T. & Bhatia, S. N. (2001) Advances in bioartificial liver devices. *Hepatology,* 34**,** 447-455.

Allen, J. W., Khetani, S. R. & Bhatia, S. N. (2005) In vitro zonation and toxicity in a hepatocyte bioreactor. *Toxicological Sciences,* 84**,** 110-119.

Anon, Facts about liver disease [online]. British Liver Trust. Available from: http://www.britishlivertrust.org.uk/home/media-centre/facts-about-liver-disease.aspx [Accessed 10 December 2008]

Anon, Overall Indications and Results [online]. European Liver Transplant Registry. Available from: http://www.eltr.org/publi/results.php3?id_rubrique=47 [Accessed 18 February 2009]

Anon, 2008. Vital Therapies Factsheet [online]. Vital Therapies. Available from: http://www.vitaltherapies.com/pdf/VTI_Fact_Sheet_1108.pdf [Accessed 15 January 2009]

Baptista, P. M., Orlando, G., Mirmalek-Sani, S.-H., Siddiqui, M., Atala, A., et al. (2009) Whole organ decellularization - a tool for bioscaffold fabrication and organ bioengineering. *Conf Proc IEEE Eng Med Biol Soc,* 2009**,** 6526-9.

Belfort, G. & Nagata, N. (1985) Fluid-Mechanics and Cross-Flow Filtration - Some Thoughts. *Desalination,* 53**,** 57-79.

Bernal, W., Hall, C., Karvellas, C. J., Auzinger, G., Sizer, E., et al. (2007) Arterial ammonia and clinical risk factors for encephalopathy and intracranial hypertension in acute liver failure. *Hepatology,* 46**,** 1844-1852.

Beyenal, H. & Tanyolac, A. (1994) A Mathematical-Model for Hollow-Fiber Biofilm Reactors. *Chemical Engineering Journal and the Biochemical Engineering Journal,* 56**,** B53-B59.

Brotherton, J., He, D., Asslani, S. & Millis, M. (2007) ELAD (R) cellular and system performance improvements. *Hepatology,* 46**,** 855.

Brotherton, J. D. & Chau, P. C. (1996) Modeling of axial-flow hollow fiber cell culture bioreactors. *Biotechnology Progress,* 12**,** 575-590.

Cabrera, M. I., Luna, J. A. & Grau, R. J. (2001) Solving design equations for a hollow fiber bioreactor with arbitrary kinetics. *Chemical Engineering Journal,* 84**,** 445-461.

Camp, J. P. & Capitano, A. T. (2007) Induction of zone-like liver function gradients in HepG2 cells by varying culture medium height. *Biotechnology Progress,* 23**,** 1485-1491.

Cascio, S. M. (2001) Novel strategies for immortalization of human hepatocytes. *Artificial Organs,* 25**,** 529-538.

Catapano, G. & De Bartolo, L. (2002) Combined effect of oxygen and ammonia on the kinetics of ammonia elimination and oxygen consumption of adherent rat liver cells. *International Journal of Artificial Organs,* 25**,** 151-157.

Catapano, G. & Debartolo, L. (1996) Importance of the kinetic characterization of liver cell metabolic reactions to the design of hybrid liver support devices. *International Journal of Artificial Organs,* 19**,** 670-676.

Chamuleau, R., Flendrig, L. M., Di Florio, E., Mancini, A., Ceriello, A., et al. (1998) Significant improvement of survival time in pigs with complete liver ischemia treated with a novel bioartificial liver (AMC-BAL). *Hepatology,* 28**,** 929.

Chan, C., Berthiaume, F., Nath, B. D., Tilles, A. W., Toner, M., et al. (2004) Hepatic tissue engineering for adjunct and temporary liver support: Critical technologies. *Liver Transplantation,* 10**,** 1331-1342.

Chen, G. & Palmer, A. F. (2009) Hemoglobin-Based Oxygen Carrier and Convection Enhanced Oxygen Transport in a Hollow Fiber Bioreactor. *Biotechnology and Bioengineering,* 102**,** 1603-1612.

Chen, X. P., Xue, Y. L., Li, X. J., Zhang, Z. Y., Li, Y. L., et al. (2001) Experimental research on TECA-I bioartificial liver support system to treat canines with acute liver failure. *World Journal of Gastroenterology,* 7**,** 706-709.

Cho, C. H., Park, J., Nagrath, D., Tilles, A. W., Berthiaume, F., et al. (2007) Oxygen uptake rates and liver-specific functions of hepatocyte and 3T3 fibroblast co-cultures. *Biotechnology and Bioengineering,* 97**,** 188-199.

Consolo, F., Fiore, G. B., Truscello, S., Caronna, M., Morbiducci, U., et al. (2009) A Computational Model for the Optimization of Transport Phenomena in a Rotating Hollow-Fiber Bioreactor for Artificial Liver. *Tissue Engineering Part C-Methods,* 15**,** 41-55.

Craig, D. G. N., Lee, A., Hayes, P. C. & Simpson, K. J. (2010) Review article: the current management of acute liver failure. *Alimentary Pharmacology & Therapeutics,* 31**,** 345-358.

Damak, K., Ayadi, A., Zeghmati, B. & Schmitz, P. (2004) A new Navier-Stokes and Darcy's law combined model for fluid flow in crossflow filtration tubular membranes. *Desalination,* 161**,** 67-77.

Das, D. B. (2007) Multiscale simulation of nutrient transport in hollow fibre membrane bioreactor for growing bone tissue: Sub-cellular scale and beyond. *Chemical Engineering Science,* 62**,** 3627-3639.

Davidson, A. J., Ellis, M. J. & Chaudhuri, J. B. (2010) A Theoretical Method to Improve and Optimize the Design of Bioartificial Livers. *Biotechnology and Bioengineering,* 106**,** 980-988.

Davis, M. E. & Watson, L. T. (1985) Analysis of a Diffusion-Limited Hollow Fiber Reactor for the Measurement of Effective Substrate Diffusivities. *Biotechnology and Bioengineering,* 27**,** 182-186.

De Bartolo, L., Catapano, G., Della Volpe, C. & Drioli, E. (1999) The effect of surface roughness of microporous membranes on the kinetics of oxygen consumption and ammonia elimination by adherent hepatocytes. *Journal of Biomaterials Science-Polymer Edition,* 10**,** 641-655.

De Bartolo, L., Salerno, S., Curcio, E., Piscioneri, A., Rende, M., et al. (2009) Human hepatocyte functions in a crossed hollow fiber membrane bioreactor. *Biomaterials,* 30**,** 2531-43.

De Groot, H., Littauer, A. & Noll, T. (1988) Metabolic and pathological aspects of hypoxia in liver cells. IN ACKER, H. (Ed.) *Oxygen Sensing in Tissue.* New York, Springer-Verlag.

De Rave, S., Tilanus, H. W., Van Der Linden, J., De Man, R. A., Van Der Berg, B., et al. (2002) The importance of orthotopic liver transplantation in acute hepatic failure. *Transplant International,* 15**,** 29-33.

Demetriou, A. A., Brown, R. S., Busuttil, R. W., Fair, J., Mcguire, B. M., et al. (2003) Prospective, randomized, multicenter, controlled trial of a bioartificial liver in treating acute liver failure. *115th Annual Session of the Southern-Surgical-Association.* Hot Springs, VA, Lippincott Williams & Wilkins.

Diekmann, S., Bader, A. & Schmitmeier, S. (2006) Present and future developments in hepatic tissue engineering for liver support systems - State of the art and future developments of hepatic cell culture techniques for the use in liver support systems. *Cytotechnology,* 50**,** 163-179.

Dulong, J. L. & Legallais, C. (2007) A theoretical study of oxygen transfer including cell necrosis for the design of a bioartificial pancreas. *Biotechnology and Bioengineering,* 96**,** 990-998.

Ellis, A. J., Hughes, R. D., Wendon, J. A., Dunne, J., Langley, P. G., et al. (1996) Pilot-controlled trial of the extracorporeal liver assist device in acute liver failure. *Hepatology,* 24**,** 1446-1451.

Ellis, M. J. & Chaudhuri, J. B. (2007) Poly(lactic-co-glycolic acid) hollow fibre membranes for use as a tissue engineering scaffold. *Biotechnology and Bioengineering,* 96**,** 177-187.

Falkenhagen, D., Strobl, W., Vogt, G., Schrefl, A., Linsberger, I., et al. (1999) Fractionated plasma separation and adsorption system: A novel system for blood purification to remove albumin bound substances. *Artificial Organs,* 23**,** 81-86.

Gebhardt, R. (1992) Metabolic Zonation of the Liver - Regulation and Implications for Liver-Function. *Pharmacology & Therapeutics,* 53**,** 275-354.

Gerlach, J., Trost, T., Ryan, C. J., Meissler, M., Hole, O., et al. (1994) Hybrid liver support system in a short-term application on hepatectomized pigs. *International Journal of Artificial Organs,* 17**,** 549-553.

Gerlach, J. C., Zeilinger, K., Sauer, I. M., Mieder, T., Naumann, G., et al. (2002) Extracorporeal liver support: Porcine or human cell based systems? *International Journal of Artificial Organs,* 25**,** 1013-1018.

Giorgio, T. D., Moscioni, A. D., Rozga, J. & Demetriou, A. A. (1993) Mass transfer in a hollow fiber device used as a bioartificial liver. *Asaio J,* 39**,** 886-92.

Gullino, P. M., Grantham, F. H. & Smith, S. H. (1965) Interstitial Water Space of Tumors. *Cancer Research,* 25**,** 727-&.

Hassanein, T. I., Tofteng, F., Brown, R. S., Mcguire, B., Lynch, P., et al. (2007) Randomized controlled study of extracorporeal albumin dialysis for hepatic encephalopathy in advanced cirrhosis. *Hepatology,* 46**,** 1853-1862.

Hay, P. D., Veitch, A. R. & Gaylor, J. D. S. (2001) Oxygen transfer in a convection-enhanced hollow fiber bioartificial liver. *Artificial Organs,* 25**,** 119-130.

Hay, P. D., Veitch, A. R., Smith, M. D., Cousins, R. B. & Gaylor, J. D. S. (2000) Oxygen transfer in a diffusion-limited hollow fiber bioartificial liver. *Artificial Organs,* 24**,** 278-288.

Hillebrand, D. J., Frederick, R. T., Williams, W. W., Brown, R. S., Napotilano, L. M., et al. (2010) Safety and Efficacy of the Extracorporeal Liver Assist Device (ELAD(R)) in Patients with Acute on Chronic Liver Failure. *Journal of Hepatology,* 52**,** S323-S324.

Hsu, W. M., Carraro, A., Kulig, K. M., Miller, M. L., Kaazempur-Mofrad, M., et al. (2010) Liver-Assist Device With a Microfluidics-Based Vascular Bed in an Animal Model. *Annals of Surgery,* 252**,** 351-357.

Jayaraman, V. K. (1992) The Solution of Hollow Fiber Bioreactor Design Equations. *Biotechnology Progress,* 8**,** 462-464.

Jungermann, K. & Kietzmann, T. (2000) Oxygen: Modulator of metabolic zonation and disease of the liver. *Hepatology,* 31**,** 255-260.

Kietzmann, T. & Jungermann, K. (1996) Modulation by oxygen of zonal gene expression in liver studied in primary rat hepatocyte cultures. *International Congress on Hepatocytes - Applications in Cell Biology, Toxicology and Medicine.* Tubingen, Germany, Kluwer Academic Publ.

Kinasiewicz, A., Gautier, A., Lewinska, D., Smietanka, A., Legallais, C., et al. (2008a) Three-dimensional growth of human hepatoma C3A cells within alginate beads for fluidized bioartificial liver. *International Journal of Artificial Organs,* 31**,** 340-347.

Kinasiewicz, A., Smietanka, A., Gajkowska, B. & Werynski, A. (2008b) Impact of Oxygenation of Bioartificial Liver Using Perfluorocarbon Emulsion Perftoran on Metabolism of Human Hepatoma C3A Cells. *Artificial Cells Blood Substitutes and Biotechnology,* 36**,** 525-534.

Kleine, M., Schrem, H., Borlak, J. & Klempnauer, J. (2008) Clinical versatility of porcine hepatocytes in the light of interspecies differences in cytochrome P450 regulation and expression. *Xenotransplantation,* 15**,** 208-217.

Krogh, A. (1919) The number and distribution of capillaries in muscles with calculations of the oxygen pressure head necessary for supplying the tissue. *J Physiol,* 52**,** 409-15.

Kuddus, R., Patzer, J. F., Lopez, R., Mazariegos, G. V., Meighen, B., et al. (2002) Clinical and laboratory evaluation of the safety of a bioartificial liver assist device for potential transmission of porcine endogenous retrovirus. *Transplantation,* 73**,** 420-429.

Kumar, A., Ergas, S. J., Yuan, X., Fitch, M., Min, K. N., et al. (2010) Modeling of a hollow fiber membrane biofilm reactor for nitric oxide removal: Model development and experimental validation. *Journal of Chemical Technology and Biotechnology,* 85**,** 423-428.

Kundu, P. K. & Cohen, I. M. (2001) *Fluid mechanics,* Boston, Mass. ; London, Academic Press.

Labecki, M., Bowen, B. D. & Piret, J. M. (1996) Two-dimensional analysis of protein transport in the extracapillary space of hollow-fibre bioreactors. *Chemical Engineering Science,* 51**,** 4197-4213.

Labecki, M., Piret, J. M. & Bowen, B. D. (1995) 2-Dimensional Analysis of Fluid-Flow in Hollow-Fiber Modules. *Chemical Engineering Science,* 50**,** 3369-3384.

Labecki, M., Piret, J. M. & Bowen, B. D. (2004) Effects of free convection on three-dimensional protein transport in hollow-fiber bioreactors. *Aiche Journal,* 50**,** 1974-1990.

Lee, W. M., Squires, R. H., Nyberg, S. L., Doo, E. & Hoofnagle, J. H. (2008) Acute liver failure: Summary of a workshop. *Hepatology,* 47**,** 1401-1415.

Lindros, K. O. (1997) Zonation of cytochrome P450 expression, drug metabolism and toxicity in liver. *General Pharmacology,* 28**,** 191-196.

Mareels, G., Poyck, P. P. C., Eloot, S., Chamuleau, R. a. F. M. & Verdonck, P. R. (2006) Three-dimensional numerical modeling and computational fluid dynamics simulations to analyze and improve oxygen availability in the AMC bioartificial liver. *Annals of Biomedical Engineering,* 34**,** 1729-1744.

Margaria, R. (1963) A Mathematical Treatment of the Blood Dissociation Curve for Oxygen. *Clin Chem,* 9**,** 745-762.

Mazariegos, G. V., Kramer, D. J., Lopez, R. C., Shakil, A. O., Rosenbloom, A. J., et al. (2001) Safety observations in Phase I clinical evaluation of the Excorp Medical Bioartificial Liver Support System after the first four patients. *Asaio Journal,* 47**,** 471-475.

Mazariegos, G. V., Patzer, J. F., Lopez, R. C., Giraldo, M., Devera, M. E., et al. (2002) First clinical use of a novel bioartificial liver support system (BLSS). *American Journal of Transplantation,* 2**,** 260-266.

Mccuskey, R. S. (2008) The hepatic microvascular system in health and its response to toxicants. *Anatomical Record-Advances in Integrative Anatomy and Evolutionary Biology,* 291**,** 661-671.

Millis, J. M., Cronin, D. C., Johnson, R., Conjeevaram, H., Conlin, C., et al. (2002) Initial experience with the modified extracorporeal liver-assist device for patients with fulminant hepatic failure: System modifications and clinical impact. *Transplantation,* 74**,** 1735-1746.

Mishra, A. & Starly, B. (2009) Real time in vitro measurement of oxygen uptake rates for HEPG2 liver cells encapsulated in alginate matrices. *Microfluidics and Nanofluidics,* 6**,** 373-381.

Miyazaki, M., Bai, L., Tsuboi, S., Seshimo, K. & Namba, M. (1991) Effects of Anitoxidants on Survival of Adult Rat Hepatocytes Under Various Oxygen-Tensions in Serum-Free Primary Culture. *Acta Medica Okayama,* 45**,** 441-444.

Moll, W. (1968) Influence of Hemoglobin Diffusion on Oxygen Uptake and Release by Red Cells. *Respiration Physiology,* 6**,** 1-&.

Morelli, S., Salerno, S., Rende, M., Lopez, L. C., Favia, P., et al. (2007) Human hepatocyte functions in a galactosylated membrane bioreactor. *Journal of Membrane Science,* 302**,** 27-35.

Morgan, S. M., Tilley, S., Perera, S., Ellis, M. J., Kanczler, J., et al. (2007) Expansion of human bone marrow stromal cells on poly-(DL-lactide-co-glycolide) (P(DL)LGA) hollow fibres designed for use in skeletal tissue engineering. *Biomaterials,* 28**,** 5332-5343.

Morsiani, E., Brogli, M., Galavotti, D., Pazzi, P., Puviani, A. C., et al. (2002) Biologic liver support: Optimal cell source and mass. *International Journal of Artificial Organs,* 25**,** 985-993.

Moussy, Y. (2003) Convective flow through a hollow fiber bioartificial liver. *Artificial Organs,* 27**,** 1041-1049.

Mullon, C. & Pitkin, Z. (1999) The HepatAssist bioartificial liver support system: clinical study and pig hepatocyte process. *Expert Opin Investig Drugs,* 8**,** 229-35.

Neto, C., Evans, D. R., Bonaccurso, E., Butt, H. J. & Craig, V. S. J. (2005) Boundary slip in Newtonian liquids: a review of experimental studies. *Reports on Progress in Physics,* 68**,** 2859-2897.

Nyberg, S. L., Remmel, R. P., Mann, H. J., Peshwa, M. V., Hu, W. S., et al. (1994) Primary Hepatocytes Outperform Hep G2 Cells as the Source of Biotransformation Functions in a Bioartificial Liver. *Annals of Surgery,* 220**,** 59-67.

Ohashi, K., Yokoyama, T., Yamato, M., Kuge, H., Kanehiro, H., et al. (2007) Engineering functional two- and three-dimensional liver systems in vivo using hepatic tissue sheets. *Nature Medicine,* 13**,** 880-885.

Palsson, B. O. (2004) *Tissue Engineering*, Pearson Prentice Hall.

Patzer, J. F. (2004) Oxygen consumption in a hollow fiber bioartificial liver-revisited. *Artificial Organs,* 28**,** 83-98.

Patzer, J. F., Campbell, B. & Miller, R. (2002a) Plasma versus whole blood perfusion in a bioartificial liver assist device. *Asaio Journal,* 48**,** 226-233.

Patzer, J. F., Mazariegos, G. V., Lopez, R. & Invest, B. L. P. (2002b) Preclinical evaluation of the Excorp Medical, Inc, bioartificial liver support system. *Journal of the American College of Surgeons,* 195**,** 299-310.

Patzer, J. F., Mazariegos, G. V., Lopez, R., Molmenti, E., Gerber, D., et al. (1999) Novel Bioartificial Liver Support System: Preclinical Evaluation. *Annals of the New York Academy of Sciences,* 875**,** 340-352.

Peszynski, P., Peters, E. & Schmidt, R. (2001) Albumin dialysis: single pass vs. recirculation (MARS). *3rd International Rostock Symposium on Albumin Dialysis in Liver Disease.* Rostock, Germany, Blackwell Munksgaard.

Pillarella, M. R. & Zydney, A. L. (1990) Theoretical Analysis of the Effect of Convective Flow on Solute Transport and Insulin Release in a Hollow Fibre Bioartificial Pancreas. *Journal of Biomechanical Engineering-Transactions of the Asme,* 112**,** 220-228.

Piret, J. M. & Cooney, C. L. (1990) Mammalian-cell and protein distributions in ultrafiltration hollow fiber bioreactors. *Biotechnology and Bioengineering,* 36**,** 902-910.

Piret, J. M. & Cooney, C. L. (1991) Model of Oxygen-Transport Limitations in Hollow Fiber Bioreactors. *Biotechnology and Bioengineering,* 37**,** 80-92.

Pless, G. & Sauer, I. M. (2005) Bioartificial liver: Current status. *Transplantation Proceedings,* 37**,** 3893-3895.

Podger, C., 1999. Setback for animal to human transplants [online]. BBC. Available from: http://news.bbc.co.uk/1/hi/sci/tech/265933.stm [Accessed 17 December 2008]

Poyck, P. P. C., Pless, G., Hoekstra, R., Roth, S., Van Wijk, A. C. W. A., et al. (2007) In vitro comparison of two bioartificial liver support systems: MELS CellModule and AMC-BAL. *International Journal of Artificial Organs,* 30**,** 183-191.

Pryor, H. I. & Vacanti, J. P. (2008) The promise of artificial liver replacement. *Frontiers in Bioscience,* 13**,** 2140-2159.

Qian, Y., Lanjuan, L., Jianrong, H., Jun, L., Hongcui, C., et al. (2003) Study of severe hepatitis treated with a hybrid artificial liver support system. *International Journal of Artificial Organs,* 26**,** 507-513.

Radisic, M., Deen, W., Langer, R. & Vunjak-Novakovic, G. (2005) Mathematical model of oxygen distribution in engineered cardiac tissue with parallel channel array perfused with culture medium containing oxygen carriers. *American Journal of Physiology-Heart and Circulatory Physiology,* 288**,** H1278-H1289.

Renkin, E. M. (1954) Filtration, diffusion, and molecular sieving through porous cellulose membranes. *J Gen Physiol,* 38**,** 225-43.

Rifai, K. (2008) Extracorporeal albumin dialysis. *Hepatology Research,* 38**,** S41-S45.

Rifai, K., Ernst, T., Kretschmer, U., Bahr, M. J., Schneider, A., et al. (2003) Prometheus (R) - a new extracorporeal system for the treatment of liver failure. *Journal of Hepatology,* 39**,** 984-990.

Ross, S. M. (1974) Mathematical-Model of Mass-Transport in a Long Permeable Tube with Radial Convection. *Journal of Fluid Mechanics,* 63**,** 157-175.

Rozga, J. (2006) Liver support technology - an update. *Xenotransplantation,* 13**,** 380-389.

Rozga, J., Holzman, M. D., Ro, M. S., Griffin, D. W., Neuzil, D. F., et al. (1992) Development of a Hybrid Bioartificial Liver. *104th Annual Meeting of the Southern Surgical Assoc.* Aventura, Fl, Lippincott-Raven Publ.

Saito, A. (2003) Development of bioartificial kidneys. *Nephrology,* 8**,** S10-S15.

Sander, R., 2007. Compilation of Henry's Law Constants for Inorganic and Organic Species of Potential Importance in Environmental Chemistry (Version 3) [online].

Mainz: Max Planck Institute for Chemistry. Available from: http://www.henrys-law.org [Accessed 10 August 2008]

Sardonini, C. A. & Dibiasio, D. (1992) An Investigation of the Diffusion-Limited Growth of Animal-Cells around Single Hollow Fibers. *Biotechnology and Bioengineering,* 40**,** 1233-1242.

Sardonini, C. A. & Dibiasio, D. (1993) Growth of Animal-Cells around Hollow Fibers - Multifiber Studies. *Aiche Journal,* 39**,** 1415-1419.

Sauer, I. M. & Gerlach, J. C. (2002) Modular extracorporeal liver support. *Artificial Organs,* 26**,** 703-706.

Sauer, I. M., Goetz, M., Steffen, I., Walter, G., Kehr, D. C., et al. (2004) In vitro comparison of the molecular adsorbent recirculation system (MARS) and single-pass albumin dialysis (SPAD). *Hepatology,* 39**,** 1408-1414.

Sauer, I. M., Kardassis, D., Zeillinger, K., Pascher, A., Gruenwald, A., et al. (2003) Clinical extracorporeal hybrid liver support - phase I study with primary porcine liver cells. *Xenotransplantation,* 10**,** 460-469.

Sauer, I. M., Schwartlander, R., Van Der Jagt, O., Steffen, I., Efimova, E., et al. (2005) In vitro evaluation of the transportability of viable primary human liver cells originating from discarded donor organs in bioreactors. *Artificial Organs,* 29**,** 144-151.

Sauer, I. M., Zeilinger, K., Obermayer, N., Pless, G., Grunwald, A., et al. (2002) Primary human liver cells as source for modular extracorporeal liver support - a preliminary report. *International Journal of Artificial Organs,* 25**,** 1001-1005.

Saxena, R., Zucker, S. D. & Crawford, J. M. (2003) Anatomy and Physiology of the Liver. IN ZAKIM, D. & BOYER, T. D. (Eds.) *Hepatology : a textbook of liver disease.* 4th ed. Philadelphia ; London, Saunders.

Scanlon, V. C. & Sanders, T. (2003) *Essentials of anatomy and physiology,* Philadelphia, F.A. Davis Co.

Schonberg, J. A. & Belfort, G. (1987) Enhanced Nutrient Transport in Hollow Fiber Perfusion Bioreactors - a Theoretical-Analysis. *Biotechnology Progress,* 3**,** 80-89.

Shaffer, E. A., 2007. Merck Manual of Medical Information [online]. Second Home Edition. Merck. Available from: http://www.merck.com/mmhe/ag/print/sec10/ch138/ch138a.html [Accessed 7 January 2009]

Shen, C. N., Horb, M. E., Slack, J. M. W. & Tosh, D. (2003) Transdifferentiation of pancreas to liver. *Mechanisms of Development,* 120**,** 107-116.

Shipley, R. J., Davidson, A. J., Chan, K., Chaudhuri, J. B., Waters, S. L., et al. (2011) A Strategy to Determine Operating Parameters in Tissue Engineering Hollow Fiber Bioreactors. *Biotechnology and Bioengineering,* 108**,** 1450-1461.

Shipley, R. J., Waters, S. L. & Ellis, M. J. (2010) Definition and Validation of Operating Equations for Poly(Vinyl Alcohol)-Poly(Lactide-Co-Glycolide) Microfiltration Membrane-Scaffold Bioreactors. *Biotechnology and Bioengineering,* 107**,** 382-392.

Sielaff, T. D., Nyberg, S. L., Rollins, M. D., Hu, M. Y., Amiot, B., et al. (1997) Characterization of the three-compartment gel-entrapment porcine hepatocyte bioartificial liver. *Cell Biology and Toxicology,* 13**,** 357-364.

Stadlbauer, V., Davies, N. A., Sen, S. & Jalan, R. (2008) Artificial liver support systems in the management of complications of cirrhosis. *Seminars in Liver Disease,* 28**,** 96-109.

Stadlbauer, V., Wright, G. a. K. & Jalan, R. (2009) Role of artificial liver support in hepatic encephalopathy. *Metab Brain Dis,* 24**,** 15-26.

Stange, J., Mitzner, S. R., Risler, T., Erley, C. M., Lauchart, W., et al. (1999) Molecular adsorbent recycling system (MARS): Clinical results of a new membrane-based blood purification system for bioartificial liver support. *Artificial Organs,* 23**,** 319-330.

Strain, A. J. & Neuberger, J. M. (2002) A bioartificial liver - State of the art. *Science,* 295**,** 1005-+.

Sullivan, J. P., Gordon, J. E., Bou-Akl, T., Matthew, H. W. T. & Palmer, A. F. (2007) Enhanced oxygen delivery to primary hepatocytes within a hollow fiber bioreactor facilitated via hemoglobin-based oxygen carriers. *Artificial Cells Blood Substitutes and Biotechnology,* 35**,** 585-606.

Sullivan, J. P., Harris, D. R. & Palmer, A. F. (2008) Convection and hemoglobin-based oxygen carrier enhanced oxygen transport in a hepatic hollow fiber bioreactor. *Artificial Cells Blood Substitutes and Biotechnology,* 36**,** 386-402.

Sullivan, J. P. & Palmer, A. F. (2006) Targeted oxygen delivery within hepatic hollow fiber bioreactors via supplementation of hemoglobin-based oxygen carriers. *Biotechnology Progress,* 22**,** 1374-1387.

Sussman, N. L., Koussayer, T., He, D. E. & Kelly, J. H. (1991) Rescue from Fulminant Hepatic-Failure with an Extracorporeal Liver Assist Device (ELAD). *Hepatology,* 14**,** A95-A95.

Telford, I. R. & Bridgman, C. F. (1995) Digestive System III - Pancreas, Liver , and Biliary Tract. *Introduction to Functional Histology.* 2nd ed. New York ;, HarperCollins College Publishers.

Tilles, A. W., Baskaran, H., Roy, P., Yarmush, M. L. & Toner, M. (2001) Effects of oxygenation and flow on the viability and function of rat hepatocytes cocultured in a microchannel flat-plate bioreactor. *Biotechnology and Bioengineering,* 73**,** 379-389.

Tosh, D., Shen, C. N. & Slack, J. M. W. (2002) Differentiated properties of hepatocytes induced from pancreatic cells. *Hepatology,* 36**,** 534-543.

Uygun, B. E., Soto-Gutierrez, A., Yagi, H., Izamis, M. L., Guzzardi, M. A., et al. (2010) Organ reengineering through development of a transplantable recellularized liver graft using decellularized liver matrix. *Nature Medicine,* 16**,** 814-U120.

Van De Kerkhove, M. P., Hoekstra, R., Chamuleau, R. a. F. M. & Van Gulik, T. M. (2004) Clinical application of bioartificial liver support systems. *Annals of Surgery,* 240**,** 216-230.

Wigg, A. J. & Padbury, R. T. (2005) Liver support systems: Promise and reality. *Journal of Gastroenterology and Hepatology,* 20**,** 1807-1816.

Willaert, R., Smets, A. & De Vuyst, L. (1999) Mass transfer limitations in diffusion-limited isotropic hollow fiber bioreactors. *Biotechnology Techniques,* 13**,** 317-323.

Williams, S. N. O., Callies, R. M. & Brindle, K. M. (1997) Mapping of oxygen tension and cell distribution in a hollow-fiber bioreactor using magnetic resonance imaging. *Biotechnology and Bioengineering,* 56**,** 56-61.

Woodley, J. M. & Titchener-Hooker, N. J. (1996) The use of windows of operation as a bioprocess design tool. *Bioprocess Engineering,* 14**,** 263-268.

Wurm, M., Lubei, V., Caronna, M., Hermann, M., Buttiglieri, S., et al. (2009) Introduction of a Novel Prototype Bioartificial Liver Support System Utilizing Small Human Hepatocytes in Rotary Culture. *Tissue Engineering Part A,* 15**,** 1063-1073.

Wurm, M., Woess, C., Libiseller, K., Beer, B. & Pavlic, M. (2010) Challenging small human hepatocytes with opiates: further characterization of a novel prototype bioartificial liver. *Tissue Eng Part A,* 16**,** 807-13.

Xue, Y. L., Zhao, S. F., Yun-Luo, Li, X. J., Duan, Z. P., et al. (2001) TECA hybrid artificial liver support system in treatment of acute liver failure. *World Journal of Gastroenterology,* 7**,** 826-829.

Ye, H., Das, D. B., Triffitt, J. T. & Cui, Z. F. (2006) Modelling nutrient transport in hollow fibre membrane bioreactors for growing three-dimensional bone tissue. *Journal of Membrane Science,* 272**,** 169-178.

Yu, C. B., Pan, X. P. & Li, L. J. (2009) Progress in bioreactors of bioartificial livers. *Hepatobiliary & Pancreatic Diseases International,* 8**,** 134-140.

Zhou, Y. H. & Titchener-Hooker, N. J. (1999) Visualizing integrated bioprocess designs through "windows of operation". *Biotechnology and Bioengineering,* 65**,** 550-557.

Appendix

A.1 Matlab Scripting

A.1.1 Zonation profile script

```
function [Z2 Z10 Z25 Z35 Z60 Z70] = hollowfibreBAL(pO2_inlet, Vmax,
Cell_layers, membrane_thickness) %returns boundary positions for
particular BAL set-ups
Z2=[]; % define arrays which hold the axial positions of the relevant
zone boundaries
Z10=[];
Z25=[];
Z35=[];
Z60=[];
Z70=[];
w = membrane_thickness;
pO2 = pO2_inlet;
CL = Cell_layers;
    for ubar = 1e-3:1.5e-3:7e-3 %loop through the range of plasma flow
rates, finding the zonation profile in each case
        Rl = 1.4e-4;
        Rm = Rl+w;
        Rk = Rl+w+CL*25e-6;


        % COMSOL Multiphysics Model M-file
        % Generated by COMSOL 3.5a (COMSOL 3.5.0.606, $Date: 2009/04/29
09:11:29 $)

        flclear fem

        % COMSOL version
        clear vrsn
        vrsn.name = 'COMSOL 3.5';
        vrsn.ext = 'a';
        vrsn.major = 0;
        vrsn.build = 606;
        vrsn.rcs = '$Name: v35ap $';
        vrsn.date = '$Date: 2009/04/29 09:11:29 $';
        fem.version = vrsn;


        % Constants
        fem.const = {'ubar',ubar, ...
            'Rl', Rl ...
           'Vmax',Vmax};

        % Geometry
        g1=rect2(Rl,1e-3/CL,'base','corner','pos',{'0','0'},'rot','0');
        g2=rect2(Rm,1e-3/CL,'base','corner','pos',{'0','0'},'rot','0');
        g3=rect2(Rk,1e-3/CL,'base','corner','pos',{'0','0'},'rot','0');

        % Analyzed geometry
        clear s
        s.objs={g1,g2,g3};
        s.name={'R1','R2','R3'};
        s.tags={'g1','g2','g3'};
```

```
fem.draw=struct('s',s);
fem.geom=geomcsg(fem);

% Initialize mesh
fem.mesh=meshinit(fem, ...
                  'hauto',5);

% Refine mesh
fem.mesh=meshrefine(fem, ...
                    'mcase',0, ...
                    'rmethod','regular');
fem.mesh=meshrefine(fem, ...
                    'mcase',0, ...
                    'rmethod','regular');

% (Default values are not included)

% Application mode 1
clear appl
appl.mode.class = 'ConvDiff';
appl.mode.type = 'axi';
appl.module = 'CHEM';
appl.sshape = 2;
appl.assignsuffix = '_chcd';
clear prop
prop.analysis='static';
appl.prop = prop;
clear bnd
bnd.c0 = {0,0,pO2,0,0};
bnd.type = {'N0','cont','C','ax','Nc'};
bnd.ind = [4,3,5,2,1,1,2,1,1,1];
appl.bnd = bnd;
clear equ
equ.dtensor = {{{3e-9;0}},{{3e-9;0}},{{2e-9;0}}};
equ.v = {'2*ubar*(1-(r/Rl)^2)/1000',0,0}; %Poisueille flow in
lumen
equ.R = {0,0,'-481*Vmax*c/(c+3)'}; %Michaelis-Menten kinetics
equ.dtype = 'aniso';
equ.ind = [1,2,3];
appl.equ = equ;
fem.appl{1} = appl;
fem.sdim = {'r','z'};
fem.frame = {'ref'};
fem.border = 1;
fem.outform = 'general';
clear units;
units.basesystem = 'SI';
fem.units = units;

% ODE Settings
clear ode
clear units;
units.basesystem = 'SI';
ode.units = units;
fem.ode=ode;

% Multiphysics
fem=multiphysics(fem);

% Extend mesh
```

```
        fem.xmesh=meshextend(fem);

        % Solve problem
        fem.sol=femstatic(fem, ...
              'solcomp',{'c'}, ...
              'maxiter',40, ...
              'outcomp',{'c'});

        % Save current fem structure for restart purposes
        fem0=fem;


        % Find position of each zone boundary
        [m2 d2] = postmin(fem,'sqrt((c-2)^2)','edim',1,'dl',10);
        Z2(:,end+1)=d2(2)*1000;
        [m10 d10] = postmin(fem,'sqrt((c-10)^2)','edim',1,'dl',10);
        Z10(:,end+1)=d10(2)*1000;
        [m25 d25] = postmin(fem,'sqrt((c-25)^2)','edim',1,'dl',10);
        Z25(:,end+1)=d25(2)*1000;
        [m35 d35] = postmin(fem,'sqrt((c-35)^2)','edim',1,'dl',10);
        Z35(:,end+1)=d35(2)*1000;
        [m60 d60] = postmin(fem,'sqrt((c-60)^2)','edim',1,'dl',10);
        Z60(:,end+1)=d60(2)*1000;
        [m70 d70] = postmin(fem,'sqrt((c-70)^2)','edim',1,'dl',10);
        Z70(:,end+1)=d70(2)*1000;
    end
```

A.1.2 Optimization script

```
function [Qopt1 optimal_zone_pattern1 Qopt2 optimal_zone_pattern2 ] =
HepaMate_optimum
%Return flowrates and zonation pattern for each optimization protocol


% COMSOL Multiphysics Model M-file
% Generated by COMSOL 3.5a (COMSOL 3.5.0.606, $Date: 2009/04/29 09:11:29
$)

flclear fem
Ncell=1.4e10;
Nf=4800;
Rl=1.6e-4;
Rm=1.9e-4;
L=.25;
Dl=3e-9;
Lz = [];
L70 =[];
L60 =[];
L35 =[];
L25 =[];
L10 =[];
L2=[];
epsilon = 0.5;
De=epsilon*2e-9+(1-epsilon)*Dl;
Vecs_per_fibre=Ncell*(4/3)*(3.142*12.5e-6^3)/(Nf*epsilon);
Re=sqrt((Vecs_per_fibre+Rm^2*3.142*L)/(3.142*L));
```

```
for ubar =
(250/6e7/Nf)/(3.142*Rl^2):(5/6e7/Nf)/(3.142*Rl^2):(400/6e7/Nf)/(3.142*Rl^
2); %Scan through range of flowrates, 250-400 ml/min
    % COMSOL version
    clear vrsn
    vrsn.name = 'COMSOL 3.5';
    vrsn.ext = 'a';
    vrsn.major = 0;
    vrsn.build = 606;
    vrsn.rcs = '$Name: v35ap $';
    vrsn.date = '$Date: 2009/04/29 09:11:29 $';
    fem.version = vrsn;

    % Constants
    fem.const = {'Dl',Dl, ...
      'De',De, ...
      'Vmax','5.87e-3 [mol/s/m^3]', ...
      'Km','3 [mmHg]', ...
      'epsilon',epsilon, ...
      'Rl',Rl, ...
      'Rm',Rm, ...
      'Re',Re, ...
      'ubar',ubar, ...
      'pO2_inECS','80' ...
      'L',L, ...
      'alpha','2.08e-3', ...
      'pO2_in','90', ...
      'pO2min','10', ...
      'Dm','3e-9'};

    % Geometry
    g1=rect2('1','1','base','corner','pos',{'0','0'},'rot','0');
    g2=rect2(Rm/Rl,'1','base','corner','pos',{'0','0'},'rot','0');
    g3=rect2(Re/Rl,'1','base','corner','pos',{'0','0'},'rot','0');

    % Analyzed geometry
    clear s
    s.objs={g1,g2,g3};
    s.name={'R1','R2','R3'};
    s.tags={'g1','g2','g3'};

    fem.draw=struct('s',s);
    fem.geom=geomcsg(fem);

    % Initialize mesh
    fem.mesh=meshinit(fem, ...
                      'hauto',5);

    % Refine mesh
    fem.mesh=meshrefine(fem, ...
                        'mcase',0, ...
                        'rmethod','regular');

    % Refine mesh
    fem.mesh=meshrefine(fem, ...
                        'mcase',0, ...
                        'rmethod','regular');

    % Refine mesh
    fem.mesh=meshrefine(fem, ...
                        'mcase',0, ...
```

```
                        'rmethod','regular');


    % (Default values are not included)

    % Application mode 1
    clear appl
    appl.mode.class = 'FlConvDiff';
    appl.mode.type = 'axi';
    appl.dim = {'pO2'};
    appl.sshape = 2;
    appl.assignsuffix = '_cd';
    clear prop
    prop.analysis='static';
    appl.prop = prop;
    clear bnd
    bnd.c0 = {0,0,'pO2_in',0,0};
    bnd.type = {'N0','cont','C','Nc','ax'};
    bnd.ind = [5,3,4,2,1,1,2,1,1,1];
    appl.bnd = bnd;
    clear equ
    equ.init = {'pO2_in',0,0};
    equ.dtensor =
{{{'Dl/Rl^2';'Dl/L^2'}},{{'Dm/Rl^2';'Dm/L^2'}},{{'De/Rl^2';'De/L^2'}}};
    equ.v = {'2*ubar*(1-r^2)/L',0,0};
    equ.R = {0,0,'-epsilon*Vmax*pO2/(alpha*(pO2+Km))'};
    equ.dtype = 'aniso';
    equ.ind = [1,2,3];
    appl.equ = equ;
    fem.appl{1} = appl;
    fem.sdim = {'r','z'};
    fem.frame = {'ref'};
    fem.border = 1;
    fem.outform = 'general';

    % Descriptions
    clear descr
    descr.const= {'alpha','henry constant','X','Hb fraction'};
    descr.globalexpr= {'Seq','equilibrium
saturation','RHbO2','binding/release kinetics'};
    fem.descr = descr;

    % Multiphysics
    fem=multiphysics(fem);

    % Extend mesh
    fem.xmesh=meshextend(fem);

    % Solve problem
    fem.sol=femstatic(fem, ...
                      'solcomp',{'pO2'}, ...
                      'outcomp',{'pO2'}, ...
                      'maxiter',40, ...
                      'blocksize','auto');

    % Save current fem structure for restart purposes
    fem0=fem;

         [m z] = postmin(fem,'sqrt((pO2-70)^2)','edim',1,'dl',10);
         L70(end+1)=L*z(2);
         [m2 z2] = postmin(fem,'sqrt((pO2-60)^2)','edim',1,'dl',10);
```

```
        L60(end+1)=L*z2(2);
        [m3 z3] = postmin(fem,'sqrt((pO2-35)^2)','edim',1,'dl',10);
        L35(end+1)=L*z3(2);
        [m4 z4] = postmin(fem,'sqrt((pO2-25)^2)','edim',1,'dl',10);
        L25(end+1)=L*z4(2);
        [m5 z5] = postmin(fem,'sqrt((pO2-10)^2)','edim',1,'dl',10);
        L10(end+1)=L*z5(2);
        [m6 z6] = postmin(fem,'sqrt((pO2-2)^2)','edim',1,'dl',10);
        L2(end+1)=L*z6(2);

end
Lz = [L70',L60',L35',L25',L10'];
zones=[L70/L,(L60-L70)/L,(L35-L60)/L,(L25-L35)/L,(L10-L25)/L,(L-L10)/L];
Lz = [L70',L60',L35',L25',L10'];
zones=[L70/L;(L60-L70)/L;(L35-L60)/L;(L25-L35)/L;(L10-L25)/L;(L-L10)/L]';
x=zones(:,1)+zones(:,2);
y=zones(:,4)+zones(:,5);
zopt=sqrt((((L60-L70)/L)-((L25-L35)/L)).^2); %optimize by setting
periportal=perivenous
zopt2=sqrt((x-y).^2);  %optimize by setting hyper+periportal =
perivenous+hypo
[C I]=min(zopt);
while L10(I)<L %scan through all zonation profiles, finding the optimum
    zopt(I)=10;
    [C I]=min(zopt);
end
[C2 I2]=min(zopt2);
while L10(I2)<L
    zopt2(I2)=10;
    [C2 I2]=min(zopt2);
end
ubar =
(250/6e7/Nf)/(3.142*Rl^2):(5/6e7/Nf)/(3.142*Rl^2):(400/6e7/Nf)/(3.142*Rl^
2);
optimal_zone_pattern1 = zones(I,:);
optimal_zone_pattern2 = zones(I2,:);
Qopt1 = 6e7*3.142*Rl^2*Nf*ubar(I);
Qopt2 = 6e7*3.142*Rl^2*Nf*ubar(I2);
```

Similar scripts exist for the optimization of the BLSS and ELAD systems.

List of Conferences and Papers

Conferences/Seminars

Summer Workshop in Mathematical Medicine and Biology, Nottingham University (July 2008)
Centre for Regenerative Medicine Seminar, University of Bath (Feb 2009)
Network Young Membrains (sic), Meze, France (Sept 2009)
IChemE Bioprocessing Young Researchers Meeting, University of Cambridge (April 2010)
Tissue Culture and Cell Engineering Conference, University of Manchester (July 2010)
Annual bioProcessUK Conference, Manchester (Nov 2010)
Annual Tissue Engineering and Regenerative Medicine International Society North American Conference (Dec 2010)

Papers

Davidson, A. J., Ellis, M. J. & Chaudhuri, J. B. (2010) A Theoretical Method to Improve and Optimize the Design of Bioartificial Livers. Biotechnology and Bioengineering, 106, 980-988.

Shipley, R. J., Davidson, A. J., Chan, K., Chaudhuri, J. B., Waters, S. L. & Ellis, M. J. (2010) A Strategy to Determine Operating Parameters in Tissue Engineering Hollow Fiber Bioreactors. Biotechnology and Bioengineering, 108, 1450-1461.

Davidson, A. J., Ellis, M. J. & Chaudhuri, J. B. (2011) A theoretical approach to zonation in a bioartificial liver. Biotechnology and Bioengineering, In press